AD-A164 560 MICROSCOPIC CONTROL OF SEMICONDUCTOR INTERFACE REACTIVITY(U) MINNESOTA UNIV MINNEAPOLIS DEPT OF CHEMICAL ENGINEERING AND MATERIALS SCIENCE A FRANCIOSI 1/1

UNCLASSIFIED 10 JAN 86 N00014-84-K-0545 F/G 7/4 NL

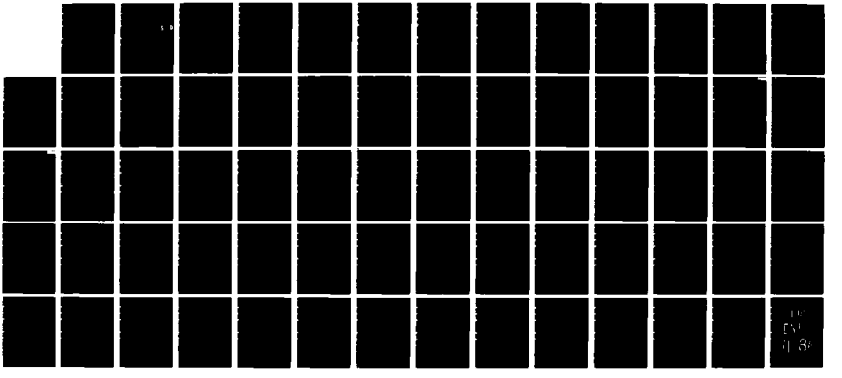

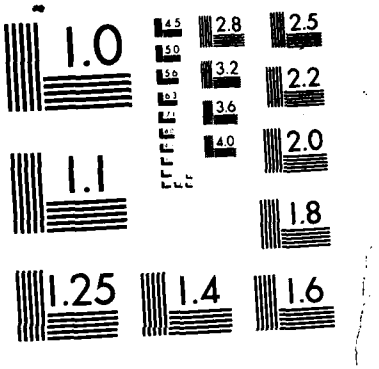

OFFICE OF NAVAL RESEARCH

ANNUAL REPORT: 08/01/84 - 07/31/85

CONTRACT # N00014-84-K-0545
TASK NR 371-162

MICROSCOPIC CONTROL OF SEMICONDUCTOR INTERFACE REACTIVITY

Principal Investigator: A. Franciosi

Department of Chemical Engineering
and Materials Science
University of Minnesota
Minneapolis, Minnesota 55455

REPORT DOCUMENTATION PAGE

READ INSTRUCTIONS BEFORE COMPLETING FORM

1. REPORT NUMBER: 7	2. GOVT ACCESSION NO.
3. RECIPIENT'S CATALOG NUMBER	
4. TITLE (and Subtitle): Annual Report 8/1/84-7/31/85	5. TYPE OF REPORT & PERIOD COVERED: Interim; 8/1/84-7/30/86
	6. PERFORMING ORG. REPORT NUMBER
7. AUTHOR(s): A. Franciosi	8. CONTRACT OR GRANT NUMBER(s): N00014-84-K-0545
9. PERFORMING ORGANIZATION NAME AND ADDRESS: University of Minnesota 1919 University Ave St Paul, MN 55104	10. PROGRAM ELEMENT, PROJECT, TASK AREA & WORK UNIT NUMBERS: task NR 372-162
11. CONTROLLING OFFICE NAME AND ADDRESS: Office of Naval Research Electronics Division (Dr. K. Hathaway) Department of the Navy, Arligton, VA 22217	12. REPORT DATE: 1/10/86 13. NUMBER OF PAGES: 64
14. MONITORING AGENCY NAME & ADDRESS (if different from Controlling Office)	15. SECURITY CLASS. (of this report): unclassified 15a. DECLASSIFICATION/DOWNGRADING SCHEDULE

16. DISTRIBUTION STATEMENT (of this Report)

Approved for publi release; unlimited distribution.

17. DISTRIBUTION STATEMENT (of the abstract entered in Block 20, if different from Report)

18. SUPPLEMENTARY NOTES

19. KEY WORDS (Continue on reverse side if necessary and identify by block number)

Interface reactivity; catalysis; metal-semiconductor interfaces

20. ABSTRACT (Continue on reverse side if necessary and identify by block number)

First year annual report for the program "Microscopic Control of Semiconductor Interface Reactivity".

DD FORM 1 JAN 73 1473 EDITION OF 1 NOV 65 IS OBSOLETE
S/N 0102-LF-014-6601

unclassified
SECURITY CLASSIFICATION OF THIS PAGE (When Data Entered)

Table of Contents

Summary of First Year Activity

In recent years a number of metal overlayers on silicon have been shown to yield an increase in silicon oxidation rate when the surface is exposed to an oxidizing atmosphere. Metals as diverse as Au, Ag, Cu, Pd all give rise to promotion effects, with the production of Si-oxide phases of variable stoichiometry. In the case of Au and Cr, the Si-oxide appears to nucleate on top of the metal overlayer. To the extent that the metal atoms increase the surface reaction kinetics and do not appear directly involved in the reaction product, i.e. the surface silicon oxide, they play the role of a catalyst. Since the magnitude of the effect depends on the overlayer-silicon interface morphology, in the absence of a more precise denomination we refer to such phenomena as interface catalytic effects.

The main goal of our program is to investigate the microscopic mechanisms which determine these effects, characterize the electronic and structural modifications that accompany the surface reactions, determine the stoichiometry of the reaction products and/or the interface composition profile, and ultimately obtain an enhanced control of the kinetics of surface reactions with gaseous species and metals. Long term practical applications include the synthesis of new insulating and metallic epitaxial layers on Si and GaAs and enhanced control of interdiffusion and contact stability.

We have conducted parallel investigations on Si(111) and GaAs(110) surfaces. Our interest in GaAs stems from both technological and fundamental reasons. The possible use of catalysts to promote the formation of new stable insulating layers on GaAs surfaces would have substantial impact on device technology, if the reacted layers would exhibit inversion and accumulation characteristics suitable for MOS fabrication. From a fundamental point of view,

our understanding of the microscopic mechanisms that determine interface catalytic effects could be greatly improved by considering GaAs-metal interfaces, which may exhibit for a given metal different chemistry and different local morphology relative to the silicon case.

We have conducted a number of synchrotron radiation photoemission studies of the effect of different metal overlayers on the oxidation rate of GaAs and Si surfaces. We have concentrated on low pressure, low temperature reaction with oxygen or water, and on semiconductor substrates cleaved in situ, in order to simplify the experimental procedures and to expedite the build-up of a substantial systematics. The objective was to establish correlations between the specific catalytic activity of a given overlayer, the chemistry of the metal and the properties of the semiconductor surface.

Investigation of the interaction of Si and GaAs surfaces with oxygen in the presence of Ag, Au, and Cr overlayers, and of semiconductor-water reaction in the presence of Cr and Mo overlayers show that the magnitude of the oxidation promotion effect depends on the chemistry of the overlayer, on the local morphology of the interface region and on the nature of the gaseous reactants. For example Au shows catalytic activity both on GaAs and Si, while Ag exhibit some measure of activity on Si, where it forms an intermixed, diffuse interface, but not on GaAs, where the interface morphology is sharp and unreacted. We find that the promotion effect in the series is maximum in the presence of Cr overlayers, and that the nature of the surface reaction products changes if oxygen or water is employed. For example, in the case of oxygen on GaAs, Ga and As oxide phases are found with high atomic oxidation states present. If water is employed, only Ga oxide/hydroxyl phases are found at the surface, on top of a Cr-As subsurface layer that remains largely unaffected by oxidation.

The strong catalytic activity of Cr overlayers on both Si and GaAs surfaces stimulated our interst in examining the role of Cr on other semiconductor substrates with different type of bonding. Semiconductor of the II-VI family are known to exhibit substantial ionic character in the bonding and to give rise to strong exchange reactions following metal deposition. We choose $Hg_{1-x}Cd_xTe$ alloys for their technological interest for infrared applications. We characterized the local interface morphology of Cr overlayers onto $Hg_{1-x}Cd_xTe(110)$ surfaces. Our results show that the local interface morphology is far more complex than for GaAs or Si, with Cr replacing Hg atoms at room temperature in a 10-13Å thick subsurface layer. Studies of the potential role of Cr in controlling $Hg_{1-x}Cd_xTe$ surface reactivity with oxygen are in progress.

In all of the catalytic studies performed in our program, the oxidation of the interface species resulted in their decomposition into stable oxide phases. If this process leads to saturation of the chemisorption process, then the technological implications would be minor. However, in all cases we have examined thus far we did not observe saturation at the highest exposures explored at room temperature. This suggests that when the mass-transfer problem is solved by low-temperature annealing of the substrate during reaction, relatively thick oxidized layers can be grown. Even at room temperature thicknesses larger than 20-30 Å are easily obtained. The metal atoms that remain relatively unreacted in the first oxidation stage, appear oxidized at high exposure. This, however, may not eliminate catalytic effects, since transition metal mixed oxide phases show considerable catalytic activity for a number of chemical reactions, and explain why saturation is not observed.

The evidence that the chemistry of the metal is of primary importance in determining the promotion effect is unambiguous, but the metal overlayers

discussed so far have relatively high electronegativity and varying degree of d-character at the Fermi level E_F. We speculated that metals with low electronegativity, relatively high p character at E_F and intermixed interface morphology might give rise to unprecedented oxidation enhancement effects, since they would play the double role of "catalyst" and electronic "promoter" of the oxidation reaction. Promotion and poisoning effects of catalytic reactions, such as is observed, for example, during co-adsorption of CO with K or S on Ni, seems far removed from semiconductor chemistry, but the thought was rather stimulating, so we extended our study to low electronegativity metal overlayers, namely Cs, Na, and Sm.

Although some of our results are still preliminary, we found evidence of dramatic oxidation promotion effects induced by Cs and especially by Sm overlayers. Surprisingly the magnitude of the effect is smaller for Na overlayers. The unprecedented magnitude of the promotion effect for Sm overlayers is consistent with our model, since Sm is a low electronegativity metal that exhibits an intermixed interface morpology both with GaAs and Si substrates. The chemisorption of Sm atoms on Si and GaAs surfaces follows a peculiar two-step process, with Sm atoms in a divalent state at submonolayer coverage, and in a mixed valent state at higher concentration. A most striking results is that the onset of the promotion effect appears related to the formation of trivalent Sm species. This result may give us invaluable insight on the connection between local bonding and interface catalytic effects. Therefore we are attempting to clarify the complex Sm chemisorption process through comparison with adsorption studies on ideally inert substrates (solid xenon crystals). A couple of papers in press will focus on electronic structure and reactivity of elemental Sm in cluster and thin film form. Structural studies of overlayers with substantial catalytic activity are

also in progress, following the successful testing of our new electron energy loss fine structure spectrometer.

Future Developments

We plan to concentrate on the synthesis and charcterization of novel insulating materials on Si and GaAs The low-pressure room temperature reaction parameters employed so far have been sufficient to study the catalytic activity of a number of metal overlayers and to synthesize thin (10-30Å) insulating layers. We plan to further extend the systematics, but we emphasize the importance of ultimately obtain device-grade materials and test MOS structures. To do that we have to synthesize thick insulating layers (1-5μm), characterize these layers for composition and structure, examine the inversion and accumulation characteristics for practical MOS applications. Since the catalyst atoms are not removed from the reaction products (the insulating layer) after the reaction is completed, they may in principle yield interface states in or below the insulating layer and give rise to junction parameters unsuitable for device applications. New thermal procedures would then have to be used in order to disperse the ultrathin catalyst layer in the semiconductor matrix without perturbing the insulating layer. The growth of MOS test structures for electrical characterization is the most effective way of examining these problems.

Low-pressure/low temperature systematics:

We will continue our investigation on Si and GaAs cleavage surfaces, and extend it to thermally cleaned (100) surfaces and "technological" chemically etched surfaces. New chemisorption studies will deal with transition metal overlayers such as Mo and Nb, and low electronegativity overlayers such as Be,

Ca, Yb. The puzzling contrast between the catalytic activity of Cs and Na overlayers will be examined through structural and electronic analysis of the local overlayer morphology, via electron energy loss fine structure and photoemission investigation. Subject to time availability, we plan to examine near noble metal overlayers and compare their specific catalytic activity with noble metal case examined previously. Tne goal is to construct a detailed microscopic model of the interface catalytic effect that will guide our future studies.

Thin film processing:

We will study the suitability of interface catalytic effects for producing good quality insulating layers in the 1-5μm thickness range. We will focus on some of tne metal overlayers most effective in promoting low-pressure and low-temperature reactions (Sm, Cs, Cr) and perform chemisorption studies of oxyge.. and water at pressures up to 1-10 torr and temperatures up to 500-700°C. for this purpose we will construct a high pressure reaction cell where the sample can be heated through back-surface irradiation. The cell will be connected through a differentially pumped transfer stage to the existing electron spectrometer. X-ray photoemission and XPS-AES depth profiling will give information on layer composition. Ex-situ electron microscopy and Rutheford backscattering studies will provide information on the structures and composition of the thicker layers. Special emphasis will be given to examining the final distribution of catalyst atoms in the reaction products, and the influence of thermal processing on this distribution.

A positive conclusion of the thin film processing stage should enable us to start the preparation of MOS test structures for electrical characterization. Having identified the most promising catalytic process, we will proceed to form

insulating layers and suitable contact patterns on wafer samples. Our existing spectrometers are still suitable for our purpose, provided that suitable metallization patterns can be obtained beforehand on the wafers and maintained stable during the following processing steps. Automated electrical testing equipment is available to us through external collaborations within the Minnesota Microelectronic community (Honeywell, Department of Electrical Engineering).

Cumulative List of Publications

84-K0545-1 A. Franciosi, S. Chang, P. Philip, C. C. Caprile and J. Joyce, "Microscopic Control of Semiconductor Surface Oxidation", J. Vac. Sci. Technol. A3, 933 (1985)

84-K-0545-2 P. Philip. A. Franciosi, and D. J. Peterman, "Interface Chemistry of $Hg_{1-x}Cd_xTe$", J. Vac. Sci. Technol A3, 1007 (1985).

84-K-0545-3 A. Franciosi, D. W. Niles, G. Margaritondo, C. Quaresima, M. Capozi and P. Perfetti, "Au-Si Interface Formation: The Other Side of the Problem", Phys. Rev. B32, 6917 (1985).

84-K-0545-4 A. Franciosi, P. Philip and D. J. Peterman, "Interface Chemistry of Ternary Semiconductors: Local Morphology of the $Hg_{1-x}Cd_xTe$(110)-Cr Interface", Phys. Rev. B32, 8100 (1985).

84-K-0545-5 S. Chang, A. Rizzi, C. Caprile, P. Philip, A. Wall, and A. Franciosi, "Overlayer-induced Enhanced Oxidation of GaAs Surfaces", J. Vac. Sci. Technol. A (in press).

84-K-0545-6 C. Caprile, A. Franciosi, D. Wielickza, and C. G. Olson, "Experimental Determination of the Electronic Structure of Small Metal Particles", J. Vac. Sci. Technol. A (in press).

Graduate Students/Postdoc/Visitors

Personnel involved in the project. In parenthesis we give the supporting institution.

Dr. C. Caprile	Postdoctoral Associate	(MEIS*)
S. Chang	Graduate Student	(MEIS*)
A. Wall	Graduate Student	(MEIS*)
P. Philip	Graduate Student	(MEIS*)
Dr. A. Rizzi	Visiting Investigator from University of Modena, Italy	(MEIS*)
Prof. P. Soukiassian	Visiting Investigator from University of Reims, France	
Prof. S. Nannarone	Visiting Investigator from University of Rome, Italy	(Italian National Research Council)
Prof. E. Colavita	Visiting Investigator from University of Calabria, Italy	(Italian National Research Council)

* Microelectronic and Information Science Center of Minnesota, and industrial consortium that includes Sperry, 3M, Honeywell, Control Data Corporations and the State of Minnesota.

External Collaborations

A number of researchers from industrial and academic institutions have had access to equipment purchased with ONR funding, within the following ongoing collaborative projects:

- McDonnell Douglas Corporation (Dr. D. J. Peterman, McDonnell Douglas Research Laboratories, Department 224, St. Louis, MO). Enhanced Control of Interface Reactivity for Mercury-Cadmium-Telluride.

- Purdue University, Department of Physics (Professors R. Reifenberger and J. K. Furdyna). Enhanced Control of Interface Reactivity for Ternary Semiconductors.

- University of Rome, Italy, Department of Physics (Professors S. Nannarone and M. DeCrescenzi). Structural Aspects of Interface Reactions for Si and GaAs.

9

OFFICE OF NAVAL RESEARCH

PUBLICATIONS/PATENTS/PRESENTATIONS/HONORS REPORT

for

1 August 1984 through 31 July 1985

CONTRACT # N00014-84-K-0545

TASK NR 371-162

MICROSCOPIC CONTROL OF SEMICONDUCTOR INTERFACE REACTIVITY

A. Franciosi

Department of Chemical Engineering
and Materials Science
University of Minnesota
Minneapolis, Minnesota 55455

Publications/Patents/Presentations/Honors Report

1 August 1984 through 31 July 1985

A. Papers Submitted

1. A. Franciosi, S. Chang, P. Philip, C. Caprile and J. Joyce, "Microscopic Control of Semiconductor Surface Oxidation", J. Vac. Sci. Technol. A3, 933 (1985), supported in part by MEIS* and by the Graduate School of the University of Minnesota.

2. P. Philip. A. Franciosi, and D. J. Peterman, "Interface Chemistry of $Hg_{1-x}Cd_xTe$", J. Vac. Sci. Technol A3, 1007 (1985), supported in part by MEIS*, by the McDonnell Douglas Independent Research and Development program, and by the Graduate School of the University of Minnesota.

3. A. Franciosi, D. W. Niles, G. Margaritondo, C. Quaresima, M. Capozi and P. Perfetti, "Au-Si Interface Formation: The Other Side of the Problem", Phys. Rev. B32, 6917 (1985), supported in part by MEIS*.

4. A. Franciosi, P. Philip and D. J. Peterman, "Interface Chemistry of Ternary Semiconductors: Local Morphology of the $Hg_{1-x}Cd_xTe(110)$-Cr Interface", Phys. Rev. B32, 8100 (1985), support in part by MEIS*, by McDonnell Douglas Independent Research and Development program, and by the Graduate School of the University of Minnesota.

5. S. Chang, A. Rizzi, C. Caprile, P. Philip, A. Wall, and A. Franciosi, "Overlayer-induced Enhanced Oxidation of GaAs Surfaces", J. Vac. Sci. Technol. A (in press), supported in part by MEIS*

6. C. Caprile, A. Franciosi, D. Wielickza, and C. G. Olson, "Experimental Determination of the Electronic Structure of Small Metal Particles", J. Vac. Sci. Technol. A (in press), supported in part by MEIS*.

* Microelectronic Center of Minnesota, an industrial consotium including 3M, Honeywell, Sperry and Control Data Corporations.

B., C., D., E., F., G.

None

H. Presentation

1. A. Franciosi and P. Philip, "Microscopic Control of Silicon Interface Reactivity", 31st Meeting American Vacuum Society, Reno, Nevada, December 4-7, 1984.

2. A. Franciosi, P. Philip and D. J. Peteman, "Interface Chemistry of MCT", 1984 Annual Meeting Materials Research Society, Boston, Massachusetts, November 26-30, 1984.

3. A. Franciosi, S. Chang, P. Philip, and C. Caprile, "Microscopic Control of Semiconductor Oxidation", 1985 March Meeting of the American Physical Society, Baltimore (Maryland), March 25-29, 1985.

4. A. Rizzi, C. Caprile, P. Philip, A. Wall, and A. Franciosi, "Catalytic Role of Transition of Metals on Si and GaAs Surfaces", 32nd Symposium of the American Vacuum Society, Houston (Texas), November 19-22, 1985.

5. C. Caprile, A. Franciosi, D. Wieliczka, and C. Olson, "Experimental Determination of the Electronic Structure of Small Metal Particles", 32nd Symposium of the American Vacuum Society, Houston (Texas), November 19-22, 1985.

6. A. Franciosi, "Surface and Interface Properties of Ternary Semiconductors for Infrared Applications" (invited), 1985 Annual Meeting of the Italian National Research Council, Surface Division, Modena (Italy), December 16-18 (1985).

7. E. Colavita, M. De Crescenzi, S. Nannarone, S. Chang, P. Philip, A. Wall, and A. Franciosi, "Surface Extended Electron Energy Loss Fine Structure *Above the 2p Core Level of Cr*", 1985 Annual Meeting of the Italian National Research Council, Surface Division, Modena (Italy), December 16-18, 1985.

I. Honors/Awards/Prizes

The following matching grants were awarded for the above research:

1. $187,000, Microelectronic and Information Science Center (a consortium including Honeywell, Sperry, Control Data Corporation, 3M and the State of Minnesota).

2. $25,000, Graduate School, University of Minnesota.

Equipment

The following capital equipment items were aquired in the first year of the program.

1.	Turbomolecular pump LH TMP 150/D4A	$ 6,125
2.	Ionization gauges Granville Phillips and controller 271-003	1,713
3.	Lock in amplifier EGbG PAR 128 A	3,831
4.	Thermoionics COV-2000 pump system	13,640
5.	Electron energy analyzer LH EA10/100	36,292
6.	UHV chamber LH REZ 10/11	5,554
7.	Electron gun LH EQ 22/35	9,039
8.	X-ray source LH RQ 20-35	27,665
9.	Picoammeter Keithley 485	813
10.	Microvoltmeter Keithley 197	848
11.	Oscilloscope Tektronix 2235	1,551
12.	Ion gun LH IQE 10/35	5,333
	TOTAL	$112,404

These aquisitions were possible because of the extensive matching funding for personel expenses that became available during the first year of the program.

Matching Funding

The following matching grants were awarded for our research program.

$187,000	From the Microelectronic and Information Science Center of Minnesota, a consortium including 3M, Honeywell, Sperry, Control Data Corporations and the State of Minnesota - Grants # 0910-4791 and 0912-4991.
$ 25,000	From the Graduate School of the University of Minnesota, Grants # 0100-4908-32 and 0100-4969-02.

Microscopic control of semiconductor surface oxidation

A. Franciosi, Shu Chang, P. Philip, and C. Caprile
Department of Chemical Engineering and Materials Science, University of Minnesota, Minneapolis, Minnesota 55455

J. Joyce
Materials Science Program, University of Wisconsin, Madison, Wisconsin 53713

(Received 29 November 1984; accepted 17 February 1985)

We examined the effect of ultrathin (0.1–10 Å) chromium overlayers on the reactivity with oxygen of Si(111) and GaAs(110) cleavage surfaces. Synchrotron radiation photoemission shows that for Cr coverages below a critical threshold coverage the overlayer does not affect substantially the oxygen adsorption rate. For chromium coverage *above* threshold the overlayer sharply enhances the oxygen adsorption kinetics so that most semiconductor atoms in the surface and near surface region appear oxidized at activated oxygen exposures as low as 100 L. The critical threshold coverage corresponds to the onset of reactive interdiffusion at the Si(111)–Cr and GaAs(110)–Cr interfaces. Therefore we suggest that ultrathin Si–Cr and As–Cr reacted phases created at the surface act as activation layers for semiconductor oxidation.

Thin metal overlayers deposited on atomically clean semiconductor surfaces can change dramatically the reactivity of the surface for reactions with gas species[1–4] and metals.[5,6] We have recently shown, for example, that thin Cr overlayers on Si(111) surfaces can act both as passivating layers and as catalysts for Si(111)–Au interface reaction, so that one can control and modulate interdiffusion by varying the thickness of the Cr interlayer.[6] Similar effects have been observed by Brillson and co-workers for Al atoms at the GaAs(110)–Au interface.[5] As far as reactions with gaseous species are concerned, a few pioneering studies have addressed the effect of Ag and Au overlayers[1,3] on the oxidation of silicon surfaces, while the presence of an Al overlayer has been shown to induce the formation of a potentially stable new oxide phase on Ge(111) surfaces.[2] An understanding of these phenomena requires a search for systematic correlations of the observed "catalytic" trends with the different local morphology of the metal/semiconductor surface layers. The goal is to establish a connection between the microscopic bonding situation of semiconductor and metal atoms at the surface and the observed specific catalytic activity.

We report here on the interaction of Si(111) and GaAs(110) surfaces with activated oxygen O_2^* in the presence of ultrathin (0.1–10 Å) Cr overlayers deposited *in situ*. We selected the Si–Cr and GaAs–Cr systems because these are within the interfaces best characterized at room temperature.[7,8] Furthermore, chromium compounds show considerable catalytic activity for a number of chemical reactions.[9] Interaction with oxygen was selected as prototype reaction with oxidizing gas phases, and because of extensive literature existing on this subject.[10–13] Our results indicate a qualitatively similar effect of the Cr overlayer on the kinetics of Si and GaAs oxidation. While only limited oxygen adsorption is possible on the clean semiconductor surfaces at the highest activated oxygen exposures explored (10^4 L) we see an enhancement of several orders of magnitude in the semiconductor oxidation rate for Cr coverages above a critical threshold coverage (1.3 Å for Si). We relate this enhancement to the thin intermixed Si–Cr and As–Cr species that start to form at the surface at the critical threshold coverage. These intermixed species act as catalysts and dramatically increase the semiconductor oxidation kinetics. Most of the silicon, gallium, and arsenic atoms in the surface and near surface layers appear oxidized at oxygen exposures as low as 100 L. The major reaction product identified at the Si surface is a Si–oxide with average Si–oxygen coordination between 3 and 4. For GaAs, an As oxide similar to As_2O_3 is observed, together with a Ga–oxide phase that involves an effective Ga–oxygen coordination greater than for Ga_2O_3.

The experiments were performed on a clean Si(111)2×1 and GaAs(110)1×1 surfaces obtained through cleavage of *n*-type single crystals inside a photoelectron spectrometer, at operating pressure $<5\times10^{-11}$ Torr. Cr was deposited from a W coil at pressure $<3\times10^{-10}$ Torr, with overlayer thickness measured by a quartz thickness monitor. Since the clean semiconductor surfaces are relatively inert upon oxygen exposure, we elected to use activated oxygen in the pressure range 10^{-5} Torr to enhance reaction kinetics.[14,15] A tungsten ionization filament was therefore positioned in line of sight of the substrate during oxygen exposure. The photoemission measurements were performed by positioning the sample at the focus of a synchrotron radiation beam and of a commercial double pass cylindrical mirror analyzer. The radiation from the 240 MeV electron storage ring Tantalus at the Synchrotron Radiation Center of the University of Wisconsin–Madison was monochromatized by means of a 3 m toroidal grating monochromator in the 21–130 eV photon energy range. The overall experimental energy resolution (electrons and photons) was typically 0.3–0.4 eV for the valence band and Ga 3*d* core levels, and of about 0.6–0.8 eV for the As 3*d* and Si 2*p* core data.

Photoelectron energy distribution curves for the Ga 3*d* and As 3*d* core levels are shown in Figs. 1 and 2, respectively, as a function of O_2^* exposure ($10–10^4$ L) of the clean

 0734-2101/85/030933-05$01.00

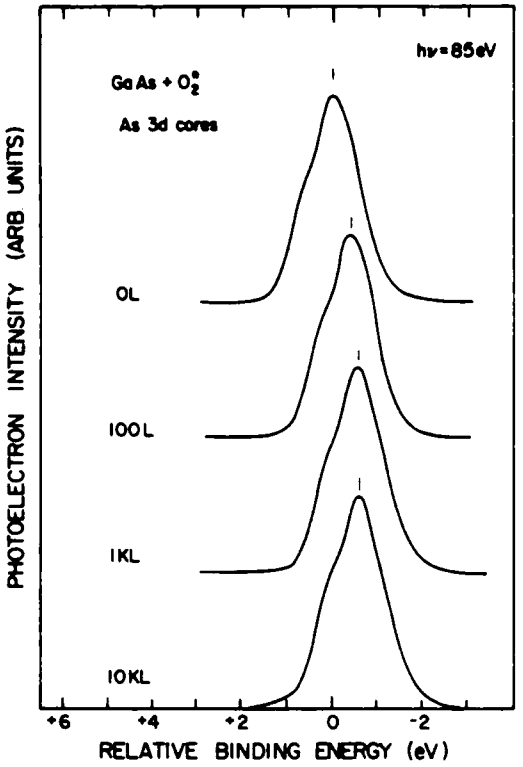

FIG. 1. Photoelectron energy distribution curves (EDC's) for the As 3*d* core emission from cleaved GaAs(110). Spectra displaced downward show the effect of exposure to increasing amount (100, 10^3, 10^4 L) of activated oxygen. The rigid shift of the core line reflects the variation in band bending from the initial flat-band situation.

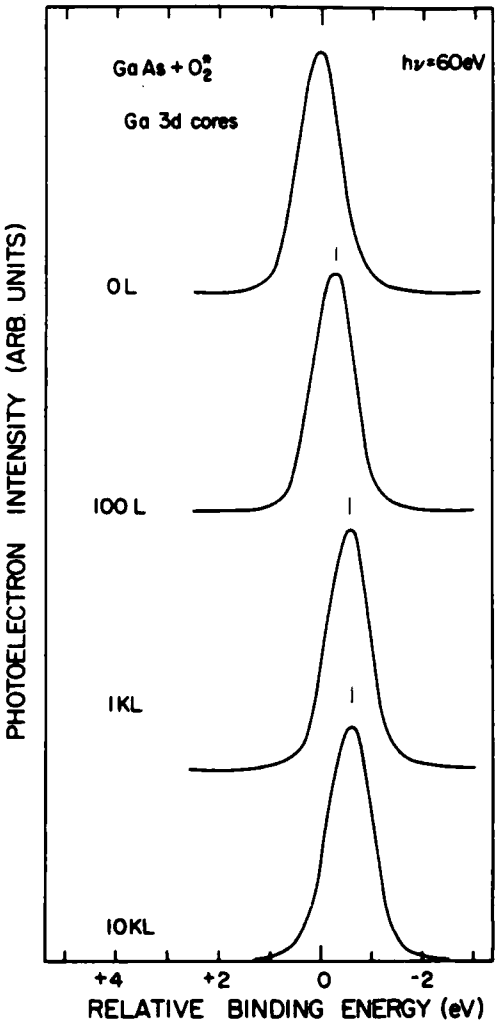

FIG. 2. EDC's for the Ga 3*d* core emission from cleaved GaAs(110). Spectra displaced downward show the effect of exposure to increasing amounts of activated oxygen. The rigid shift of the core line reflects the variation in band bending.

GaAs(110) surface. The zero of the binding energy scale corresponds to initial flat-band core binding energy. Exposures up to 10^4 L yield a rigid shift of the core levels that reflects the change in band bending, and attenuation of the As 3*d* surface contribution, visible as structure on the low binding energy side of the main As 3*d* line. These changes reflect the relatively low oxygen adsorption rate observed on cleaved GaAs(110) surfaces.[12,13] Even at the highest exposures explored here, the oxygen coverage is only a fraction of a monolayer.[12] The quasisaturation value of band bending for 10^3 L exposure (0.65 eV) corresponds to the value observed by Lindgren *et al.*[12] at 10^4–10^5 L exposure to ground state molecular oxygen, so that the use of activated oxygen in our case yields a 10 to 100-fold enhancement in adsorption.

Results for the Si(111) surface are summarized in Fig. 3. In the top section we show the Si 2*p* core emission for a clean Si(111)2×1 surface (dashed line) and for the same surface after exposure to 100 L of activated oxygen (solid line). Weak oxygen-induced features appear on the high binding energy side of the main line. Vertical bars 0.9, 1.8, 2.6, and 3.5 eV below the main line mark the position of the chemically shifted Si 2*p* contributions associated by Hollinger and Himpsel[10] with silicon atoms bonded to 1,2,3, and 4 oxygen atoms, respectively. Further exposure to oxygen (10^3 L) yields a three to fourfold increase of the oxygen-induced features, that saturate in intensity and show little change[4] upon further oxygen exposure (10^4 L), in agreement with the 1–1.5 monolayer oxygen saturation coverage observed in Ref. 10.

The spectra for the oxidation of the clean surface all show[4] the presence of one, two, and threefold silicon–oxygen coordination, as expected in the submonolayer and monolayer oxygen coverage range.[10] The effect of Cr overlayer on the oxygen adsorption kinetics is shown in the middle and bottom sections of Fig. 3. We distinguish two qualitatively different regions as a function of Cr coverage θ. For θ below a critical threshold coverage of 1.3 ± 0.3 Å the Cr overlayer affects relatively little the silicon oxidation rate. For example, in the midsection of Fig. 3 we show EDC's for the Si 2*p* emission at $\theta = 0.6$ before (dashed line) and after exposure to 100 L of activated oxygen (solid line). Deposition of 0.6 Å of Cr onto the clean Si(111) cleavage surface[7] attenuates slightly the Si 2*p* emission with no visible line shape changes. Exposure to 100 L of activated oxygen gives rise to the same oxygen-induced feature observed for oxygen adsorption on the clean Si(111) surface.

The situation changes dramatically if Cr coverages above threshold are employed. This is shown in the bottom section of Fig. 3 for $\theta = 2$ Å. Exposure of the Cr-activated semiconductor surface to 100 L of activated oxygen (solid line) yields a main oxide-induced feature centered 3.0 eV below the main

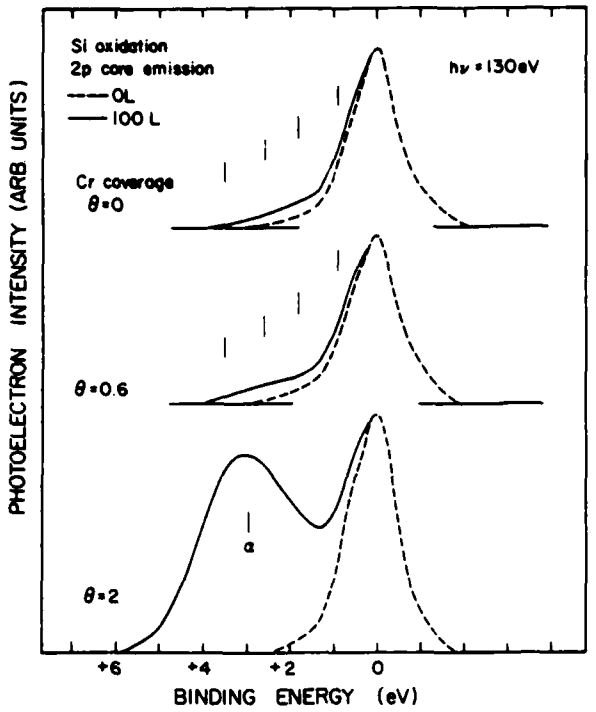

FIG. 3. Si 2*p* core emission from cleaved Si(111)2×1 surfaces. Top: Clean surface emission before (dashed line) and after exposure (solid line) to 100 L of activated oxygen. The vertical bars mark the position of Si 2*p* oxide features associated by Hollinger and Himpsel (Ref. 10) with silicon atoms coordinated with one, two, three, and four oxygen atoms. Midsection: A 0.6 Å Cr overlayer was deposited on a freshly cleaved Si(111) surface. The resulting Si 2*p* core emission is shown before (dashed line) and after (solid line) oxygen exposure. The vertical bars mark Hollinger and Himpsel's Si 2*p* oxide features. Bottom: Effect of a 2 Å Cr overlayer on the Si(111) surface oxidation. The Si 2*p* core line shape before oxidation (dashed line) is similar to the initial Si 2*p* line. After exposure to 100 L of activated oxygen (solid line) a major oxide band emerges. The vertical bar marks the position of a major Si 2*p* oxide features identified by Riedel *et al.* (Ref. 16) during oxidation of amorphous silicon.

line. Further oxygen exposure[4] increases this feature relative to the Si 2*p* substrate line, indicating that no saturation of oxygen adsorption is observed in this exposure range (10–10^4 L). The width of the Si 2*p* oxide line suggests that several different oxidation states may coexist, and its binding energy, intermediate between those observed for Si atoms locally bonded to 3 and 4 oxygen atoms,[10] shows that threefold and fourfold coordination are likely to be dominant in the silicon oxidized layer.

The results of Fig. 3 indicate that Cr coverages above the critical threshold coverage change dramatically the reactivity of the semiconductor surface and enhances several orders of magnitude the silicon oxidation rate at room temperature. The observation of enhanced oxygen adsorption kinetics for Ag[3] overlayers on silicon has been related to the disruption of the ordered Si(111) surface upon Ag deposition. The effect of "amorphization" of the Si(111) surface on the Si oxidation rate can be estimated by the results of Riedel *et al.*[16] who recently studied amorphous Si and Ge layers upon exposure to activated oxygen. The vertical bar in the bottom section of Fig. 3 indicates the position of the dominant Si 2*p* oxide feature observed by Riedel *et al.*[16] The similarity with our results suggests that in both cases silicon atoms locally coordinated to 3 and 4 oxygen atoms are likely to coexist and give rise to the broad Si 2*p* oxide band observed experimentally. Comparison of the intensity of the Si 2*p* oxide feature relative to the main line, however, indicates that the oxygen adsorption rate on the Cr-activated Si surface is 20 to 30 times higher than on amorphous silicon layers.[4,16] We conclude that while the nature of the surface reaction products appears the same in both cases, the origin of enhanced oxidation has to be found in the Cr-induced modification of surface chemistry rather than in the amorphization of the semiconductor surface layer. In earlier studies of the Si(111)–Cr interface[7] we proposed that for Cr coverages below 1.5 monolayer the Cr atoms participate in weak chemisorption bonds that affect only slightly the stability of the Si–Si bonds in the surface and near surface region. At coverage above 1.5 monolayers a reactive interdiffusion interface formation stage is established, with formation of disordered Si–Cr intermixed species. The onset of reactive interdiffusion coincides within experimental uncertainty with the critical threshold coverage for oxidation determined in this work. The correspondence suggests that the silicidelike surface species formed above threshold act as catalyst for the oxidation of the semiconductor atoms in the surface and near-surface region.

In recent work Cros[17] suggested that the enhanced oxidation of the room temperature grown Si–noble metal interfaces may be explained by the low stability of the intermixed surface phases and on the metalliclike density of states at E_F which may ease the breaking of the oxygen molecule and/or the creation of atomic oxygen excited states. These mechanisms may indeed be active also in the Si–Cr case at chromium coverages above the critical threshold and contribute to the enhanced oxidation effect. However, one word of caution is necessary, since for refractory metals on silicon the stability of the intermixed phase is expected to be higher, as indicated by the trend of the corresponding silicide formation enthalpies, and, as observed by Cros,[17] since the presence of *two* species (Si and refractory metal) with very strong tendencies to oxidize, changes the nature of the problem with respect to the Si–noble metal case.

The morphology and room-temperature revolution of the Si(111)–Cr and GaAs(110)–Cr interfaces present many similarities. Both interfaces react at room temperature only for coverages above 1.5 Å(Si[7]) and 2 Å (GaAs[8]). Reactive interdiffusion occurs in a limited coverage range of $1.5 < \theta < 9$ (Si[7]) and $2 < \theta < 20$ (GaAs[8]) and yields silicidelike species on Si and arsenidelike phases on GaAs. Further Cr deposition gives rise to an unreacted metal film on top of the reacted interface.[7,8] The chemical bonding for the main interface reaction products (silicide or arsenidelike) involves in both cases dominant coupling of the metal-*d* states with anion-*p* states, with similar modifications of the electronic density of states. These similarities between the two interfaces suggest that an oxidation promotion effect may be found also for GaAs–Cr above a critical threshold coverage value of $\theta \simeq 2$ Å. In Figs. 4 and 5 we summarize the effect of exposure to activated oxygen on the As 3*d* and Ga 3*d* core level emission. In the top section of Figs. 4 and 5 we show the clean surface

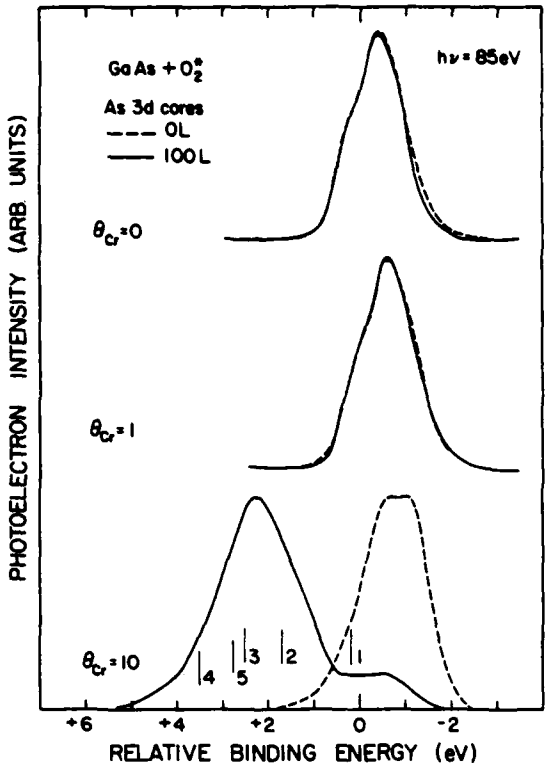

FIG. 4. Effect of thin Cr overlayers on the oxidation of As at the GaAs(110) surface. Top: Clean surface As 3*d* emission before (dashed line) and after (solid line) oxygen exposure. Midsection: A 1 Å Cr overlayer was deposited on a freshly cleaved GaAs(110) surface. The resulting As 3*d* emission is shown before (dashed line) and after (solid line) oxygen exposure. Bottom: Effect of a 10 Å Cr overlayer on the GaAs(110) surface oxidation. The As 3*d* core line shape before oxidation (dashed line) is composed of a low binding energy reacted As 3*d* feature from Cr–As interface species, and of a high binding energy segregated As/substrate contribution (Ref. 8). Upon oxidation (solid line) most of the As atoms appear oxidized. The vertical bars 1–4 mark the position of the oxidized As 3*d* features observed by Landgren *et al.* (Ref. 12) for As coordinated with one to four oxygen atoms. The vertical bar 5 marks the position of the As 3*d* core level in As_2O_3, from Su *et al.* (Ref. 18).

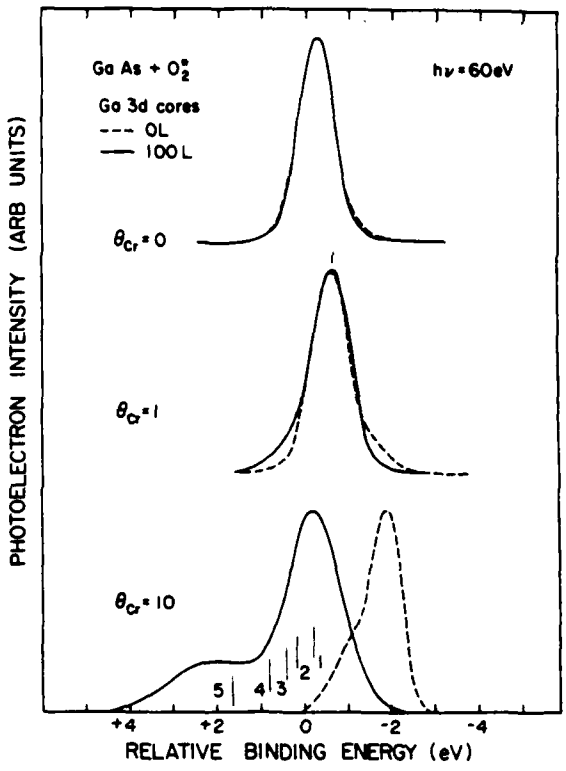

FIG. 5. Effect of thin Cr overlayers on the oxidation of Ga at the GaAs(110) surface. Top: Clean surface Ga 3*d* emission before (dashed line) and after (solid line) oxygen exposure. Midsection: A 1 Å Cr overlayer was deposited on a freshly cleaved GaAs(110) surface. The resulting Ga 3*d* exposure is shown before (dashed line) and after (solid line) oxygen exposure. Bottom: Effect of a 10 Å Cr overlayer. The Ga 3*d* core line before oxidation (dashed line) includes a main contribution from dissociated Ga atoms or from Ga atoms in a Cr matrix (Ref. 8). Upon oxidation (solid line) most of the Ga atoms appear oxidized. The vertical bars 1–4 mark the position of oxidized Ga 3*d* features observed by Landgren *et al.* (Ref. 12). The vertical bar 5 marks the position of the Ga 3*d* core level i. Ga_2O_3, from Su *et al.* (Ref. 20).

core emission before (dashed line) and after (solid line) oxygen exposure. In the midsection we show the corresponding results for a Cr overlayer with $\theta = 1$, i.e., below the critical threshold coverage. In the bottom-most sections of Figs. 4 and 5 we present results for $\theta = 10$. Again, the dashed line and solid line indicate, respectively, results before and after oxygen exposure. The zero of the binding energy scale corresponds to the flat-band initial core binding energy, and the spectra have been arbitrarily normalized to emphasize line shape changes. As indicated in Figs. 1 and 2, and in the topmost section of Figs. 4 and 5, the clean GaAs surface is relatively inert and only low oxygen coverage can be obtained at room temperature. For $\theta = 1$ the Cr overlayer yields only relatively small modifications in the oxygen uptake rate. The spectra at $\theta = 10$, instead, show dramatic modification of the As 3*d* and Ga 3*d* line shape upon oxidation. At $\theta = 10$ the As 3*d* and Ga 3*d* lines before oxidation (dashed line) both include two distinct components.[8] For As (tic marks) a low binding energy As reacted 3*d* line appear above the initial clean surface emission, and a second line shifted to higher binding energy represents segregated arsenic and residual substrate emission.[8] For Ga (dashed line, bottom-most section) the main contribution corresponds to free gallium atoms that are a by-product of the As–Cr interface reaction and/or gallium atoms dispersed in a Cr matrix.[8] Upon exposure to 100 L of activated oxygen most of the As and Ga atoms within the experimental sampling depth are oxidized. We find an increase of several orders of magnitude in the overall surface oxygen uptake, and no evidence of saturation in the exposure range explored (10–10^4 L). The character of the oxidation reaction products can be examined by comparing the observed oxide-induced As 3*d* features with those reported by Landgren *et al.*[12] 0.8, 2.3, 3.2, and 4.2 eV below the initial substrate As 3*d* line (vertical bars[1–4] in Fig. 4) and related to the presence of As coordinated, respectively, with one, two, three, and four oxygen atoms, and with a 3.4–3.5 eV feature reported in Refs. 18 and 19 for As in As_2O_3 (vertical bar 5 in Fig. 4). The broad experimental oxide band suggests that several arsenic–oxygen bonding configurations must coexist in the surface and near surface region, with a dominant contribution coming from high oxidation states that are barely detectable on the oxidized GaAs surface[12] at coverages of 10^{14} L.

For the Ga 3*d* lines during oxidation of GaAs Landgren *et al.*[12] observed chemically shifted components 0.45 and 1.0 eV below the main line at low exposure (10^6 L molecular

oxygen), components at 0.8 and 1.4 eV at high exposure (10^{14} L). These are indicated by vertical bars 1–4 in Fig. 5. While Landgren *et al.*[12] suggest that the 1.4 eV component may correspond to Ga in Ga_2O_3, Su *et al.* report[20] a Ga 3*d* broad oxide feature centered some 2.2 eV below the main Ga $3d_{5/2}$ line for Ga_2O_3. This is marked by vertical bar 5 in Fig. 5. The results in the bottom-most section of Fig. 5 indicate that several nonequivalent oxidation states for Ga coexist within the sampling depth. Furthermore we note that a major spectral contribution derives from Ga 3*d* features shifted 3 eV below the pinned Ga 3*d* position (midsection of Figs. 2 and 5), i.e., from higher oxidation states than previously observed for Ga in Ga_2O_3. The nature of these new oxide species is not clear at present. It may involve mixed Cr–Ga oxide phases, but valence band results are consistent[21] with a main Cr_2O_3 oxidation state for Cr, with no evidence of mixed oxides. In analogy with the present case, we mention that Al overlayers on Ge[2] appear to stabilize a higher oxidation state for Ga atoms upon oxygen exposure at room temperature. Also in this case the morphology of the new potentially stable oxide phase remains unclear.

In summary, we have shown that thin Cr overlayers on Si and GaAs surfaces can dramatically enhance the semiconductor oxidation rate if Cr coverages above a critical threshold coverage are employed. This critical coverage corresponds to the onset of reactive interdiffusion of Cr and semiconductor atoms at the interface. The enhancement of several orders of magnitude in the oxygen adsorption kinetics is presumably related to the catalytic activity of ultrathin silicide and arsenidelike overlayers formed for Cr coverages above threshold.[1,4] The end products of oxidation involve semiconductor atoms in several different coexisting oxidation states, with high oxidation states largely dominant. For silicon, for example, dominant three and fourfold oxygen coordination was observed, with compelling analogies to α-Si oxidation processes.

ACKNOWLEDGMENTS

This work was supported by the Office of Naval Research (G. Wright) under Contract No. N00014-84-K-0545 and by the Center for Microelectronic and Information Science of the University of Minnesota. We thank G. Margaritondo and J. H. Weaver for communicating their results to us prior to publication and for generously providing equipment. The Synchrotron Radiation Center of the University of Wisconsin–Madison is supported by the National Science Foundation under Grant No. DMR-8020164 and we gratefully acknowledge the cheerful support of its staff.

[1] A. Cros, J. Derrien, and F. Salvan, Surf. Sci. **110**, 471 (1981); J. Derrien and F. Ringeisen, *ibid.* **124**, L35 (1983).
[2] A. D. Katnani, P. Perfetti, T.-X. Zhao, and G. Margaritondo, Appl. Phys. Lett. **40**, 619 (1982).
[3] G. Rossi, L. Caliari, I. Abbati, L. Braicovich, I. Lindau, and W. E. Spicer, Surf. Sci. Lett. **116**, L202 (1982).
[4] A more detailed analysis of the results for silicon will be presented in a forthcoming paper: A. Franciosi, P. Philip, and C. Caprile (to be published).
[5] L. J. Brillson, G. Margaritondo and N. G. Stoffel, Phys. Rev. Lett. **44**, 667 (1980).
[6] A. Franciosi, D. G. O'Neill, and J. H. Weaver, J. Vac. Sci. Technol. B **1**, 524 (1983); A. Franciosi, J. H. Weaver and D. G. O'Neill, Phys. Rev. B **28**, 4889 (1983).
[7] Extensive results for Si(111)–Cr at room temperature have been presented in A. Franciosi, D. J. Peterman, J. H. Weaver, and V. L. Moruzzi, Phys. Rev. B **25**, 4981 (1982).
[8] Results for the GaAs(110)–Cr interface at room temperature were available to us in the form of a preprint: J. H. Weaver, M. Grioni, and J. Joyce (to be published).
[9] See, for example, C. N. Satterfield, *Heterogeneous Catalysis in Practice* (McGraw-Hill, New York, 1980).
[10] We will not try to summarize the extensive literature available on this subject. See, for example, G. Hollinger and F. J. Himpsel, Phys. Rev. B **28**, 3651 (1983); J. Vac. Sci. Technol. A **1**, 640 (1982), and references therein.
[11] C. M. Garner, I. Lindau, C. Y. Su, P. Pianetta, and W. E. Spicer, Phys. Rev. B **19**, 3944 (1979); C. Y. Su, P. R. Skeath, I. Lindau, and W. E. Spicer, J. Vac. Sci. Technol. **19**, 481 (1981), and references therein.
[12] See, for example, G. Landgren, R. Ludeke, Y. Jugnet, J. F. Morar, and F. J. Himpsel, J. Vac. Sci. Technol. B **2**, 351 (1984); T. Miller and T.-C. Chiang, Phys. Rev. B **29**, 7034 (1984), and references therein.
[13] C. Y. Su, I. Lindau, P. W. Chye, P. R. Skeath, and W. E. Spicer, Phys. Rev. B **24**, 4045 (1982), and references therein.
[14] In these conditions the "activated" species consist mostly of excited molecular oxygen and atomic oxygen. See J. A. Silberman, D. Laser, I. Lindau, W. E. Spicer, and A. Wilson, J. Vac. Sci. Technol. A **1**, 1706 (1983).
[15] P. Pianetta, I. Lindau, C. M. Garner, and W. E. Spicer, Phys. Rev. B **18**, 2792 (1978).
[16] R. A. Riedel, M. Turowski, G. Margaritondo, P. Perfetti, and C. Quaresima (unpublished).
[17] A. Cros, J. Phys. (Paris) **44**, 707 (1983), and references therein.
[18] C. Y. Su, I. Lindau, P. R. Skeath, I. Hino and W. E. Spicer, Surf. Sci. **118**, 257 (1982).
[19] R. Holm and S. Storp, Appl. Phys. **9**, 217 (1976).
[20] C. Y. Su, P. R. Skeath, I. Lindau, and W. E. Spicer, Surf. Sci. **118**, 248 (1982).
[21] S. Chang and A. Franciosi (unpublished).

Interface chemistry of $Hg_{1-x}Cd_xTe$

P. Philip and A. Franciosi
Department of Chemical Engineering and Materials Science, University of Minnesota, Minneapolis, Minnesota 55455

D. J. Peterman
McDonnell Douglas Research Laboratories, St. Louis, Missouri 63166

(Received 19 November 1984; accepted 17 February 1985)

We present preliminary studies of room temperature formation of the $Hg_{1-x}Cd_xTe(110)$–Cr interface. For Cr coverages below 2 Å, Cr atoms replace Hg atoms in a 10–13 Å thick semiconductor layer while elemental Te is released at the surface. The typical high coverage interface morphology consists of an elemental Te surface, a metallic Cr film, a Hg-depleted subsurface layer where Cr is bonded to Te, and finally the ternary semiconductor bulk. This complex interface chemistry is compared with recent results for $Hg_{1-x}Cd_xTe$ interfaces with simple and noble metals.

Mercury–cadmium–telluride is probably the most studied ternary semiconductor in recent years because of its widespread application for infrared detectors. The use of this material for device fabrication requires us to meet a number of challenges. Lattice, surface, and interface instabilities in the alloy[1] are caused by the weakening of the Hg–Te bond relative to the Cd–Te bond.[2,3] Large changes in electronic properties are possible as a result of mechanical stress and may arise, for example, during metal contact fabrication. The relationship between local stoichiometry and semiconductor surface/interface properties is still largely unexplored. Recent pioneering studies have related the Schottky barrier height for the $Hg_{1-x}Cd_xTe$–Al[4] and $Hg_{1-x}Cd_xTe$–Au[5] interfaces to the nonstoichiometric composition of the semiconductor surface layer. In this paper we present preliminary results of investigations of the local morphology of the $Hg_{1-x}Cd_xTe(110)$–Cr interface. Results concerning the establishment of the Schottky barrier have been published previously.[6] To our knowledge this is the first investigation of a HgCdTe–refractory metal interface by means of surface sensitive techniques. Our study indicates that important differences exist in interface morphology and interface parameters (Schottky barrier height, interface width) relative to HgCdTe–noble and simple metal systems and emphasizes that careful analysis of the local environment of each elemental species during interface formation is the only way to obtain a complete picture of the local interface structure.

We performed synchrotron radiation photoemission measurements of interfaces prepared *in situ* by direct Cr sublimation on cleaved $Hg_{0.78}Cd_{0.22}Te(110)$ substrates. The HgCdTe single crystals were grown at McDonnell Douglas Research Laboratories using a modified Bridgman method. The bulk crystals exhibited a band gap of 0.175 ± 0.01 eV and *p*-type conductivity with a room-temperature carrier concentration of $2\times10^{16}\,cm^{-3}$ as determined from infrared transmission and Hall effect measurements, respectively. The samples were introduced into the photoelectron spectrometer (operating pressure $< 5\times10^{11}$ Torr) through a fast insertion device and cleaved *in situ* with varying degrees of success at obtaining mirrorlike surfaces. Interfaces were prepared by Cr sublimation from a W basket at pressures of 5×10^{-10} Torr with coverage θ monitored by a quartz thickness monitor. The photoemission measurements were performed using monochromatized synchrotron radiation from a Grasshopper grazing incidence monochromator and the Tantalus electron storage ring at the Synchrotron Radiation Center of the University of Wisconsin–Madison. The photo-

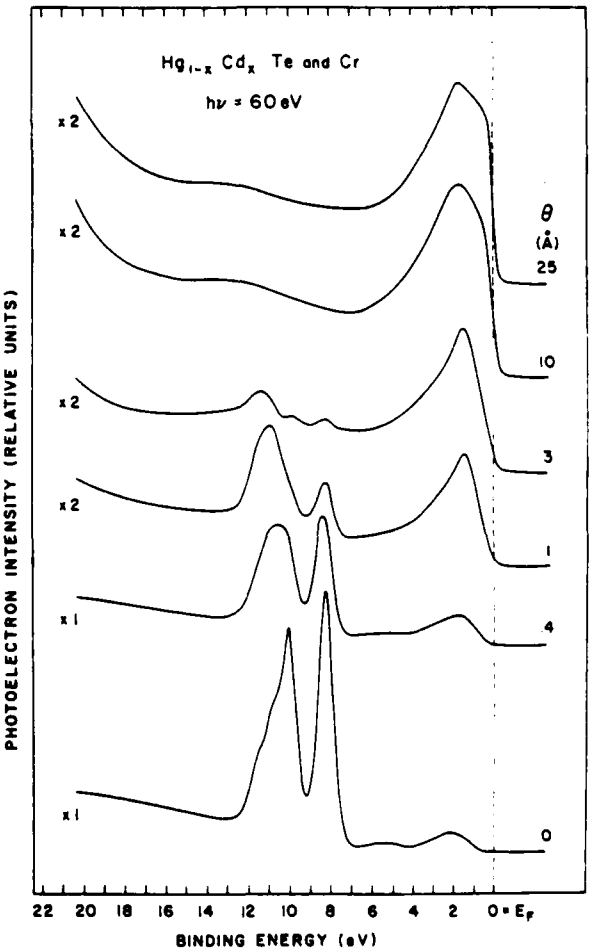

FIG. 1. EDC's for the valence bands and Hg $5d_{3/2}$, Hg $5d_{1/2}$, and Cd 4*d* core levels for the $Hg_{1-x}Cd_xTe(110)$–Cr interface. The spectra are given in relative units and the topmost EDC's are shown expanded by a scale factor of 2.

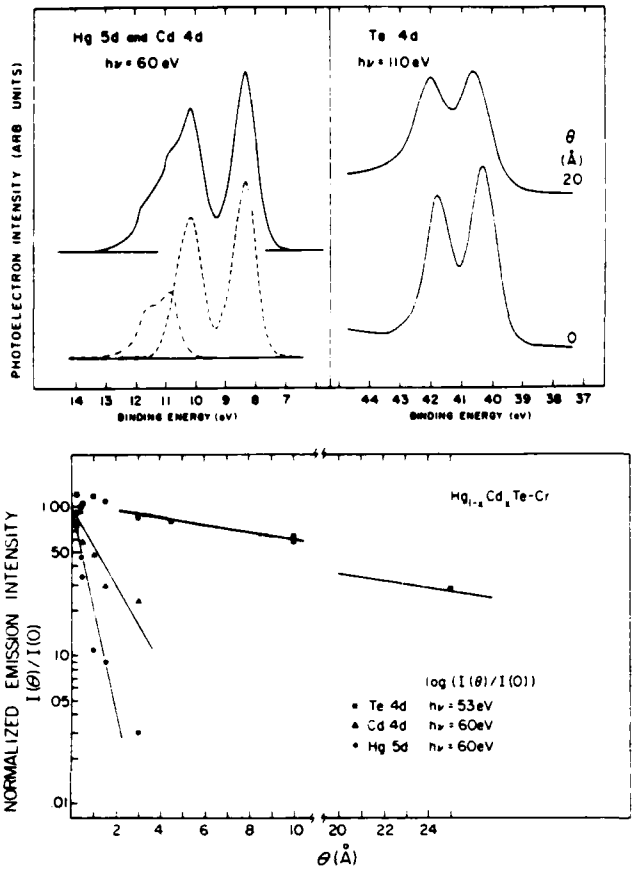

FIG. 2. Top, left: decomposition of the Hg 5*d* (dashed line) and Cd 4*d* (dot–dashed line) core emission from the clean HgCdTe surface. Top, right: Te 4*d* emission at $h\nu = 110$ eV, for the clean HgCdTe surface and for the HgCdTe–Cr interface at $\theta = 20$. Bottom: integrated intensity of the Hg 5*d*, Cd 4*d*, and Te 4*d* core emission is shown in a semilogarithmic plot after normalization to the clean surface emission and to monochromator output.

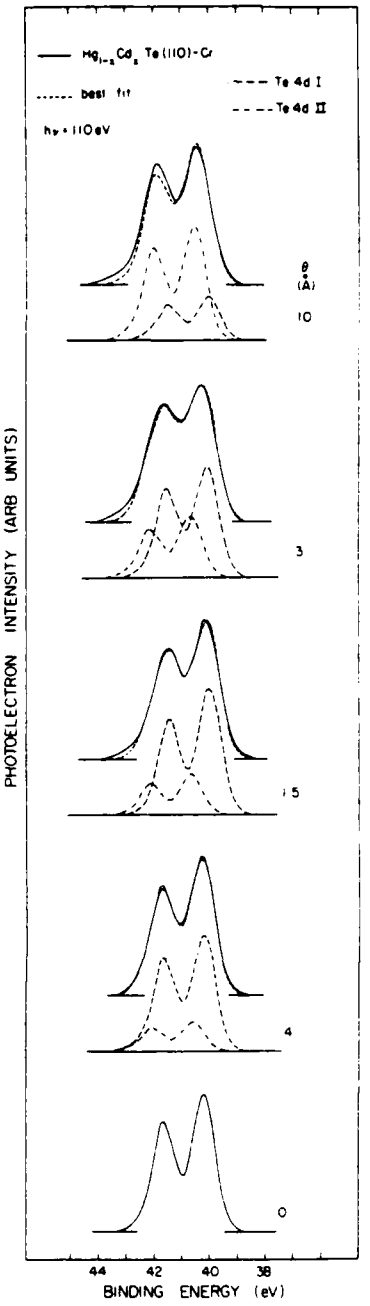

FIG. 3. Te 4*d* core emission from the $Hg_{1-x}Cd_xTe$–Cr interface. Solid line: experiment. Short-dashed line: result of a best fit in terms of a Te I subsurface component (long-dashed line) and a Te II surface component (dot–dashed line).

electrons were energy analyzed by means of a commercial double pass cylindrical mirror analyzer, with a typical overall resolution (electrons + photons) of 0.4–0.7 eV for $h\nu < 90$ eV, and 0.8–1.0 eV at higher photon energies.

In Fig. 1 we show representative photoelectron energy distribution curves (EDC's) for the valence band emission from the clean and Cr-covered semiconductor surface, at $h\nu = 60$ eV. The EDC for the clean surface is in good agreement with the results of Silberman *et al.*[8] and Spicer *et al.*[9] and exhibits a Te *p*-derived density of states (DOS) feature within 3.5 eV of the Fermi level E_F and a second structure (4–7 eV) derived from unresolved Cd-*s* and Hg-*s* DOS features. Structure in the 8–12 eV binding energy range corresponds to the Hg $5d_{5/2}$ and $5d_{3/2}$ core levels and the unresolved Cd 4*d* doublet. This is more clearly seen from Fig. 2. In the left-most top section we show a decomposition of the core emission in terms of a Hg 5*d* line shape (dashed line) and a Cd 4*d* line (dot–dashed line) for the clean HgCdTe surface. The Hg and Cd core line shapes were obtained from HgSe and CdSe samples measured in the same experimental conditions. The emission from the Te 4*d* cores was also monitored with comparable surface sensitivity at $h\nu = 110$ eV. As an example, we show in the right-most top section of Fig. 2 the Te 4*d* line from a clean HgCdTe surface and from the same surface with 20 Å Cr coverage. The integrated intensities of the Hg, Cd, and Te emission, normalized to the clean surface emission, is shown as a function of metal coverage in a semilogarithmic plot in the bottom-most section of Fig. 2.

The effect of Cr deposition can be seen in Figs. 1–2 from the fast attenuation of the Cd 4*d* and especially of the Hg 5*d* core emission. Solid lines in Fig. 2 correspond to exponential attenuation of the core emission. The resulting attenuation length of 0.7 Å for the Hg 5*d* cores is far more rapid than can be reasonably expected from an escape-depth-driven mechanism, that would correspond to an attenuation length of 4–5. This indicates that Hg atoms migrate away from the surface layer. Since the binding energy of the Hg cores remains unchanged,[7] this process is likely to produce a surface layer completely depleted in Hg rather than a layer with graded Hg content, that would give rise to several inequivalent envi-

ronments for Hg atoms within the sampling depth and possibly to broadening and shifts of the Hg 5*d* cores. Assuming a photoelectron escape depth of 4–5 Å, the residual Hg 5*d* emission observed at $\theta = 2$ is consistent with complete Hg depletion of a 13–16 Å thick surface layer.

The relatively small attenuation of the Te 4*d* emission in Fig. 2 is mainly related to the presence of dissociated Te released at the overlayer surface. The existence of two different environments for the Te atoms at the interface is clearly shown Fig. 3, where the experimental EDC's for the Te 4*d* core emission (solid line) can be successfully fitted (short-dashed line) in terms of two 4*d* components shifted ~0.5 eV from each other. Escape depth-dependent studies[7] demonstrate that the Te II component corresponds to a Te-rich surface layer. Its binding energy corresponds to the one reported for elemental Te,[10] 0.4–0.5 eV above the Te 4*d* binding energy value for the clean HgCdTe surface. The Te I component starts at the clean surface binding energy value and then shifts 0.25 eV to lower binding energy as the Cr coverage increases up to 2 Å. This may reflect the interaction of the Te I atoms with Cr, which has a lower electronegativity relative to Hg. The attenuation of the Te 4*d* emission as a function of metal coverage is shown in Fig. 4. The top section shows a semilogarithmic plot of the Te II integrated intensity, normalized to the clean surface Te 4*d* emission. The bottom-most section shows the analogous plot for the Te I component. Figure 4 indicates that Te II is released at the surface for $0 < \theta < 2$ Å while Hg leaves the subsurface layer and Cr interacts directly with Te atoms (type I) in the semiconductor. The lower section of Fig. 4 shows that the Te I ($h\nu = 53$ eV) attenuation for $\theta > 2$ Å follows an exponential behavior with attenuation length of 7–8 Å. Since this value is consistent, within experimental uncertainty, with the photoelectron escape depth, the Te I "substrate" emission shows, therefore, no evidence of Cr–Te interdiffusion at high metal coverage ($\theta > 2$).

For $\theta < 2$ the Hg depletion of the surface layer and the shift of Te I 4*d* emission may both be related to the replacement of Hg–Te bonds with Cr–Te bonds. This is suggested by the difference in formation enthalpy of refractory metal tellurides relative to HgTe,[11] that makes a Hg–Cr exchange reaction thermodynamically favored. This is supported by a comparison of the attenuation of the Hg emission with the Cr atomic density. At $\theta = 2$ we have observed a 13–16 Å Hg depletion layer from the film surface. The Te II surface contribution accounts for approximately 3 Å.[7] The remaining 10–13 Å thick subsurface layer contains $(1.2\text{–}1.5) \times 10^{15}$ atoms/cm^2, to be compared with a Cr coverage of 1.6×10^{15} atoms/cm^2 at $\theta = 2$. Therefore the Hg attenuation is roughly consistent with a one-to-one exchange reaction between Cr and Hg atoms, followed by diffusion of the dissociated Hg away from the surface and subsurface layer.[12]

Our suggestion of a Hg–Cr exchange reaction for $0 < \theta < 2$ is based on (a) the thermodynamic trends, (b) the Hg depletion of the surface layer and its quantitative relationship with θ, (c) the binding energy change of the Te I 4*d* line for $\theta < 2$. More quantitive studies of the Te I 4*d* and Cr 3*p* core intensities, as well as of the Cr 3*p* binding energy are in progress to confirm this picture.[13] We emphasize that the term "exchange reaction" is used here to summarize a process in which initially Hg atoms are bonded to Te atoms in the homogeneous semiconductor and, upon Cr deposition, the surface and subsurface layers appear depleted of Hg while Cr–Te bonds are established.[15]

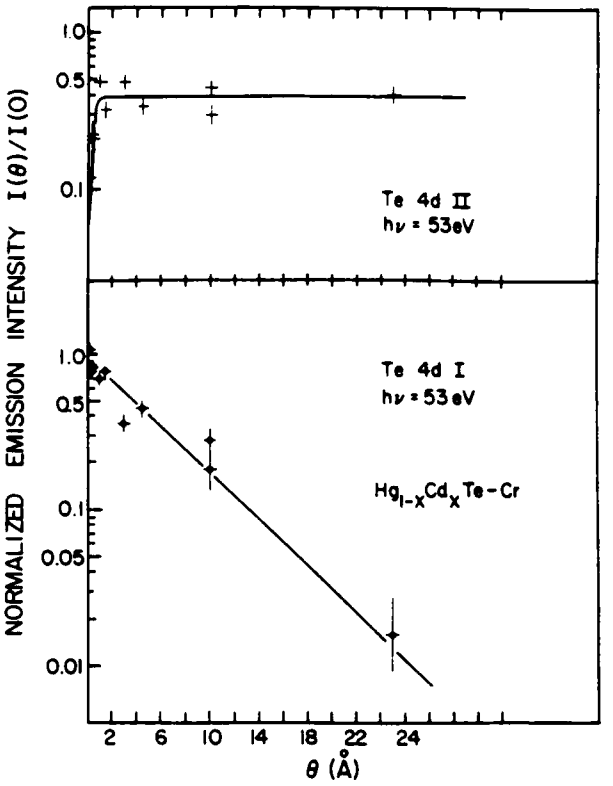

FIG. 4. Semilogarithmic plot of the integrated intensity of the Te 4*d* core emission from the $Hg_{1-x}Cd_xTe$–Cr interface, normalized to the Te 4*d* emission from the clean surface. Top: The Te II component corresponds to dissociated Te released at the surface during the first interface formation stage. Bottom: The Te I component corresponds mostly to Te atoms in the subsurface layer, where the Cr–Hg exchange reaction takes place for $\theta < 2$ Å.

As for the Cd atoms in the interface region, at this preliminary stage it is not possible for us to determine if and to what extent a Cr–Cd reaction takes place. If it does, it cannot involve more than 10%–15% of the Cd atoms in the subsurface region. A more complete discussion of this point will have to wait for a future report.[7]

The description of the $Hg_{1-x}Cd_xTe(110)$–Cr interface formation process that stems from this work is rather complex. At low metal coverages ($\theta < 2$ Å) Cr atoms replace all the Hg atoms in a 10–13 Å thick layer of the semiconductor, while some Te atoms are released from the semiconductor and form an elemental Te layer at the surface. Further Cr deposition ($\theta > 2$ Å) gives rise to a metallic Cr film covered by the dissociated Te species. This picture is rather different from the one proposed for the HgCdTe–Au[5] and HgCdTe–Al[4] interfaces. For HgCdTe–Au, Davis *et al.*[5] did report significant Te outdiffusion in the Au film, but no chemical shift of the Te 4*d* core was observed, leading to the conclusion that elemental Te was not the dominant species present Furthermore, no change in the Hg/Cd ratio was observed a

low metal coverage, when a 0.2 eV decrease of the band bending was observed relative to the clean surface. For the HgCdTe–Al interface, Daniels *et al.*[4] do not present any Te core data, but observe Hg depletion near the surface and a large decrease of the Hg/Cd ratio at low metal coverage. An apparent 0.2 eV change of the interface position of the Fermi level was related by these authors to the variation of the Hg/Cd surface ratio. In the case of the $Hg_{1-x}Cd_xTe(110)$–Cr interface one has to distinguish the properties of the relatively thin surface and subsurface layers from those of the underlying semiconductor bulk. The subsurface layer forms with the exchange reactions that yield the dramatic variations observed in the Hg/Cd ratio. The surface layer is constituted of dissociated Te that seems only a by-product of the exchange reaction that takes place in the subsurface layer. The information on the underlying "near-surface" bulk is carried primarily by the residual Hg 5*d* core emission, while the Te core and valence band emission primarily reflect the surface and subsurface electronic structure. We did not observe any variation in the Hg 5*d* core binding energy throughout the coverage range explored and we suggest that neither the local stoichiometry nor the band bending in the near surface region is affected by the reactions that take place in the two uppermost layers. In particular, interface reactions do not change the *n*-degenerate character[6] of the near-surface region.

ACKNOWLEDGMENTS

This work was supported in part by the Office of Naval Research under Contract No. N00014-84-K-0545, by the Graduate School of the University of Minnesota under Grant No. 0100490832, and by the McDonnell Douglas Independent Research and Development program. We wish to acknowledge J. H. Hollister, B. J. Morris, and D. S. Wright for their assistance in sample preparation and characterization. We thank G. D. Davis and G. Margaritondo for communicating their results to us prior to publication. Finally, we gladly acknowledge the cheerful support of the entire staff of the University of Wisconsin, Synchrotron Radiation Center, supported by NSF Grant No. DMR-8020164.

[1]W. E. Spicer, J. A. Silberman, I. Lindau A.-B. Chen, A. Sher, and J. A. Wilson, J. Vac. Sci. Technol. A 1, 1735 (1983).
[2]W. A. Harrison, J. Vac. Sci. Technol. A 1, 1672 (1983).
[3]A.-B. Chen, A. Sher, W. E. Spicer, J. Vac. Sci. Technol. A 1, 1674 (1983).
[4]R. R. Daniels, G. Margaritondo, G. D. Davis, and N. E. Byer, Appl. Phys. Lett. 42, 50 (1983); G. D. Davis, N. E. Byer, R. R. Daniels, and G. Margaritondo, J. Vac. Sci. Technol. A 1, 1726 (1983).
[5]G. D. Davis, W. A. Beck, N. E. Byer, R. R. Daniels, and G. Margaritondo (unpublished).
[6]D. J. Peterman and A. Franciosi, Appl. Phys. Lett. 45, 1305 (1984).
[7]A description of the deconvolution procedure for the Hg 5*d* and Cd 4*d* cores, as well as of the Te 4*d* line shape analysis will be presented in a longer paper: A. Franciosi, P. Philip, and D. J. Peterman (unpublished).
[8]J. A. Silberman, D. Laser, I. Lindau, and W. E. Spicer, J. Vac. Sci. Technol. 21, 154 (1982).
[9]W. E. Spicer, J. A. Silberman, J. Morgen, I. Lindau, J. A. Wilson, A.-B. Chen, and A. Sher, Phys. Rev. Lett. 49, 948 (1982).
[10]U. Solzbach and H. J. Richter, Surf. Sci. 97, 191 (1980).
[11]The equilibrium phase diagram of the Cr–Te binary system is still not completely understood. The existence of CrTe, Cr_3Te_4, Cr_2Te_3, $CrTe_2$, and Cr_7Te_8 have been proposed, in some cases following observation of relatively wide ranges of homogeneity of the $Cr_{1-x}Te$ alloy, ranges associated with the coexistence of two or more of the above stoichiometries. See for example, F.A. Shunk, *Constitution of Binary Alloys*, 2nd supplement (McGraw–Hill, New York, 1969).

The standard formation enthalpies of Cr tellurides are not known. However, their higher stability relative to HgTe is expected from a number of thermodynamic trends. Apart from the lower electronegativity of Cr relative to Hg, that suggest a larger ionic contribution to the bonding, we note that the known formation enthalpies of refractory metal tellurides are all well above the value of -7.6 kcal/mol appropriate for HgTe. In particular, most values are in the -20 to -40 kcal/mol range (for example TiTe -29.9; MnTe -26.6; $MoTe_2$ -32; WTe_2 -32; etc.) and none was reported below the ~ -13.5 kcal/mol value of $NiTe_{1.1}$ and Ti_2Te. See K. C. Mills, *Thermodynamic Data For Inorganic Sulphides, Selenides and Tellurides* (Butterworths, London, 1974). Therefore, the formation of Cr–Te phases at the HgCdTe–Cr interface should be thermodynamically favored, at the expenses of the weaker Hg–Te bonds.
[12]The local Cr/Te ratio in the subsurface region near the HgCdTe–Cr interface can be roughly estimated at $\theta = 2$ from the number of vacant Hg sites and by the number of Te atoms initially in the subsurface layer minus those that segregated at the surface and do not react with Cr. The result is consistent with CrTe, Cr_3Te_4, Cr_7Te_8 and possibly with Cr_2Te_3 stoichiometries, within the relatively large experimental uncertainty.
[13]Studies of the Cr 3*p* line require complex deconvolutions of the Cr 3*p* and Te 4*d* lines at photon energies near threshold. The Cr 3*p* line is partially superimposed on the Te $4d_{3/2}$ component. Due to centrifugal barrier effects emission from the Cr 3*p* states can be emphasized relative to the 4*d* emission for photon energy near threshold while it is negligible, for example, in the spectra of Fig. 3, obtained at $h\nu = 110$ eV.
[14]See, for example, L. J. Brillson, Surf. Sci. Rep. 2, 123 (1982) and references therein.
[15]The expression "exchange reaction" does not imply here as in the case of GaAs–Al (Ref. 16) that the adatom (Al) takes up cation (Ga) sites in the lattice, forming an ordered reacted layer (AlAs) of the same crystal structure. A conclusion of this kind would require a detailed structural analysis by means of LEED or SEXAFS or other scattering techniques that is not available at the present time.

PHYSICAL REVIEW B VOLUME 32, NUMBER 10 15 NOVEMBER 1985

Rapid Communications

The Rapid Communications section is intended for the accelerated publication of important new results. Manuscripts submitted to this section are given priority in handling in the editorial office and in production. A Rapid Communication may be no longer than 3½ printed pages and must be accompanied by an abstract. Page proofs are sent to authors, but, because of the rapid publication schedule, publication is not delayed for receipt of corrections unless requested by the author.

Au-Si interface formation: The other side of the problem

A. Franciosi
Department of Chemical Engineering and Materials Science, University of Minnesota, Minneapolis, Minnesota 55455

D. W. Niles and G. Margaritondo
Department of Physics, University of Wisconsin, Madison, Wisconsin 53706

C. Quaresima, M. Capozi, and P. Perfetti
Laboratorio di Struttura della Materia, Via Enrico Fermi 38, 00044 Frascati, Italy

(Received 6 August 1985)

Most metal-semiconductor interface-formation studies investigate the chemisorption of metal adatoms on semiconductor substrates. We extended the investigation of the Si-Au interface to the chemisorption of Si atoms on Au. We found that the formation of an extended, alloyed interface region is a common feature of both interface-formation processes. Thus, the changes in the surface and bulk substrate thermodynamic parameters do not affect the qualitative morphology of the interface.

The crucial importance of metal-semiconductor interfaces has stimulated a large number of photoemission studies of their formation in the past decade.[1-14] These investigations have explored the chemisorption of metal atoms on semiconductor substrates. We present the results of what is to our knowledge the first photoemission experiment investigating the chemisorption of silicon atoms on a metal substrate—Si deposited on Au. These results demonstrate that the two processes—Au deposition on Si and Si deposition on Au—are essentially symmetric. In particular, we find a systematic correlation between formation of Au-Si alloys and change in Au $5d$ crystal-field splitting[5-8] in both cases. We also find evidence that the formation of an extended alloyed interface region saturates at comparable coverages (atoms per unit surface) for Si deposited on Au and for Au deposited on Si.[9]

The experiments were performed at the PULS synchrotron radiation facility of the Frascati National Laboratory, with the beam line equipped with a Jobin-Yvon toroidal grating monochromator. Photoemission experiments were performed in the photon-energy range 20–60 eV with the experimental equipment described in Ref. 10. The overall resolution was of the order of 0.4 eV. The substrate was prepared by depositing a Au from a W coil on a Ta sheet *in situ*, at a pressure below 5×10^{-10} Torr. The thickness of the polycrystalline substrate was of several hundred angstroms. Si was deposited also *in situ* from an electron beam source at a rate of the order of 1 Å/min. The overlayer thickness was measured with a quartz thickness monitor.[9] Data taking and processing were controlled by a CAMAC system interfaced with a Tektronix 4052 microcomputer.

Figure 1 shows a series of photoelectron energy distribution curves (EDC's) taken at a photon energy of 21 eV with the horizontal scale referred to the Fermi level. Figure 2 shows the corresponding spectra taken at a photon energy of 35 eV, which enhances the cross section of the d-d antibonding states. The bottom curve in each figure corresponds to the clean Au substrate. The other curves correspond to the same substrate covered by a Si overlayer of increasing thickness. Figure 3 shows for comparison a series of EDC's taken[11] at a photon energy of 40 eV for Au deposited on cleaved Si(111).

The most important conclusions obtained from Figs. 1, 2, and 3 are the following. First, when Si is deposited on Au the antibonding d-d state signal at ~ -2.6 eV is progressively attenuated.[8,12] A symmetric increase in this signal is observed in Fig. 3 when Au is deposited on Si. Second, the d features shift to higher binding energies due to the Si adatoms on Au. This effect also has a symmetric counterpart in Fig. 3.

The similarity between the results for Si on Au and those for Au on Si is further demonstrated by a detailed comparison of the results of Figs. 2 and 3. The main effect of the Si adatoms in Fig. 2 is an apparent decrease of the energy splitting of the two main Au $5d$ features. We see in Fig. 3 a symmetric apparent increase of this splitting when the Au thickness increases. This effect has been explained[7] by the formation of a Au-Si alloy in which the Au atoms are far from each other—and therefore the splitting becomes closer to that of atomic Au, 1.5 eV.

Calculations by Bisi *et al.*[6] provided a detailed theoretical

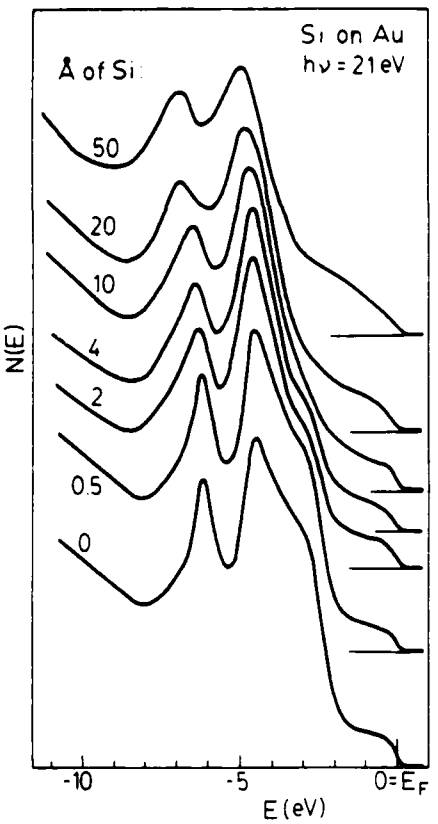

FIG. 1. Photoelectron energy distribution curves (EDC's) taken with a photon energy of 21 eV on a clean Au film and then on the same substrate covred with a Si overlayer of increasing thickness. The energy scale is referred to the Fermi level E_F.

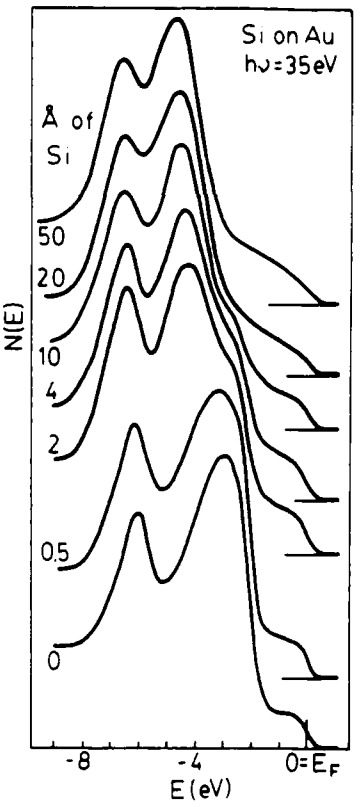

FIG. 2. EDC's similar to those of Fig. 1, taken at a photon energy of 35 eV.

background for the above explanation. The results of these authors indicate that the antibonding *d-d* states are those mostly affected by alloy or compound formation. In the case of pure Au, these states correspond to the shoulder 2–3 eV below the Fermi level in Fig. 1. For photon energies of 35–40 eV, Figs. 2 and 3, the *d-d* antibonding states dominate the shallowest-in-energy Au 5*d* feature.[12] Thus, their shift in energy is the main cause of the apparent change of the Au 5*d* splitting on going from pure Au to the Au-Si alloy.

Therefore, the behavior of the Au 5*d* energy splitting at photon energies of 35–40 eV is a good probe of the formation of a Si-Au alloy at the interface.[7] We show in Fig. 4 this splitting as a function of the overlayer thickness (in equivalent monolayers; see Ref. 9), for Si on Au and for Au on Si. We see from this figure that most of the change occurs for equivalent converages of 0–8 monolayers for Au on Si and 0–4 monolayers for Si on Au. To interpret this observation, one must consider the definition of the equivalent coverages in the two cases (Ref. 9). This definition implies that the interface layer formation is completed after depositing approximately the same number of atoms per unit substrate area in both cases, $(6–7)\times10^{15}$ atoms/cm^2. This result is somewhat surprising, since the adatom chemisorption energy was considered the dominant promoting factor for the Si-Au intermixing. Thus, the extent of the intermixing should be proportional to the number of atoms per unit substrate area. This, however, is not consistent with the results of Fig. 4, since there are approximately twice as many atoms per unit area for the Au substrate than for the Si substrate. The reason of this apparent discrepancy could be, for example, a different near-surface defect-formation enthalpy for the two cases.

We also see that the asymptotic values of the splitting for

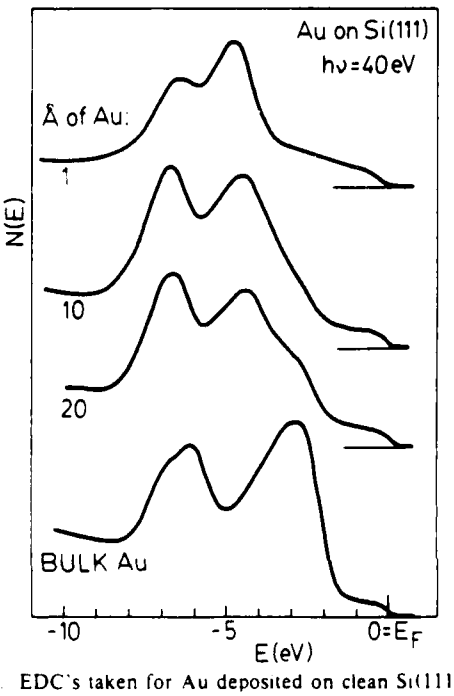

FIG. 3. EDC's taken for Au deposited on clean Si(111) at a photon energy of 40 eV. The data are from Ref. 11.

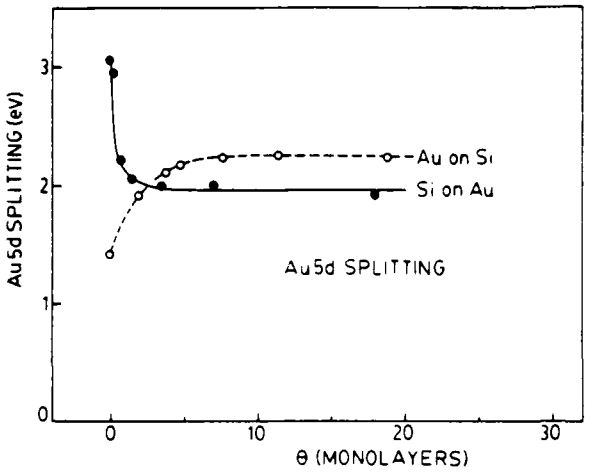

FIG. 4. The apparent Au 5*d* energy splitting as a function of the overlayer thickness for Au deposited on Si (Fig. 3) and for Si deposited on Au (Fig. 2 and Ref. 11). The overlayer thickness is expressed in equivalent monolayers in both cases, as discussed in Ref. 9.

large equivalent thicknesses are different by approximately 0.25 eV. This difference cannot be taken as evidence for a different average stoichiometry of the alloyed interface layer. In fact, the asymptotic value for Au on Si has been associated[7,13,14] with the presence of segregated Si atoms at the Au-vacuum interface. Similarly, in the case of Si on Au one could have segregated phases that give a constant Au 5*d* splitting for large coverages.

In summary, the most important result of our experiment is that interface alloyed species are formed both when Au is deposited on Si and when Si is deposited on Au. Processes of this kind, involving either alloys or interface compounds, have been observed in many investigations of metal overlayers on silicon.[1-7,15-17] Several factors have been proposed to control the formation of these extended interfaces. Our results enable us to rule out some of these factors, at least in the case of Si-Au. For example, we can rule out an important role of mass transport, of the segregation energies, and of the adatom kinetic energy. We also find similar numbers of atoms involved in the alloyed interface species for both Au on Si and Si on Au. One important result is that the changes in bulk and surface thermodynamic parameters caused by interchanging substrate and overlayer do not affect the qualitative morphology of the interface region.

This work was supported by the Office of Naval Research and by the Center for Microelectronics and Information Science of the University of Minnesota. The international collaboration Frascati-Wisconsin is supported by the National Science Foundation under Grant No. INT-81-22013 and by the Italian National Research Council.

[1]L. J. Brillson, Surf. Sci. Rep. **2**, 124 (1982).
[2]R. H. Williams, Contemp. Phys. **23**, 329 (1982).
[3]G. Margaritondo and A. Franciosi, Annu. Rev. Mater. Sci. **14**, 67 (1984).
[4]I. Lindau and W. E. Spicer, in *Synchrotron Radiation Research*, edited by H. Winick and S. Doniach (Plenum, New York, 1980), p. 159.
[5]I. Abbati, L. Braicovich, A. Franciosi, I. Lindau, P. R. Skeath, C. Y. Su, and W. E. Spicer, J. Vac. Sci. Technol. **17**, 930 (1980), and references therein.
[6]O. Bisi, C. Calandra, L. Braicovich, I. Abbati, G. Rossi, I. Lindau, and W. E. Spicer, J. Phys. C **15**, 470 (1982).
[7]L. Braicovich, C. M. Garner, P. R. Skeath, C. Y. Su, P. W. Chye, I. Lindau, and W. E. Spicer, Phys. Rev. B **20**, 5131 (1979).
[8]C. Calandra, O. Bisi, and G. Ottaviani, Surf. Sci. Rep. **4**, 271 (1984), and references therein.
[9]The definition of an equivalent monolayer thickness of Si on Au is made difficult in our case by the polycrystalline nature of the Au substrate. We assumed a prevailing (111) orientation for the microcrystallites, and used the surface density of Au(111), 13.8×10^{14} atoms/cm^2, to define the equivalent monolayer of Si on our substrate, 2.78 Å. The equivalent monolayer of Au on Si(111) is 1.32 Å.
[10]P. Perfetti, S. Nannarone, F. Patella, C. Quaresima, M. Capozi, A. Savoia, and G. Ottaviani, Phys. Rev. B **26**, 1125 (1982).
[11]A. Franciosi, D. G. O'Neill, and J. H. Weaver, J. Vac. Sci. Technol. B **1**, 524 (1983).
[12]A. Franciosi, J. H. Weaver, and D. G. O'Neill, Phys. Rev. B **28**, 4889 (1983).
[13]A. Hiraki, K. Shuto, S. Kim, W. Kamura, and M. Iwami, Appl. Phys. Lett. **31**, 611 (1977).
[14]A. K. Green and E. Bauer, J. Appl. Phys. **47**, 1284 (1976).
[15]P. S. Ho, J. Vac. Sci. Technol. A **1**, 745 (1983).
[16]P. J. Grunthaner, F. J. Grunthaner, A. Madhukar, and J. W. Mayer, J. Vac. Sci. Technol. A **19**, 649 (1983).
[17]P. Perfetti, S. Nannarone, F. Patella, C. Quaresima, A. Savoia, F. Cerrina, and M. Capozi, Solid State Commun. **35**, 151 (1980).

Interface chemistry of ternary semiconductors: Local morphology of the $Hg_{1-x}Cd_xTe(110)$-Cr interface

A. Franciosi and P. Philip
Department of Chemical Engineering and Materials Science, University of Minnesota, Minneapolis, Minnesota 55455

D. J. Peterman
McDonnell Douglas Research Laboratories, St. Louis, Missouri 63166

(Received 18 April 1985)

Synchrotron-radiation photoemission studies of interfaces prepared *in situ* on cleaved substrates show atomic interdiffusion with Cr/Hg and Cr/Cd exchange reactions taking place at room temperature for Cr coverages less than 2 Å. Correspondingly, dissociated Te is released at the surface. A subsurface region 10–13 Å thick is formed in which Cr atoms replace all of the Hg atoms and at least 20% of the Cd atoms. Below this subsurface the semiconductor maintains the bulk stoichiometry and the initial surface band bending.

Very little is known about the interface chemistry of ternary semiconductor alloys. The results available on compound semiconductors[1,2] can be extrapolated only in part to ternary alloys, where the interplay of two different kinds of chemical bonding can substantially change the character and stability of each bond with respect to those of the binary parent compounds. $Hg_{1-x}Cd_xTe$ is probably the ternary semiconductor most studied in recent years because of its widespread application for infrared detectors in the (8–14)-μm spectral range. This material poses a number of intriguing fundamental and technological problems that only now are starting to be addressed. As a ternary semiconductor alloy formed from parent compounds of very different stability, this material easily sustains composition variations. It has also been recently recognized that the interplay of ionicity and metallicity in the two kinds of chemical bonding that coexist in the matrix further weakens[3,4] one bond (Hg—Te) relative to the other (Cd—Te), causing lattice, surface, and interface instabilities in the alloy.[5] For example, dramatic composition variations have been observed in $Hg_{1-x}Cd_xTe$ as a result of processes as diverse as mechanical damage,[6,7] oxidation,[8] and metal deposition.[9,10] A detailed understanding of the interface chemistry and physics of this material requires a systematic analysis of variations in local stoichiometry, Schottky-barrier height, and interface width.

Pioneering photoemission studies have recently clarified the nature of chemical bonding in the bulk alloy,[11,12] and related the Schottky barrier height for the $Hg_{1-x}Cd_xTe(110)$-Al (Ref. 10) and $Hg_{1-x}Cd_xTe(110)$-Au (Ref. 13) interfaces to the local composition of the semiconductor surface layer. In this paper we focus on the chemistry of $Hg_{1-x}Cd_xTe$-refractory metal interfaces, which represent a new class of technologically important junctions that are largely unexplored. We have performed synchrotron radiation photoemission studies of the $Hg_{1-x}Cd_xTe(110)$-Cr interface formed *in situ*. Results concerning the connection between Schottky-barrier height and the changes in semiconductor surface composition have been presented earlier.[14] Here we describe the local morphology of the interface region in detail and relate the interface electronic properties to the local chemistry of the material.

EXPERIMENTAL DETAILS

Single crystals of $Hg_{1-x}Cd_xTe$ were prepared at McDonnell Douglas using a modified Bridgman method. Several oriented (110) posts ($3\times3\times15$ mm^3) were cut from the center of the cylindrical portion of a boule. Samples cut from each end of the cylinder showed an identical energy gap of 0.175 ± 0.01 eV and p-type conductivity with a room-temperature carrier concentration of 2×10^{16} cm^{-3}, as determined from infrared-transmission and Hall-effect measurements, respectively. The sample composition, deduced from the band gap measurements[15] was $x=0.22\pm0.01$. The posts were loaded into the photoelectron spectometer through a special fast-insertion device, thus allowing an operating pressure $<5\times10^{-11}$ Torr while avoiding sample exposure to high temperature. The posts were cleaved *in situ* with varying degrees of success at obtaining mirrorlike surfaces. The photoemission measurements were performed by positioning the samples at the common focus of the monochromatic photon beam and a commercial double pass cylindrical mirror analyzer. Photoelectron energy distribution curves (EDC's) were recorded for $40\leq h\nu\leq140$ eV using a "grasshopper" grazing incidence monochromator and synchrotron radiation from the 240-MeV electron storage ring, Tantalus, at the Synchrotron Radiation Center of the University of Wisconsin—Madison. The overall energy resolution (electrons plus photons) ranged from 0.4–0.7 eV for $h\nu<100$ eV to about 0.8–1.0 eV for the high-photon-energy studies (Te 4d and Cr 3p core levels at $h\nu=110$ eV). The interfaces were prepared *in situ* by direct Cr sublimation from a W coil and the metal coverage was monitored using a quartz thickness monitor.

RESULTS

Valence states

The experimental results are organized in two series of figures. Figures 1–4 show valence-band spectra for the clean and Cr-covered $Hg_{1-x}Cd_xTe$ surfaces, Figs. 5–10 summarize results for the core-level emission. In the photon-energy range available to us we were able to monitor the evolution of the Hg $5d$, Cd $4d$, Te $4d$, and Cr $3p$ core levels as a function of metal coverage, gaining information on the relative concentration and on the local chemical environment of each atomic species present in the interface region.

In Fig. 1 we show representative energy distribution curves for the valence-band emission of the cleaved $Hg_{1-x}Cd_xTe$ surface. The zero of the binding energy scale corresponds to the spectrometer Fermi level as derived from the Fermi level cutoff of the high-Cr-coverage EDC's. The spectra have been approximately normalized to the main emission features, and are given in arbitrary units. The EDC's show good qualitative agreement with the results of Silberman *et al.*[11] and exhibit a Tep–derived density-of-states feature within 3.5 eV of the Fermi level E_F, and a second structure between 4 and 7 eV derived primarily from unresolved Cd s and Hg s features which reflect the metal s–chalcogenide p hybridization responsible for the stability of the alloy.[16]

The emission features between 8 and 12 eV correspond to the Hg $5d$ and Cd $4d$ core levels. Deconvolution of two doublets was performed using the experimental line shape of the Hg $5d$ and Cd $4d$ levels obtained from cleaved HgSe and CdSe samples. As an example, the result of the decomposition for the clean surface is shown in the top section of Fig. 6. All cleaves resulted in identical [Hg]:[Cd]:[Te] ratios (as determined by the ratios of the Hg $5d$, Cd $4d$, and Te $4d$ integrated emissions) irrespective of cleave quality, and no time-dependent change of the surface composition was observed after cleaving. From the EDC's of Fig. 1 it is possible to estimate the position of the valence band maximum, E_v, by linearly extrapolating the valence band edge at low binding energy. From all cleaves we obtained $E_v = 0.49 \pm 0.15$ which, when compared with the measured bulk band gap of only 0.175 ± 0.01 eV, indicates a strongly inverted (n-type) character for the near surface region.

The effect of Cr deposition on the valence band emission is shown in Fig. 2 for $h\nu = 60$ eV. The bottom-most spectrum is the clean surface spectrum while EDC's displaced upward correspond to increasing Cr coverages Θ and are given in relative units. Two effects are clearly evident in Fig. 2. First, emission from the Cr $3d$ states quickly dominates the valence band spectra within 3 eV of E_F. Second, the Hg-derived emission decreases dramatically and is almost negligible at $\Theta \sim 3$ Å. These two trends are shown in more detail in Figs. 3 and 5 where we have plotted, in an expanded scale, the valence-band emission within 9 eV of E_F and the Hg $5d$–Cd $4d$ core emission, respectively. In Fig. 3 we see that initial Cr deposition gives rise to increased valence emission within 2 eV of E_F, and to a "tailing" of valence states at E_F. A true Fermi-level cutoff, however, cannot be seen until $\Theta \sim 3$ Å.

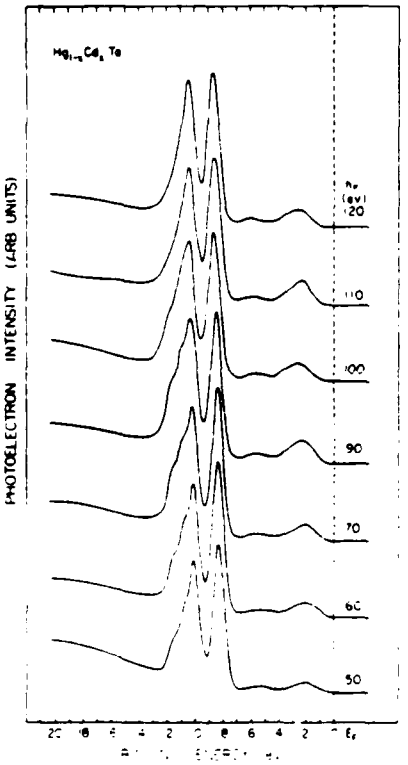

FIG. 1. EDC's for the valence-band and Hg $5d$–Cd $4d$ core-level emissions from $Hg_{1-x}Cd_xTe(110)$ surfaces obtained by cleaving $x = 0.22$ bulk crystals.

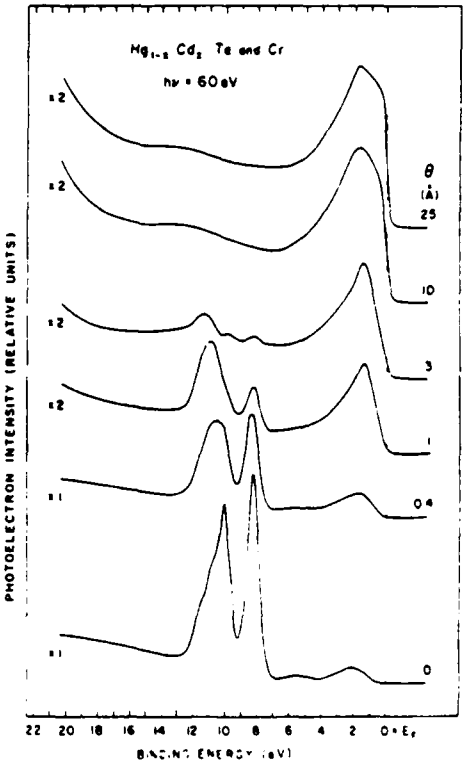

FIG. 2. Valence-band and Hg $5d$–Cd $4d$ core-level emissions for the $Hg_{1-x}Cd_xTe(110)$-Cr interface. The topmost spectra are shown multiplied by a scale factor of 2.

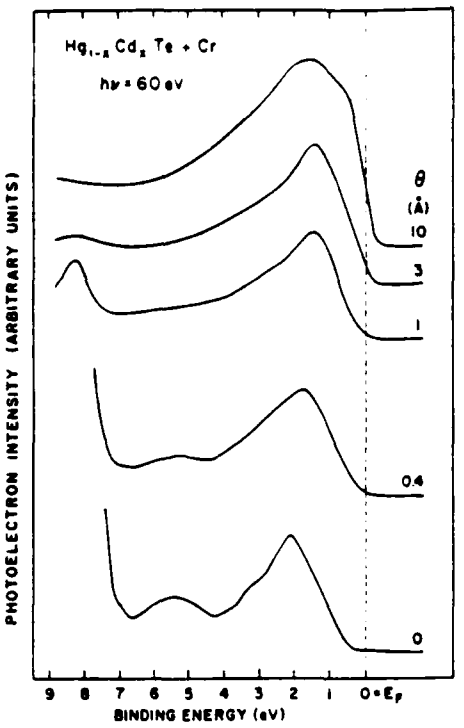

FIG. 3. Detail of the valence-band emission within 9 eV of the Fermi level E_F for the $Hg_{1-x}Cd_xTe(110)$-Cr interface. Initial Cr deposition gives rise to increased valence emission within 2 eV of the E_F and to tailing of valence states at E_F. A true Fermi level cutoff, however, can be seen only for coverages $\Theta \geq 3$.

At this point, the $3d$ emission gives rise to a main emission feature centered 1.3–1.4 eV below E_F which is relatively sharp [full width at half maximum (FWHM) ~2.7–2.8 eV] compared to the more bulklike Cr emission at $\Theta = 25$ Å. Very little change of the valence states is observed for $10 < \Theta < 25$ Å yet there are several relevant differences compared to bulk Cr. This is shown in Fig. 4 where the topmost spectrum (solid line) was obtained from a 250-Å-thick Cr film evaporated on oxidized Ta, and the bottom-most spectrum from the $Hg_{1-x}Cd_xTe$ interface with $\Theta = 25$ Å [coverage corresponding to over 30 monolayers, taking 1 ML $= 6.8 \times 10^{14}$ atoms /cm^2 equals the total surface atomic density for $Hg_{1-x}Cd_xTe(110)$]. The main differences we note (tic marks) are a shift of the main $3d$ feature by 0.2 eV to higher binding energy, increased emission within 1 eV of the Fermi level, and a rather broad density-of-states feature centered 12.5 eV below E_F.

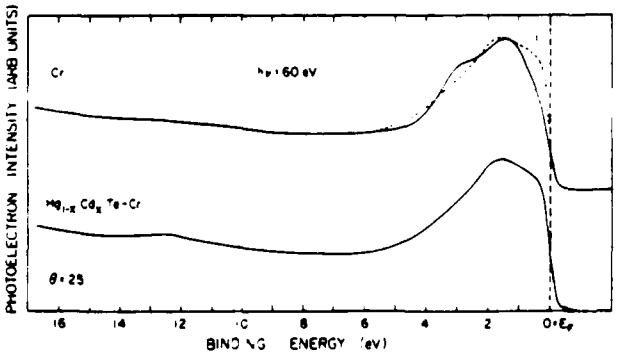

FIG. 4. Comparison of valence emission from bulk Cr (250 Å Cr film on oxidized Ta) and from the $Hg_{1-x}Cd_xTe$-Cr interface at $\Theta = 25$ Å. The 25-Å-coverage interface shows increased emission within 1 eV below E_F and a 0.2-eV shift to higher binding energy of the main $3d$ feature.

Core emission

Figure 5 shows the evolution of the Hg $5d$ and Cd $4d$ core-level line shapes in the $0 \leq \Theta \leq 3$ Å coverage range for $h\nu = 60$ eV. The spectra were obtained from the EDC's of Fig. 2 after subtraction of a smooth secondary electron background and are given in relative units. The vertical dashed lines mark the position of the Hg $5d_{5/2}$, Hg $5d_{3/2}$, and Cd $4d_{5/2}$ levels after deconvolution (see top section of Fig. 6). Emission from all cores appear strongly attenuated even at low metal coverages (note the scale factors in Fig. 5). Furthermore, the Hg-to-Cd ratio decreases dramatically with increasing metal coverage. The binding energy of the Hg $5d$ core levels remains unchanged as a function of metal coverage within experimental uncertainty (~0.1 eV). For the Cd core levels, our data show constant binding energy for $\Theta \leq 1$ Å, and suggest a sharp 0.3–0.4 eV binding energy increase for 1 Å $< \Theta < 3$ Å.[17]

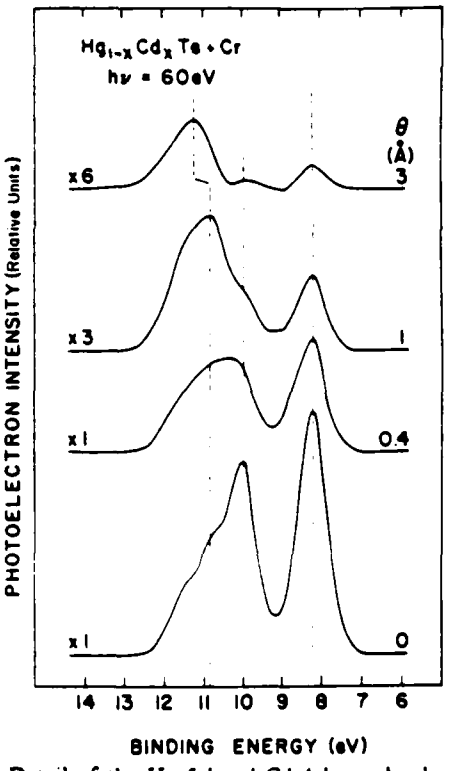

FIG. 5. Detail of the Hg $5d$ and Cd $4d$ core-level emission from the $Hg_{1-x}Cd_xTe$-Cr interface as a function of metal coverage. The vertical dashed lines indicate the corresponding binding energy as derived from the deconvolution shown in the top section of Fig. 6. Note the dramatic increase of the [Cd]/[Hg] ratio due to Hg migration away from the subsurface layer.

To examine quantitatively the surface concentration of Hg and Cd as a function of coverage, the two doublets were deconvolved as sketched in the top sections of Fig. 6. The total integrated intensity of each doublet at a given coverage Θ was normalized to the zero-coverage emission intensity, and is shown in a semilogarithmic plot in the lower section of Fig. 6. The solid lines correspond to an exponential attenuation of the core emission. The resulting attenuation lengths[18] are 0.7 and 1.7 Å, respectively, for the Hg $5d$ and Cd $4d$ core levels. The attenuation of the Cd and especially of the Hg core emission is far more rapid than can be reasonably expected from an escape-depth-driven mechanism, where an attenuation length of 4–5 Å would be expected.[19]

EDC's for the Te $4d$ core emission at $h\nu = 110$ eV and $h\nu = 53$ eV are shown (solid lines) in Figs. 7 and 8, respectively. The spectra appear all approximately normalized to the main emission feature to emphasize the line shape changes. The EDC's (solid lines) in Fig. 7 show that the sharp experimental $4d$ line shape for the clean surface is broadened asymmetrically at $\Theta = 1.5$ and 3.0 Å and shifted to lower binding energy. For $\Theta \geq 10$ Å, however, the linewidth decreases again while the doublet is shifted to higher binding energy. These nonmonotonic trends can be explained by the existence of two $4d$ lines, shifted by 0.5 eV from each other, and with coverage-dependent relative intensity. To fit the experimental spectra, we used two $4d$ line shapes obtained from the clean surface emission and, as fitting parameters, the binding energy and relative intensity of the two $4d$ components. The result of the fit is shown in Fig. 7 by a short-dashed line. The fit is remarkably good, and the experimental line shape appears to be composed of a low binding energy doublet (Te $4d$ I) that dominates at low coverage, and by a new high-binding-

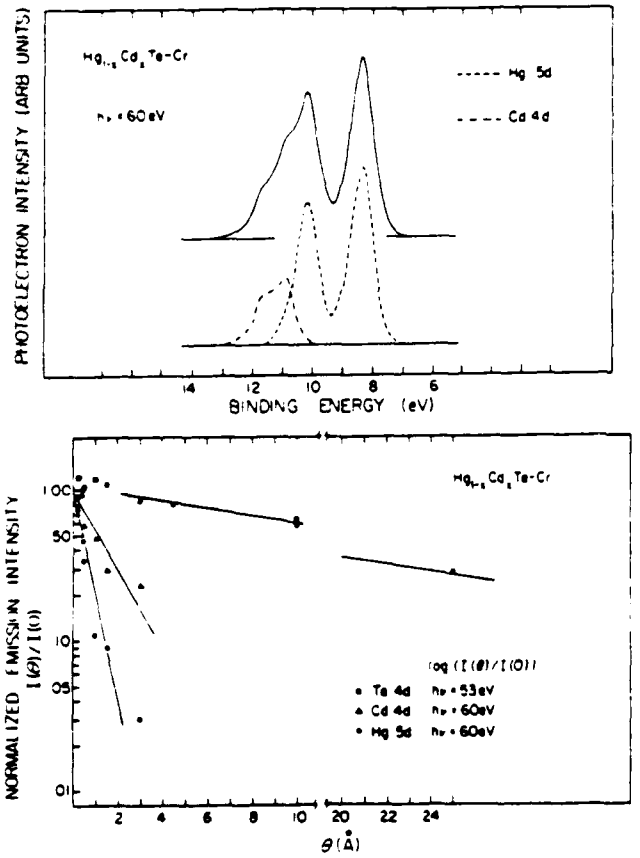

FIG. 6. Top: deconvolution of the experimental line shape (solid line) in Hg $5d$ (dashed line) and Cd $4d$ (dotted-dashed line) contributions for the clean $Hg_{1-x}Cd_xTe$ surface. The $4d$ and $5d$ line shapes were obtained from HgSe and CdSe samples. Bottom: semilogarithmic plot showing the integrated intensity of the Hg $5d$, Cd $4d$, and Te $4d$ core-level emission, normalized to the emission from the clean surface, as a function of metal coverage. As discussed in the text, the fast attenuation of the Hg and Cd emission reflects an exchange reaction in a (10–13)-Å subsurface region, where all of the Hg atoms and at least 20% of the Cd atoms are replaced by Cr atoms.

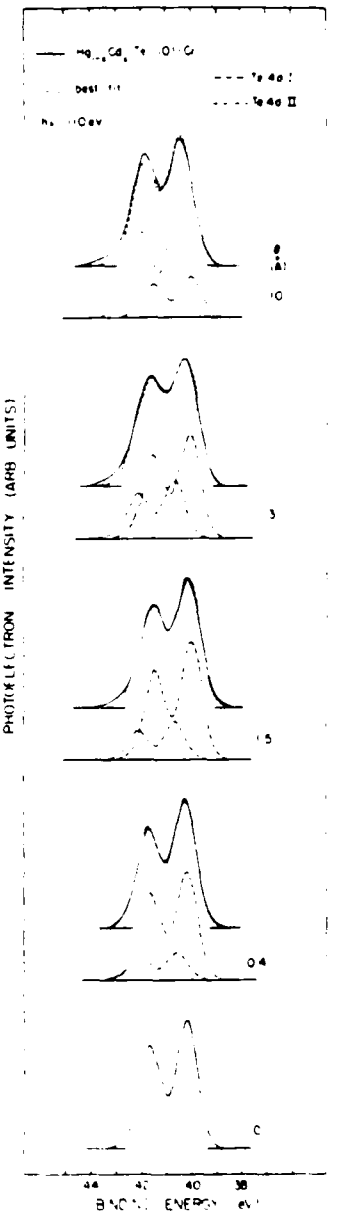

FIG. 7. Te $4d$ core emission from the $Hg_{1-x}Cd_xTe$-Cr interface at $h\nu = 110$ eV. Solid line: experiment. Short-dashed line: results of a best fit using the sum of a Te $4d$ I subsurface component (long-dashed line) and a Te $4d$ II surface component (dotted-dashed line). At $h\nu = 110$ eV the emission from the Cr $3p$ cores is negligible for $\Theta \leq 10$.

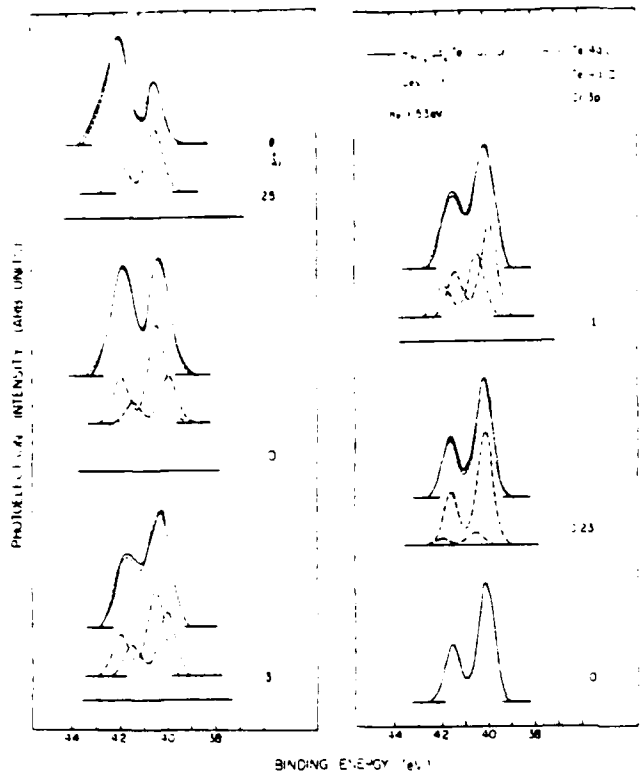

FIG. 8. Te 4*d* core emission from the $Hg_{1-x}Cd_xTe$-Cr interface at $h\nu=53$ eV. Solid line: experiment. Short-dashed line: result of a best fit using the sum of a Te 4*d* I subsurface component (long-dashed line), a Te 4*d* II surface component (dotted-dashed line), and a Cr 3*p* line (dotted line). The Cr line shape was obtained from a Cr film evaporated on an inert substrate. At $h\nu=53$ eV we are near the photoemission threshhold and the Cr signal is of the same order of magnitude as the Te signal.

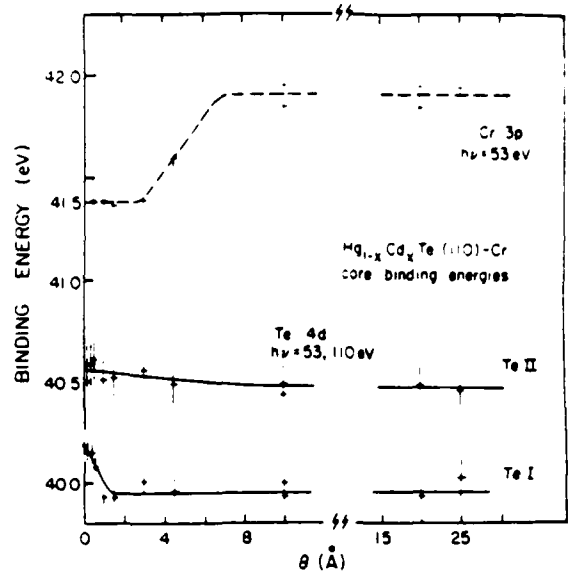

FIG. 9. Binding energy of the Cr 3*p*, Te 4*d* I, and Te 4*d* II, core-level emission from the $Hg_{1-x}Cd_xTe$-Cr interface. The binding energies were obtained from the deconvolution procedure described in Figs. 7 and 8. The high-coverage saturation values of the Cr 3*p* and Te 4*d* II binding energies are close to the elemental values.

energy component (Te 4*d* II) 0.45 eV above the main line that grows as a result of Cr deposition, and becomes the dominant feature at $\Theta=10$ Å. At coverages greater than 10 Å the Cr 3*p* core-level contribution, at a binding energy of about 42 eV, is not negligible, even for $h\nu=110$ eV, and the fit cannot be obtained by simply superimposing two Te 4*d* lines. This is demonstrated by the results at $h\nu=53$ eV in Fig. 8. At photon energies close to the photoemission threshold, one expects the centrifugal barrier to emphasize the Cr 3*p* as compared to the Te 4*d* emissions in our EDC's. The experimental line shapes in Fig. 8 (solid line) reflect, in fact, the superposition of the two 4*d* lines and a Cr 3*p* line (dotted line). Again, to reduce the number of fitting parameters, we used an experimental Cr 3*p* line shape determined from evaporated Cr films, and we let the binding energy and intensity of this line be the additional fitting parameters. The results (shown with short-dashed lines in Fig. 8) were extremely rewarding. We emphasize that the results of the fitting at $h\nu=53$ eV confirm those at $h\nu=110$ eV since the binding energy of each Te 4*d* line was identical, within experimental uncertainty, in the two cases. The binding energy of each Te component and of the Cr 3*p* line is shown in Fig. 9. The Cr 3*p* emission appears initially at constant binding energy (for $\Theta\leq 3$ Å) and then shifts toward higher binding energy. The final binding energy at high metal coverage appears close to the bulk Cr value (41.95 ± 0.1 eV versus 42.22 ± 0.15 eV). The binding energy of the Te 4*d* II component remains relatively unchanged as a function of coverage, with at most a gradual 0.1-eV decrease in the whole coverage range. The Te 4*d* I component, that starts at the clean surface position, shifts rigidly 0.25 eV to lower binding energy during initial metal deposition ($\Theta\leq 2$ Å) and then remains unchanged. The integrated intensity of each Te 4*d* component is plotted in Fig. 10 as a function of metal coverage for $h\nu=53$ eV. The overall Te 4*d* core-level emission (component I plus component II) is compared in the lower part of Fig. 6 (full squares) with the Cd 4*d* and Hg 5*d* core-level emission. It is readily seen from Fig. 6 that the attenuation of the Te 4*d* core-level emission is relatively small compared to that of the Cd and Hg core-level emissions. This is because while the Te 4*d* I component exponentially decreases in intensity (lower section, Fig. 10) the Te 4*d* II component (upper section, Fig. 10) grows dramatically during deposition of the first two monolayers. The results at $h\nu=110$ eV are similar, except for the higher saturation value of the Te 4*d* II emission, about 60–80% of the clean surface emission as opposed to 40%.

DISCUSSION

Composition variations

The results of Figs. 1–10, and in particular, of Figs. 2, 3, 9, and 10, suggest that different processes occur at the interface in the low-coverage range $0\leq\Theta<2$ Å, and in the high-coverage range $\Theta>2$ Å. In Fig. 6 we showed that dramatic changes in the relative [Hg]/[Te] and [Hg]/[Cd] concentrations at the surface occur upon Cr deposition at low coverage. For 2 Å Cr coverage the

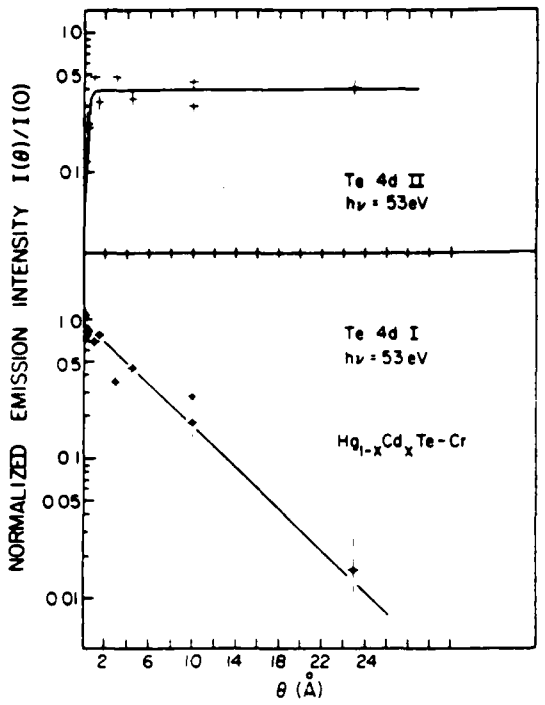

FIG. 10. Semilogarithmic plot of the integrated emission intensity of the Te 4*d* core levels from the $Hg_{1-x}Cd_xTe$-Cr interface, normalized to the Te 4*d* emission from the clean surface. Top: The Te 4*d* II component corresponds to dissociated Te released at the surface during the first interface formation stage. Bottom: The Te 4*d* I component corresponds to Te atoms in the subsurface layer, where the Cr-Hg (and Cr-Cd) exchange reaction takes place for $\Theta \leq 2$ Å.

Hg 5*d* core-level emission is reduced to about 4% of the initial value, the Cd 4*d* emission to about 30%, while the overall Te 4*d* emission remains near the clean surface value (100 %). The reduction of the Hg signal is explained by a combination of three experimental observations: (a) Hg depletion of the semiconductor surface layer, (b) layer-by-layer Cr coverage of the reacted surface, and (c) Te outdiffusion at the surface of the Cr film. The analysis of the Te 4*d* line shape gives us a guideline to interpret the remaining experimental results. Figures 7 and 8 show that two well-defined chemical environments exist for the Te atoms at the surface. The Te 4*d* I environment is related to the bulk semiconductor $Hg_{0.78}Cd_{0.22}Te$ environment, as indicated by the Te 4*d* I binding energy which starts at the clean surface value (and then shifts rigidly to lower binding energy; see Fig. 9). The Te 4*d* II environment is sharply different from the initial semiconductor environment, as indicated by the (0.4—0.5)-eV increase in 4*d* binding energy, which varies very little with further metal deposition (Fig. 9). The intensities of the Te 4*d* I and Te 4*d* II components (Fig. 10) exhibit sharply different coverage dependencies. The Te 4*d* II component increases dramatically at low coverage ($\Theta < 2$ Å), with a suggestive inverse relationship to the sharp decrease of the Hg 5*d* emission (Fig. 6). At higher coverage it saturates to a constant limit of about 40% of the initial overall Te emission ($h\nu = 53$ eV). The saturation value at $h\nu = 110$ eV is, instead, about 70%. Because of the shorter escape depth at $h\nu = 110$ eV, this last point clearly indicates the surface character of the Te 4*d* II emission. It is possible to roughly estimate the amount of Te at the film surface by calculating the thickness d of a Te layer which would give rise to the same 4*d* emission intensity observed at the highest metal coverage. Assuming the Te photoionization cross section to be similar in the semiconductor and in the Te 4*d* II environment, one obtains

$$\left.\frac{I^{II}_{Te}(\Theta)}{I_{Te}(0\ \text{Å})}\right|_{\Theta\to\infty} \simeq 1 - e^{-d/L},$$

where L is the photoelectron escape depth [$L \simeq 4$ Å at $h\nu = 110$ eV and $L \simeq 8$ Å at $h\nu = 53$ eV (Ref. 19)]. For both $h\nu = 53$ eV and $h\nu = 110$ eV we obtain $d \simeq 3$ Å, i.e., about 1.3 monolayers, in terms of the Te surface atomic density on the $Hg_{0.78}Cd_{0.22}Te(110)$ surface. The Te 4*d* II emission is therefore localized in a relatively thin surface layer of the deposited film. Further information on the chemical environment of the Te 4*d* II component can be obtained from the high-coverage Cr 3*p* (Fig. 9) and valence-band (Fig. 4) results. At high metal coverages ($\Theta \sim 25$ Å) the Te 4*d* I emission does not contribute appreciably (Fig. 10) and the results of Figs. 4 and 9 reflect the interaction of the Te 4*d* II species with the top layers of the Cr film. Correspondingly, the Te 4*d* II binding energy (0.4—0.5 eV above the initial 4*d* substrate emission) is consistent with the "elemental Te" core binding energies reported in Refs. 20 and 21, and the Cr 3*p* binding energy is close to the elemental Cr 3*p* value. This suggests a relatively small Cr-Te interaction for the Te 4*d* II environment. The valence band results of Fig. 4 are qualitatively consistent with such a picture. An elemental Te valence emission is expected to show[22] a 5*s* emission feature peaked some 12 eV below the valence band edge and a leading emission feature within 1.5 eV of the valence band edge, deriving from the Te lone-pair *p* electrons. Figure 4 shows that the high-coverage valence-band spectra exhibit indeed a 12.5-eV broad emission feature absent in Cr and increased emission within 1 eV from E_F. We therefore suggest that the Te 4*d* II species that are released at the surface during the early stages of interface formation reflect mostly an elemental Te environment.

The sharp decrease of the Hg 5*d* emission (Fig. 6) for $\Theta < 2$ Å cannot be explained simply by layer-by-layer coverage of the $Hg_{1-x}Cd_xTe$ substrate, even if one takes into account the formation of an additional Te 4*d* II surface layer. Hg has to migrate away from the surface layer. Since the binding energy of the Hg 5*d* cores (Fig. 5) remains unchanged, this process is likely to produce a surface layer completely depleted of Hg rather than a layer with graded Hg content. In the first case one would expect the residual Hg emission to come from deeper in the solid and to reflect a relatively unperturbed $Hg_{1-x}Cd_xTe$ environment. In the second case one would expect, instead, several inequivalent environments for Hg atoms within the experimental sampling depth, with consequent broadening and shift of the Hg 5*d* cores, in contrast with the results of Fig. 5. The residual 4% Hg 5*d* emission observed in Fig. 5 at $\Theta = 2$ Å, is consistent with complete Hg depletion of a (13—16)-Å thick surface layer.[23]

The residual Hg core emission would then reflect the stoichiometric $Hg_{1-x}Cd_xTe$ semiconductor below this layer. The Te emission, instead reflects both the dissociated species at the surface of the evaporated film (Te 4*d* II) and the reacted Te 4*d* I species in the subsurface layer (see next section). We emphasize that at $\Theta=2$ Å only an estimated 10–15% of the Te 4*d* I emission ($h\nu=53$ eV) originates from regions of the semiconductor deep enough in the solid so to reflect the stoichiometric situation.

Exchange reactions

In the lower part of Fig. 10 we show that the intensity of the Te 4*d* I core-level emission ($h\nu=53$ eV) decreases to about 70% of its initial value for $\Theta\sim2$ Å and, at higher metal coverages, follows an exponential behavior with attenuation length of 7–8 Å. Since this value is consistent, within experimental uncertainty, with the photoelectron escape depth, we identify the Te 4*d* I component as Te subsurface emission. Our results show, therefore, no evidence of Cr-Te interdiffusion at high metal coverages ($\Theta>2$ Å). For $\Theta\leq2$ Å, the interpretation of the results of Fig. 10 is complicated by the outdiffusion of Te 4*d* II species and by Hg migration away from the surface. For $\Theta\sim2$ Å we note that the observed Te 4*d* I intensity (70%) is consistent with the attenuation expected from the Te 4*d* II layer alone, as if the Cr did not contribute to the attenuation. This, together with the binding energy change of the Te 4*d* I core levels observed for $\Theta\leq2$ Å, argues for substrate-overlayer interdiffusion in this coverage range. The Hg depletion would be then related to the replacement of Hg—Te bonds with the more stable Cr—Te bonds. An independent check of this hypothesis can be obtained by comparing the observed attenuation of the Hg emission with the Cr atomic density. At $\Theta=2$ Å we have observed a 13–16 Å depletion layer at the film surface. The Te 4*d* II surface layer accounts for ~3 Å. The remaining 10–13 Å subsurface layer contains $\simeq(1.2-1.5)\times10^{15}$ Hg-sites/cm^2. At $\Theta\simeq2$ Å the Cr surface density is $\simeq1.67\times10^{15}$ atoms/cm^2. Therefore, the Hg attenuation is roughly consistent with a one-to-one exchange reaction between Cr and Hg atoms, followed by diffusion of the dissociated Hg away from the surface and subsurface layer.

The core binding energy results are more difficult to interpret due to the presence of a number of semiconducting and metallic species of rapidly varying composition. During the Hg-Cr exchange reaction the Te 4*d* I core shifts by about 0.25 eV to lower binding energy. This shift could reflect a net charge transfer to the Te atom because of the reduced Cr electronegativity compared to Hg. The *rigid* shift of the Te 4*d* I core level and the fact that the shift is independent of the experimental sampling depth (4 Å $<L<$ 8 Å for 110 eV $>h\nu>$ 53 eV) further confirms the picture of a Cr-Te reacted subsurface layer with a depth which is larger than L. The Cr 3*p* binding energy (Fig. 9) appears constant in the first interface formation stage ($\Theta\leq2$ Å), in agreement with a one-to-one exchange picture that yields a similar local environment for all Cr atoms in the subsurface region. After the reaction is completed, the Cr cores shift toward the bulk Cr position, as expected since no interdiffusion takes place for $\Theta\geq2$ Å. The Cr 3*p* binding energy for $\Theta\sim2$ Å is 0.5 ± 0.1 eV less than that for the final "metallic" position. This would seem to argue against a net charge transfer from Cr to Te atoms during the exchange reaction. We emphasize, however, that the observed "chemical shift" need not be related in an elementary way to the actual charge transfer.[24] Furthermore, for Cr atoms isolated in a nonmetallic matrix, as appears to be the case for $\Theta\leq2$ Å (Fig. 3), the binding energy should be measured from the vacuum level and would reflect the effective work function of the subsurface and surface species.[25] If we take, for example, the high coverage Cr 3*p* and Te 4*d* II binding energy as representative of the elemental Cr 3*p* and Te 4*d* emission, then at $\Theta\sim2$ Å both the Cr 3*p* core level and Te 4*d* I core levels exhibit an analogous ~0.5 eV shift to lower binding energy relative to the elemental state, with no clear indication of net charge transfer in any direction.

Exchange reactions between metal overlayers and semiconductor cations have been observed in II-VI compound semiconductors such as CdSe and CdTe.[1,2] In these materials dissociated Cd has been reported in the interface region and its presence has been related to the production of Ohmic contacts onto the semiconductor surface. These dissociated Cd species are characterized by a 0.5–0.6 eV *lower* 4*d* binding energy compared to Cd in the II-VI-semiconductor environment.[26] Our results show that the Cd emission from the $Hg_{1-x}Cd_xTe$-Cr interface decreases more slowly in intensity than the Hg emission, and that the binding energy of the Cd 4*d* cores seems to increase by about 0.3 eV at $\Theta=3$ Å. Therefore, while the subsurface region does contain a substantial amount of Cd, these atoms appear to be neither bulk-$Hg_{1-x}Cd_xTe$-like nor dissociated. A possible explanation is that the Cd atoms in the subsurface region interact with Cr when Cr replaces the neighboring Hg atoms with a charge transfer from Cd to Cr. Due to the higher stability of the Cd—Te bond as compared to the Hg—Te bond, the probability of Cr replacing Cd in the structure is smaller. If the exchange occurs, Cd atoms must migrate away from the subsurface region since we have no evidence of dissociated Cd within the experimental sampling depth. Both Cd and Hg, in fact, exhibit large diffusion coefficients in $Hg_{1-x}Cd_xTe$ at room temperature.[6] From the reduction in intensity of the Cd emission at $\Theta\sim2$ Å we can estimate a lower limit for this Cr-induced Cd deficiency in the subsurface layer of $(0.7-1.0)\times10^{14}$ atoms/cm^2. This would be consistent with the difference between the Cr surface concentration at $\Theta\sim2$ Å of 1.67×10^{15} atoms/cm^2 and the available Hg sites in the subsurface layer [$\sim(1.2-1.5)\times10^{15}$ atoms/cm^2]. In this picture, upon metal deposition Cr atoms would replace all of the Hg atoms and at least 20% of the Cd atoms in the subsurface layer. The model implies that the residual Hg 5*d* emission seen at $\Theta\simeq2$ Å is representative of the bulk semiconductor underlying the subsurface layer and its binding energy reflects the bulk stoichiometry and the near-surface band bending.[14] Systematic investigation with variable escape depth and high

resolution for the Cd 4*d* core levels is necessary to further verify the validity of this model.

CONCLUSIONS

The local morphology of the $Hg_{1-x}Cd_xTe(110)$-Cr interface is rather complex compared to those reported for the $Hg_{1-x}Cd_xTe$-Al and $Hg_{1-x}Cd_xTe$-Au interfaces. A description of this morphology was possible only through systematic studies of the core emission from each of the chemical species involved and, in particular, through careful line shape analysis of the Te 4*d* emission. Valence and core results are consistent with a first interface formation stage ($\Theta \leq 2$ Å) where Cr replaces all of the Hg atoms and at least 20% of the Cd atoms in a (10–13)-Å thick layer of the semiconductor. At the same time Te atoms are released from the semiconductor and form an elemental Te layer at the surface. When the exchange reaction is completed ($\Theta \sim 2$ Å), about $(1.2-1.5)\times 10^{15}$ Hg atoms in the subsurface layer have been replaced by Cr atoms. Further Cr deposition gives rise to a metallic Cr film covered by the dissociated Te species produced during the first stage of interface reaction (~ 1.3 monolayers). The typical high coverage interface morphology consists, therefore, of an elemental Te surface, a metallic Cr film, and a Hg-depleted 10–13 Å subsurface region where Cr—Te and Cd—Te bonds coexists, on top of the ternary semiconductor bulk. The Hg core emission from the underlying bulk remains at a constant binding energy indicating that the bulk environment and the semiconductor band bending[14] remain unchanged beneath the surface and subsurface layers.

ACKNOWLEDGMENTS

This work was supported, in part, by the Graduate School of the University of Minnesota under Grant No. 0100490832, by the Office of Naval Research, Department of the Navy, under Contract No. N00014-84-K-0545, and by the McDonnell Douglas Independent Research and Development program. We wish to acknowledge J. H. Hollister, B. J. Morris, and D. S. Wright for their assistance in sample preparation and characterization. We thank G. D. Davis and G. Margaritondo for useful discussions and for communicating their results to us prior to publication. Finally, we are grateful for the friendly support of the entire staff of the University of Wisconsin, Synchrotron Radiation Center at Stoughton (supported by National Science Foundation Grant No. DMR-76-15089).

[1]For an extensive review, see L. J. Brillson, Surf. Sci. Rep. 2, 123 (1982).

[2]G. Margaritondo and A. Franciosi, Ann. Rev. Mater. Sci. 14, 67 (1984) and references therein.

[3]W. A. Harrison, J. Vac. Sci. Technol. A 1, 1672 (1983).

[4]A.-B. Chen, A. Sher, and W. E. Spicer, J. Vac. Sci. Technol. A1, 1675 (1983).

[5]W. E. Spicer, J. A. Silberman, I. Lindau, A.-B. Chen, A. Sher, and J. A. Wilson, J. Vac. Sci. Technol. A 1, 1735 (1983).

[6]H. M. Nitz, O. Ganschow, V. Kaiser, L. Wiedmann, and A. Benninghoven, Surf. Sci. 104, 365 (1981).

[7]A. Lastras-Martinez, V. Lee, J. Zehnder, and P. M. Raccah, J. Vac. Sci. Technol. 21, 157 (1982).

[8]J. A. Silberman, D. Laser, I. Lindau, and W. E. Spicer, J. Vac. Sci. Technol. A 1, 1706 (1983).

[9]G. D. Davis, N. E. Byer, R. R. Daniels, and G. Margaritondo, J. Vac. Sci. Technol. A 1, 1706 (1983).

[10]R. R. Daniels, G. Margaritondo, G. D. Davis, and N. E. Byer, Appl. Phys. Lett. 42, 50 (1983).

[11]J. A. Silberman, P. Morgen, I. Lindau, W. E. Spicer, and J. A. Wilson, J. Vac. Sci. Technol. 21, 154 (1982).

[12]W. E. Spicer, J. A. Silberman, J. Morgen, I. Lindau, J. A. Wilson, An-Ban Chen, and A. Sher, Phys. Rev. Lett. 49, 948 (1982).

[13]G. D. Davis, W. A. Beck, N. E. Byer, R. R. Daniels, and G. Margaritondo, J. Vac. Sci. Technol. A 2, 546 (1984).

[14]D. J. Peterman and A. Franciosi, Appl. Phys. Lett. 45, 1305 (1984).

[15]M. W. Scott, J. Appl. Phys. 40, 4077 (1969).

[16]A.-B. Chen, A. Sher, and W. E. Spicer, J. Vac. Sci. Technol. A1, 1674 (1983).

[17]The reduced intensity of the Cd 4*d* emission at this coverage, the evident line broadening, and the emergence of a broad emission feature centered some 12.5 eV below E_F all yield some uncertainty in the estimate of the Cd 4*d* binding energy change. High-resolution photoemission studies of this coverage range are necessary before further discussion of this point.

[18]We will avoid using the expression "escape depth" to denote these parameters, since they do not represent the photoelectron escape depth at $h\nu = 60$ eV, as will become clear in the following discussion.

[19]These values for the escape depth of 4*d* photoelectrons from the Cr-Te overlayer are only rough estimates. See, for example, I. Lindau and W. E. Spicer, J. Electron. Spectrosc. 3, 49 (1974).

[20]V. Solzbach and H. J. Richter, Surf. Sci 97, 191 (1980).

[21]G. D. Davis, T. S. Sun, S. P. Buchner, and N. E. Byer, J. Vac. Sci. Technol. 19, 472 (1981).

[22]M. Schlüter, J. D. Joannopoulos, M. L. Cohen, L. Ley, S. P. Kowalczyk, R. A. Pollak, and D. A. Shirley, Solid State Commun. 15, 1007 (1974).

[23]Including the $\simeq 3$ Å Te 4*d* II layer.

[24]See, for example, R. E. Watson and M. L. Perlman, Struct. Bonding (Berlin) 24, 82 (1975).

[25]P. H. Citrin and G. K. Wertheim, Phys. Rev. B 27, 3176 (1983).

[26]C. F. Brucker and L. J. Brillson, Thin Solid Films 93, 67 (1982).

OVERLAYER-INDUCED ENHANCED OXIDATION OF GaAs SURFACES

S. Chang, A. Rizzi, C. Caprile,
P. Philip, A. Wall and A. Franciosi

Department of Chemical Engineering and
Materials Science
University of Minnesota
Minneapolis, Minnesota 55455

ABSTRACT

Thin metal overlayers deposited on GaAs (110) cleavage surfaces enhance the surface oxidation rate several orders of magnitude above the clean surface value. The magnitude of this effect depends on the chemistry of the overlayer, on the local morphology of the overlayer-semiconductor interface region and on the nature of the gaseous reactants. We present a synchrotron radiation photoemission investigation of the GaAs surface interaction with oxygen in the presence of Ag, Au and Cr overlayers, and of the GaAs-H_2O reaction in the presence of Cr overlayers. We find that the promotion effect is maximum in the presence of Cr overlayers, and that the nature of the surface reaction products changes if oxygen or water is employed. In particular, in the case of oxygen, Ga and As-oxide phases are found with high atomic oxidation states present. If water is employed, only Ga oxide/hydroxyl phases are found at the surface, on top of a Cr-As subsurface layer that remains largely unaffected by oxidation.

INTRODUCTION

A number of metal overlayers on silicon yield an increase in silicon oxidation rate when the surface is exposed to an oxidizing atmosphere. Metals as diverse as Au[1,2], Ag[3,4], Cu[5], Pd[5] and Cr[6] have all been shown to give rise to promotion effects, with the production of Si-oxide phases of variable stoichiometry. In the case of Au[1] and Cr[6-7], the Si-oxide appears to nucleate on top of the metal overlayer. To the extent that the metal atoms increase the surface reaction kinetics and do not appear directly involved in the reaction product, i.e. the surface silicon oxide, they play the role of a catalyst. Since the magnitude of the effect depends on the overlayer-silicon interface morphology, in the absence of a more precise denomination we refer to such phenomena as interface catalytic effects.

In this paper we discuss a few examples of interface catalytic effects observed for GaAs. Our interest in GaAs stems from both technological and fundamental reasons. The possible use of practical catalysts to promote the formation of new stable insulating layers on GaAs surfaces would have substantial impact on device technology, if the reacted layers would exhibit inversion and accumulation characteristics suitable for MOS fabrication. From a fundamental point of view, our understanding of the microscopic mechanisms that determine interface catalytic effects could be greatly improved by considering GaAs-metal interfaces, which may exhibit for a given metal different chemistry and different local morphology relative to the silicon case.

The information on GaAs interface catalytic effects is very scarce. We are aware of only one other photoemission study[8], showing that enhanced oxidation effects are produced by submonolayer Cs deposition onto the GaAs(110) surface. We have previously reported[6] that Cr overlayers greatly enhance the GaAs-O_2

reaction at room temperature. Here we compare the effect of Cr overlayers with the effect of Ag and Au overlayers and examine the role of the metal chemistry and the metal-semiconductor interface structure. Ag and Au have similar chemistry, exhibiting relatively low reactivity for oxidizing species, but exhibit different interface morphologies. Several authors[9-10] have indicated a rather sharp GaAs(110)-Ag interface with little or no atomic interdiffusion and possible island formation. For GaAs(110)-Au most authors concur[11-13] in indicating substantial atomic interdiffusion, with the formation of an extended intermixed interface region. Correspondingly, we find evidence of Au-induced oxidation promotion, while no promotion effects are observed for Ag-overlayers. A quantitative comparison with the GaAs:Cr-O_2 case indicates that the promotion effect is greatly enhanced by the use of Cr, a refractory metal exhibiting an extended intermixed interface region with GaAs. Clearly the chemistry of the metal and the interface morphology both play a relevant role. We have also examined the effect of Cr overlayers on the GaAs interaction with H_2O. We have chosen H_2O as a prototype molecular oxidizing species because of its relevent technological role in silicon processing[14]. It has recently been suggested that the chemisorption of H_2O on GaAs shows similarities with GaAs-O_2 interaction[15-17]. We find, however, very dissimilar behavior in the presence of Cr. We do observe enhanced reaction kinetics in both cases, and H_2O chemisorption does not trigger a decomposition of the arsenide-like surface species, but selectively yields oxidation of Ga at the surface. This result appears related to the formation of Ga-oxide or hydroxyl phases where low Ga oxidation states dominate, rather than to the synthesis of Ga_2O_3 at the surface.

EXPERIMENTAL DETAILS

The experiments were performed on GaAs(110) surfaces obtained by cleaving 4 x 4 x 10 mm^3 single crystals of n-type, Te-doped, 10Ω x cm GaAs in-situ in our photoelectron spectrometer at operating pressure < 5 x 10^{-11} torr. Overlayers of Ag, Au and Cr were deposited in-situ from W-coil resistively heated evaporators at pressures below 4 x 10^{-10} torr. Overlayer thickness was monitored with a quartz thickness monitor. Exposure to water or oxygen was performed at pressures in the 10^{-7}-10^{-5} torr range. Ion pumps were isolated from the spectrometer during exposure and the system was pumped down in the 10^{-9} torr range with a cryopump prior to opening to the ion pump. Pressure during exposure was monitored with a low-emission ion gauge that was not directly in line-of-sight of the sample surface. Even with such precautions, we expect a definite contribution of excited molecular species to the gas composition during exposure. For comparison, we also conducted chemisorption studies of the GaAs(110) surface in the same conditions. Promotion effects (or the lack of them) due to the overlayer are defined by comparison with the results for the free surface.

The samples were positioned at the focus of a monochromatic synchrotron radiation beam and an electron energy analyzer. A toroidal grating monochromator or a "grasshopper" grazing incidence monochromator was used to disperse the radiation from the 240 MeV electron storage ring Tantalus at the Synchrotron Radiation Center of the University of Wisconsin-Madison. We used a commercial double pass cylindrical mirror analyzer to energy-analyze the photoelectrons in the GaAs:Ag case, and a hemispherical analyzer for the other studies. Angular-integrated photoelectron energy distribution curves (EDC's) were recorded for 40 < hν < 140eV with an overall energy resolution (electrons & photons) of 0.4 eV for all studies except GaAs:Ag (0.7-0.8eV) and are shown in figs. 1 to 7 after

subtraction of a smooth secondary background estimated with a polynomial fit of the high and low energy spectral range. Here we focus mostly on a systematic comparison of results for the Ga 3d and As 3d core line emission. More complete results concerning the valence states and metal cores from selected interfaces will be presented elsewhere[18-20].

RESULTS AND DISCUSSION

Oxidation

Studies of GaAs oxidation in the presence of Au, Cr and Ag overlayers are summarized in figs. 1-3. We explored overlayer thicknesses in the 0.1 - 15 A range and oxygen exposures in the 10 - 10^4L range. The spectra have been approximately normalized to the intensity (peak height) of the main emission feature in order to emphasize the lineshape changes and are given in arbitrary units. The zero of the binding energy scale corresponds to the initial core binding energy for the clean surface in flat-band conditions. The metal coverage is given in A or monolayers[21].

In the top section of fig. 1 and 2 we show the lineshape of the As 3d and Ga 3d cores, respectively, for the clean surface (solid line) and after exposure to 1000L of oxygen. Note that the clean spectra (solid line) have been shifted 0.60 eV to lower binding energy to compensate for band bending and emphasize lineshape changes. Except for the band bending variation, very little change is observed in the core lineshape as a result of oxygen exposure. This is in agreement with the results of Landgren et al.[22] who estimate an oxygen coverage on the order of a tenth of a monolayer as a result of exposure to oxygen at room temperature in the 1-10^4 L range. When Au is predeposited onto the GaAs(110) surface, exposure to oxygen gives rise to a definite core lineshape change

(mid-section of figs. 1-2). The shaded areas emphasize new high binding energy core features that are the result of oxygen chemisorption. For comparison, the vertical bars labeled 1 to 4 in figs. 1-2 indicate the chemically shifted core features observed by Landgren et al.[22] during GaAs oxidation, and associated with As and Ga atoms coordinated with 1, 2, 3 and 4 oxygen atoms. The vertical bar labeled 5 in Fig. 1 shows the binding energy of the As 3d observed by Su et al.[23] during As oxidation and associated by these authors with stoichiometric As_2O_3. Similarly, vertical bar 5 in Fig. 2 was obtained from the results of Su et al.[24] for Ga_2O_3. Figs. 1-2 show that the presence of Au overlayers gives rise to a weak oxidation promotion effect, with the formation of an oxygen chemisorbed layer where low As-O and Ga-O coordination numbers are observed. Correspondingly, little effect is seen on the valence states[19] that mostly reflect a Au-5d derived DOS with only minor modifications following oxygen exposure. The intensity of the core oxidized features in figs. 1 and 2 appears to increase relative to the main line if higher exposures or higher metal coverages are employed. Therefore, we conclude that we did not observe saturation of oxygen chemisorption in the exposure range explored, and that the oxidation promotion effect appears related to the thickness of the Au intermixed species that are formed when Au is deposited onto the clean GaAs surface. There is some disagreement in the literature about the detailed nature and the actual thickness of such species[10-13], but most results seem to indicate an alloyed region of thickness$\geq$ 20 A.

When Cr is deposited onto the GaAs(110) surface chemically driven interdiffusion takes place[25] with the formation of two main reaction products: a Cr-As arsenide-like phase at the interface and a Cr-Ga intermetallic alloy[25]. This is visible in the core lineshape spectra (solid line) in the bottom-most sections of

figs 1 and 2. The overall As 3d line is the result of the superposition of a bulk As 3d component and of a new low binding energy component some 0.3-0.4 eV below the main line[25]. In Fig. 2, bottom-most section, the Ga 3d line (solid line) shows a broad low binding energy feature centered some 0.6-0.7 eV above the main line that corresponds to Ga atoms in several inequivalent environments in the Cr matrix.

Upon oxygen exposure (dashed line) new oxide-derived features dominate the core spectra so that most As and Ga atoms within the experimental sampling depth are oxidized. We find an increase of several orders of magnitude in the surface oxygen uptake and no evidence of saturation in the exposure range explored[6]. The oxide-derived core features are of two kinds: low oxidation state features appear near the initial flat band position in Fig. 1 for As, together with a broad oxide band centered at 2.4 eV that reflects several non-equivalent high oxidation states for As within the sampling depth. In fig. 2 (bottom-most section, dashed line) the two oxide bands are even better defined: a first feature near the zero of the relative binding energy scale reflects mostly single and double Ga-O local coordination. A second well-defined feature appears centered some 2 eV below the first one, and corresponds to higher oxidation states than previously observed for Ga. The nature of these new oxide species that appear potentially more stable than Ga_2O_3 is still a subject of investigation.

If the results for GaAs:Cr-O_2 are compared with those for GaAs: Au-O_2 important differences are found. An obvious difference is in the magnitude of the promotion effect which is several-fold higher for Cr overlayers. A second interesting difference is in the nature of the oxide species. In the case of Au overlayers the oxidized spectra show only low oxidation state features near the

zero of the relative binding energy scale. The high-stability Ga oxide phases observed (bottom-most section of fig. 1-2) are not formed in the presence of Au overlayers. One possible suggestion is that such species involve Cr-arsenate phases, that may exhibit a relatively high oxygen content. However, our metal core and valence band results[18] indicate a main Cr_2O_3-like oxidation state for Cr, with no evidence of mixed oxides. Whatever the detailed nature of these high stability oxide phases is, clearly the chemistry of the metal overlayer determines if they form or not.

In examining the GaAs:Ag-O_2 case, we leave aside for a moment the overlayer chemistry and we focus on the importance of the interface morphology in determining interface catalytic effects. In fig. 3 we show the effect of oxidation on the Ga 3d (rightmost section) and As 3d (leftmost section) core lines for two different Ag coverages. The topmost EDC's have been obtained with a 0.1 Å Ag overlayer, the bottom-most ones for a 1 Å Ag overlayer. Relatively small metal coverages were used because of the rather sharp interface morphology reported for GaAs(110)-Ag[9-10]. The zero of the binding energy scale is referred to the clean surface flat-band position, and the EDC's for the unoxidized surface (solid lines) have been shifted 0.65 eV to lower binding energy to superimpose them on the oxidized spectra (dashed line). Notwithstanding the experimental energy resolution for the series of results above, 0.8 eV, the spectra in fig. 3 clearly show that the Ag overlayers do not give rise to an oxidation promotion effect in the exposure range explored. This fact is confirmed by our valence band results which actually suggest that, if anything, the Ag overlayers passivate the GaAs surface against oxygen adsorption.

As discussed before, Au overlayers give rise to a limited oxidation promotion effect. We have shown that despite the chemical similarity of Ag and Au, Ag

overlayers do not give rise to a promotion effect under the same conditions. We suggest that the different behavior is associated with the different metal-semiconductor interface morphology. It appears that promotion effects occur via a metallic intermixed "activation layer" from which semiconductor atoms are released. Activation effects have indeed been observed only for overlayers that intermix with the semiconductor atoms with the formation of metallic (silicide-like, arsenide-like, etc.) reaction products. Our results for GaAs-Ag vs. GaAs-Au can be compared with those for Si-Au and Si-Ag by Rossi et al.[3,5] and Cros et al.[2,4] Au and Ag overlayers on Si both give rise to oxidation promotion when intermixed phases are formed.

Water Chemisorption

Figs. 4 to 7 summarize studies of H_2O chemisorption on GaAs(110) in the presence of Cr overlayers. Fig. 4 and 6 show the effect of H_2O exposure on the As 3d and Ga 3d lineshape, respectively. The topmost EDC's show the results for the clean cleavage surface, and EDC's displaced downward show the results for increasing Cr coverage prior to oxidation. The spectra have been arbitrarily normalized to emphasize lineshape changes. The zero of the binding energy scale corresponds to the initial core binding energy for the clean surface in flat-band conditions.

The effect of H_2O chemisorption on the clean surface is mostly visible in Fig. 4 and 6 in the rigid core binding energy shift due to band bending. In the exposure range explored, the coverage obtainable at room temperature is lower than a monolayer, and our results for the clean surface are in agreement with a number of investigations[15-17] in which molecular water was used.

The effect of Cr overlayers on the oxidation of As is visible in the lower

section of Fig. 4. Apart from the band bending, a relatively small oxide-induced feature is observed between 2 and 3 eV in the spectra at 2 and 4 A Cr coverage. These modifications appear surprisingly minor when compared to the oxidation promotion effects described in the previous section. In Fig. 5 we compare the As 3d core lineshape during oxidation of the clean surface (topmost curve) and for H_2O and O_2 chemisorption in the presence of Cr overlayers of similar thickness (mid and bottom-most section). The interaction with H_2O does not produce any major oxide feature, indicating that the arsenide-like interface region is essentially stable against water exposure in the exposure range examined.

The situation is drastically different for Ga, as can be seen by comparing Figs. 5 and 7 . Before water exposure the result of increasing Cr deposition is the emergence of a broad low binding energy feature some 0.7-0.8 eV below the main line. This feature increases with Cr coverage and has been associated[25] with the formation of Cr-Ga intermetallic alloy. The effect of exposure to 1000 L of H_2O is shown by a dashed line for each Cr coverage. The "alloyed" low binding energy feature is removed in all cases, and new high binding energy features appear between 1 and 3 eV below the main line. Since the intensity of the oxidized feature scales with the initial intensity of the alloyed feature, we suggest that water chemisorption selectively involves the surface Ga atoms possibly through decomposition of the Cr-Ga surface alloy[20]. In fig. 7 we compare the Ga 3d core lineshape during oxidation of the clean surface (topmost EDC) and for H_2O and O_2 chemisorption in the presence of Cr overlayers of similar thickness (mid- and bottom-most section). The vertical bars 1-4 indicate the Ga 3d binding energies observed by Landgren et al.[22] for Ga atoms coordinated to 1, 2, 3 and 4 oxygen atoms. Vertical bar 5 was obtained from the results of Su et al.[24] for Ga_2O_3, vertical bar 6 from the results of Webb and

Lichtensteiger[26] for H_2O chemisorption on GaAs. The authors assigned this feature to Ga-OH bond formation. Fig. 7 shows that during water exposure the new Ga 3d oxidized features indicate relatively low oxidation states. No hint is found of the high stability Ga-oxide feature observed during oxygen exposure. Instead, the relatively broad and structured oxidized feature is qualitatively consistent with Ga-hydroxyl bond formation and/or Ga oxide phases with low Ga-O coordination and lower stability than Ga_2O_3.

The very dissimilar behavior observed in comparing the two bottom-most sections in Fig. 7 is somewhat surprising in view of the suggestion by Childs et al.[15] that water and oxygen chemisorption on GaAs give rise to similar local bonding at the semiconductor surface. Clearly the chemistry of the metal-semiconductor interface yields a drastic asymmetry of the two chemisorption processes. These results argue for a substantially different chemisorption energy in the two cases. The stability of the Cr-As subsurface layer has been effectively compared to the energy gained through the formation of chemisorption bonds, and the layer appears stable only against water chemisorption.

CONCLUSIONS

We have presented what is just the start of a systematic study of overlayer-induced promotion effects for GaAs surface reaction. The chemistry of ternary systems of this kind (semiconductor/overlayer/gaseous species) is both intriguing and complex. Promotion effects are relatively common, but their magnitude depends on the interplay of the chemistry and the morphology of the overlayer-semiconductor interface. Correspondingly, metals with similar chemistry can give rise to quantitatively different promotion effects and so can overlayers with similar morphology and different chemistry.

The large reactivity encountered for these metal-semiconductor interface species is not surprising. In the case of silicon, silicide-like phases are formed at the interface, while for GaAs the reaction products include arsenide-like species. Oxygen chemisorption studies on bulk silicides have shown higher oxygen uptake rates than for elemental silicon, the presence of high silicon oxidation states and a prefential oxygen bonding to silicon atoms that leaves the metal atoms relatively unaffected, at least in the first chemisorption stage[27-28]. It was proposed that the metal atoms are effective in dissociating the O_2 molecule at the silicide surface and consequently promote silicon oxidation[28]. While a detailed understanding of this mechanism is still missing, the similarities in the chemical bonding between arsenides[29] and silicides[30-32] suggest that similar effects can take place at metal-GaAs interfaces.

The oxidation of the interface species results in their decomposition into stable oxide phases. If this process leads to saturation of the chemisorption process, then the technological implications would be minor. However, in all cases we have examined thus far we did not observe saturation at the highest exposures explored at room temperature. This suggests that when the mass-transfer problem is solved by annealing the substrate during reaction, relatively thick oxidized layers can be grown. Even at room temperature thicknesses larger than 20-30 A[18-20] are easily obtained. The metal atoms that remain relatively unreacted in the first oxidation stage[18,27-28], appear oxidized at high exposure. This, however, may not eliminate catalytic effects, since transition metal mixed oxide phases show considerable catalytic activity for a number of chemical reactions[33], and explain why saturation is not observed.

In this connection, we notice that the metal overlayers examined so far have relatively high electronegativity and varying degrees of d-character at E_F. We

suggest that metals with low electronegativity, relatively high d-character at E_F and intermixed interface morphology may give rise to unprecedented oxidation enhancement effects, since they would play the double role of "catalyst" and electronic "promoter" of the oxidation reaction[33,34]. Promotion and poisoning effects of catalytic reactions, such as is observed, for example, during co-adsorption of CO with K or S on Ni(001)[34], seems far removed from semiconductor chemistry, but the thought is rather stimulating, and we plan to extend our study to low electronegativity metal overlayers such as Ca and Sm.

ACKNOWLEDGEMENTS

This work was supported in part by the Office of Naval Research under contract No. 0014-84-K-0545 and by the Center for Microelectronic and Information Science of the University of Minnesota. We are in debt to O. Bisi, S. Valeri, J. H. Weaver, and M. Grioni for communicating their results to us prior to publication. We thank L. Braicovich and R. Ludeke for useful discussions. The Synchrotron Radiation Center of the University of Wisconsin-Madison is supported by the National Science Foundation under grant No. DMR-8020164 and we gratefully acknowledge the cheerful support of its staff.

REFERENCES

1. A. Hiraki, M. A. Nicolet, and J. W. Mayer, Appl. Phys. Lett. 18, 178 (1971); T. Narusawa, S. Komiya, and A. Hiraki, Appl. Phys. Lett. 20, 278 (1972).

2. A. Cros, J. Derrien, and F. Salvan, Surf. Sci. 110, 471 (1981); J. Derrien, and F. Ringeisen, Surf. Sci. 124, L35 (1983).

3. G. Rossi, L. Caliari, I. Abbati, L. Braicovich, I. Lindau, and W. E. Spicer, Surf. Sci. Lett. 116, L202 (1982).

4. A. Cros, J. Physique (Paris) 44, 707 (1983).

5. I. Abbati, G. Rossi, L. Calliari, L. Braicovich, I. Lindau, and W. E. Spicer, J. Vac. Sci. Technol. 21, 409 (1982).

6. A. Franciosi, S. Chang, P. Philip, C. Caprile, and J. Joyce, J. Vac. Sci. Technol A3, 933 (1985).

7. An extensive report on Si:Cr-O_2 reactions will appear in the near future: P. Philip, S. Chang, C. Caprile, and A. Franciosi, to be published.

8. C. Y. Su, P. W. Chye, P. Pianetta, I. Lindau, and W. E. Spicer, Surf. Sci. 86, 894 (1979).

9. D. Bolmont, P. Chen, F. Proix, and C. A. Sebenne, J. Phys. C15, 3639 (1982).

10. R. Ludeke, Surf. Sci. 132, 143 (1983); R. Ludeke, T. C. Chiang, and T. Miller, J. Vac. Sci. Technol. B1, 581 (1983).

11. P. Skeath, C. Y. Su, I. Hino, I. Lindau, and W. E. Spicer, Appl. Phys. Lett. 39, 349 (1981); S. H. Pan, D. Mo, W. G. Petro, I. Lindau, and W. E. Spicer, J. Vac. Sci. Technol. B1, 593 (1983).

12. L. J. Brillson, G. Margaritondo, N. G. Stoffel, R. S. Bauer, R. Z. Bachrach, and G. Hansson, J. Vac, Sci. Technol. 17 880 (1980); L. J. Brillson, R. S. Bauer, R. Z. Bachrach and G. Hansson, Phys. Rev. B23, 6204 (1981).

13. M. Grioni, J. J. Joyce, and J. H. Weaver, 32nd National AVS Symposium, Houston, TX, November 19-22, 1985; J. Vac. Sci. Technol. (in press).

14. L. E. Katz, in VLSI Technology, S. M. Sze, ed, McGraw-Hill Book Company, New York, 1983.

15. K. D. Childs, W. A. Ino, and M. G. Lagalli, J. Vac. Sci. Technol. A2, 593 (1984).

16. W. Mokwa, D. Kohl, and G. Heiland, Surf. Sci. 139, 98 91984).

17. G. Thornton, R. A. Rosenberg, V. Rehn, A. K. Green, and C. C. Parks, Solid State Commun. 40, 131 (1981).

18. Results for GaAs:Cr-O_2 will be presented by S. Chang, P. Philip, and A. Franciosi, to be published.

19. Results for GaAs:Au-O_2 will be presented by S. Chang and A. Franciosi, to be published.

20. Results for GaAs:Cr-H_2O will be presented by S. Chang, A. Rizzi and A. Franciosi, to be published.

21. Metal coverages are given in Angstroms, or in equivalent monolayers in terms of the GaAs surface atomic density of 8.9×10^{14} at/cm^2. It is 1ML = 1.06 Å of Cr, = 1.5 Å of Au, = 1.5 Å of Ag.

22. G. Landgreu, R. Ludeke, Y. Jugnet, J. F. Morar, and F. J. Himpsel, J. Vac. Sci. Technol. B2, 351 (1984).

23. C. Y. Su, I. Lindau, P. R. Skeath, I. Hino, and W. E. Spicer, Surf. Sci. 118, 257 (1982).

24. C. Y. Su, P. R. Skeath, I. Lindau, and W. E. Spicer, Surf. Sci. 118, 248 (1982).

25. M. Grioni, M. Del Giudice, J. Joyce, and J. H. Weaver, J. Vac. Sci. Technol. A3, 907 (1985); J. H. Weaver, M. Grioni, and J. Joyce, Phys. Rev. B31, 5348 (1985).

26. C. Webb and M. Lichtensteiger, J. Vac. Sci. Technol. 21, 879 (1982).

27. S. Valeri, V. del Pennino, and P. Sassaroli, Surf. Sci. 134, L537 (1983); S. Valeri, V. del Pennino, P. Lomellini, and P. Sassaroli, Surf. Sci. 145, 371 (1984).

28. S. Valeri, V. del Pennino, P. Lomellini, and G. Ottaviani, Surf. Sci. 161, 1 (1985).

29. R. Podlucky, J. Phys. F 14, L145 (1984).

30. C. Calandra, O. Bisi and G. Ottaviani, Surf. Sci. Rep. 4, 271 (1984) and references therein.

31. A. Franciosi and J. H. Weaver, Surf. Sci. 132, 324 (1983).

32. P. S. Ho, G. W. Rubloff, J. E. Lewis, V. L. Moruzzi, and A. R. Williams, Phys. Rev. B27, 4784 (1980).

33. See, for example, C. N. Satterfield, Heterogeneous Catalysis in Practice, McGraw-Hill, New York, 1980.

34. E. Wimmer, C. L. Fu and A. J. Freeman, Phys. Rev. Lett. (in press).

FIGURE CAPTIONS

Figure 1. As 3d core lineshape at $h\nu$ = 85eV before (solid line) and after (dashed line) exposure to 1000L of oxygen. The spectra have been approximately normalized to the main emission feature (peak height) in order to to emphasize lineshape changes. The zero of the energy scale corresponds to the initial flat-band core binding energy. Top: oxidation of the cleaved GaAs (110) surface. The clean spectrum (solid line) has been shifted 0.6 eV to lower binding energy to compensate for the band bending that follows oxidation. Mid-section: oxidation in the presence of a Au overlayer (2.7 monolayer) gives rise to lineshape changes. The shaded areas emphasize new high binding energy core features that are the result of oxygen chemisorption. The vertical bars 1-4 indicate the chemically shifted core features observed by Landgren et al.[22] and associated with surface As atoms coordinated to 1, 2, 3, and 4 oxygen atoms, respectively. Bottom: oxidation in the presence of a Cr overlayer (2.8 monolayers). The vertical bars 1-4 are still derived from ref. 22. Vertical bar 5 shows the binding energy of the As 3d observed by Su et al.[23] and associated with As_2O_3.

Figure 2. Ga 3d core lineshape at $h\nu$ = 60eV before (solid line) and after (dashed line) exposure to 1000L of oxygen. The zero of the energy scale corresponds to the initial flat-band core binding energy. Top: oxidation of the cleaved GaAs (110) surface. The clean spectrum (solid line) is shown shifted 0.6 eV to lower binding energy to emphasize line shape changes and compensate for the band bending that follows oxidation. Mid-section: oxidation in the presence of Au overlayer (2.7 ML) gives rise to new high binding energy features (shaded areas). Vertical bars 1-4 indicate the chemically shifted core features observed by Landgren et al.[22] and associated with Ga atoms coordinated to 1, 2, 3 and 4 oxygen atoms, respectively. Bottom: oxidation in the presence of a Cr overlayer (2.8 ML). The vertical bars 1-4 are derived from ref. 22. Vertical bar 5 was obtained from the results of Su et al[24] for Ga_2O_3.

Figure 3. As 3d (left) and Ga 3d (right) core lineshape at $h\nu$ = 85 eV and 60 eV, respectively, before (solid line) and after (dashed line) exposure to 1000L O_2. The experimental energy resolution for these results is 0.8 eV. The topmost spectra have been obtained with 0.1 A Ag overlayer, the bottom-most ones for 1A overlayer. Relatively small metal coverages were used because of the sharp GaAs-Ag interface morphology[9-10]. The spectra before oxidation (solid line) have been shifted to low binding energy to compensate for the band bending that follows oxidation and emphasize lineshape changes. No oxidation promotion effects are seen within experimental uncertainty.

Figure 4. As 3d lineshape before (solid line) and after (dashed line) exposure to 1000 L H_2O. Spectra displaced downward show the

effect of Cr overlayers of increasing thickness during oxidation. Except for the band bending changes, the effect of water chemisorption is seen in the emergence of a relatively small oxidized feature between 2 and 3 eV below the flat-band initial core binding energy. The Cr-As reacted subsurface appears mostly stable against reaction with H_2O.

Figure 5. As 3d core lineshape during oxidation of the clean surface (topmost spectra) and for H_2O (mid-section) and O_2 chemisorption (bottom-most section) in the presence of Cr overlayers of similar thickness. The core emission is shown before (solid line) and after (dashed line) exposure to 1000L. The interaction with H_2O leaves the arsenide-like interface species relatively unchanged, while high stability oxidized phases are formed during oxygen exposure.

Figure 6. Ga 3d lineshape before (solid line) and after (dashed line) exposure to 1000 L H_2O. Spectra displaced downward show the effect of Cr overlayers of increasing thickness during exposure. Before water exposure increasing Cr deposition yields a low binding energy Cr-Ga alloyed feature 0.7-0.8 eV below the main line (solid line spectra). Upon water chemisorption the alloyed feature is removed and new high binding energy oxidized features appear between 1 and 3 eV below the main line.

Figure 7. Ga 3d core lineshape during oxidation of the clean surface (topmost spectra) and for H_2O (midsection) and O_2 chemisorption (bottom-most section) in the presence of Cr overlayers of similar thickness. The core emission is shown before (solid line) and after (dashed line) exposure to 1000L. The vertical bars 1-4 indicate the chemically shifted core features observed by Landgren et al.[22] and associated with Ga atoms coordinated to 1, 2, 3, and 4 oxygen atoms, respectively. Vertical bar 5 was obtained from the results of Su et al[24] for Ga_2O_3, vertical bar 6 from the results of Webb and Lichteusteiger[26] reportedly for Ga-OH bond formation. During water exposure no high stability Ga-oxide features (see bottom-most spectrum) are observed. Relatively broad and structured oxidized features are observed instead, suggesting Ga-hydroxyl bond formation and/or Ga oxide phases with low Ga-oxygen coordination and lower stability than Ga_2O_3.

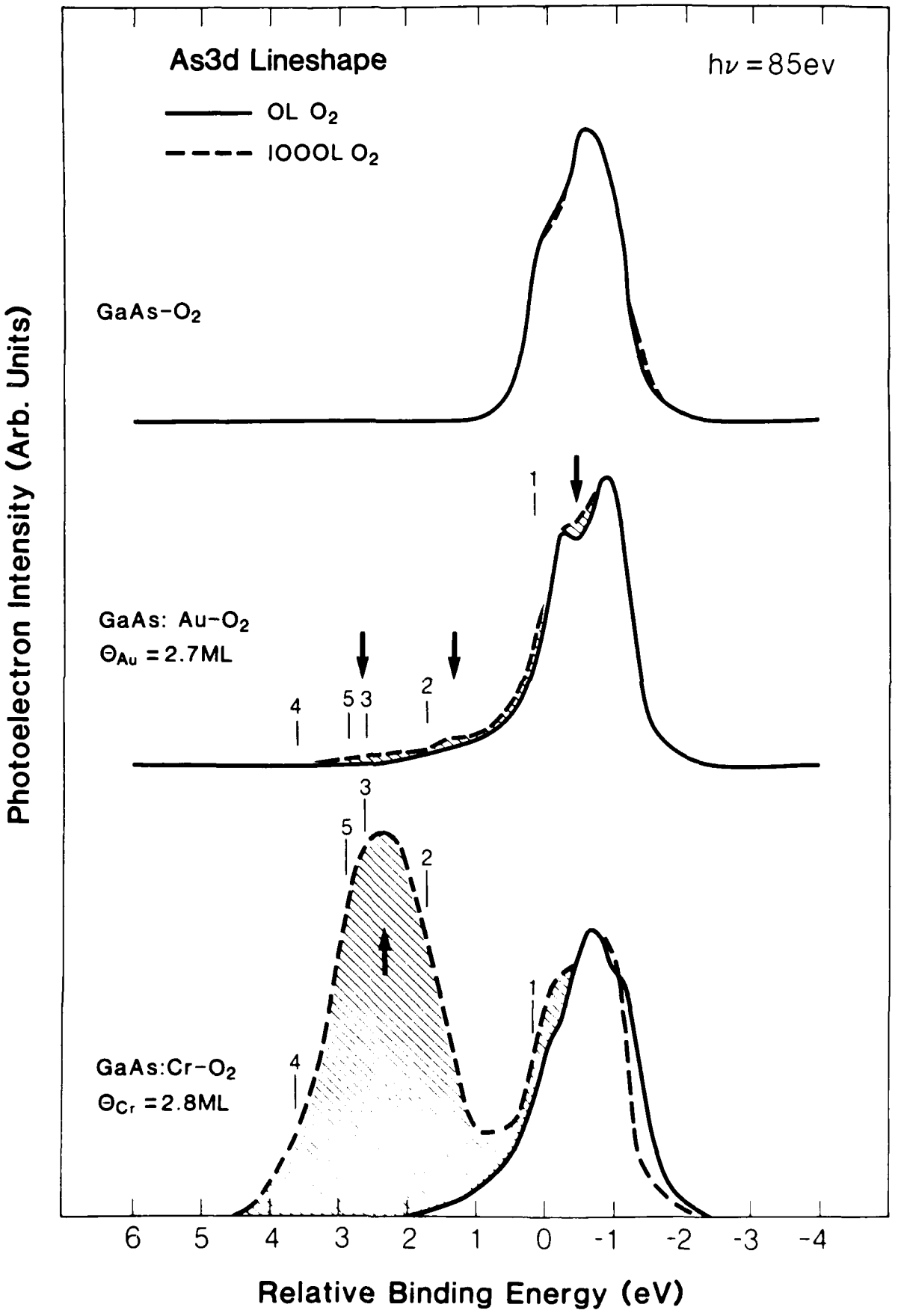
As3d Lineshape
hν = 85ev
OL O2
1000L O2
GaAs-O2
GaAs: Au-O2
ΘAu = 2.7ML
GaAs:Cr-O2
ΘCr = 2.8ML
1
2
3
4
5
Photoelectron Intensity (Arb. Units)
6 5 4 3 2 1 0 -1 -2 -3 -4
Relative Binding Energy (eV)

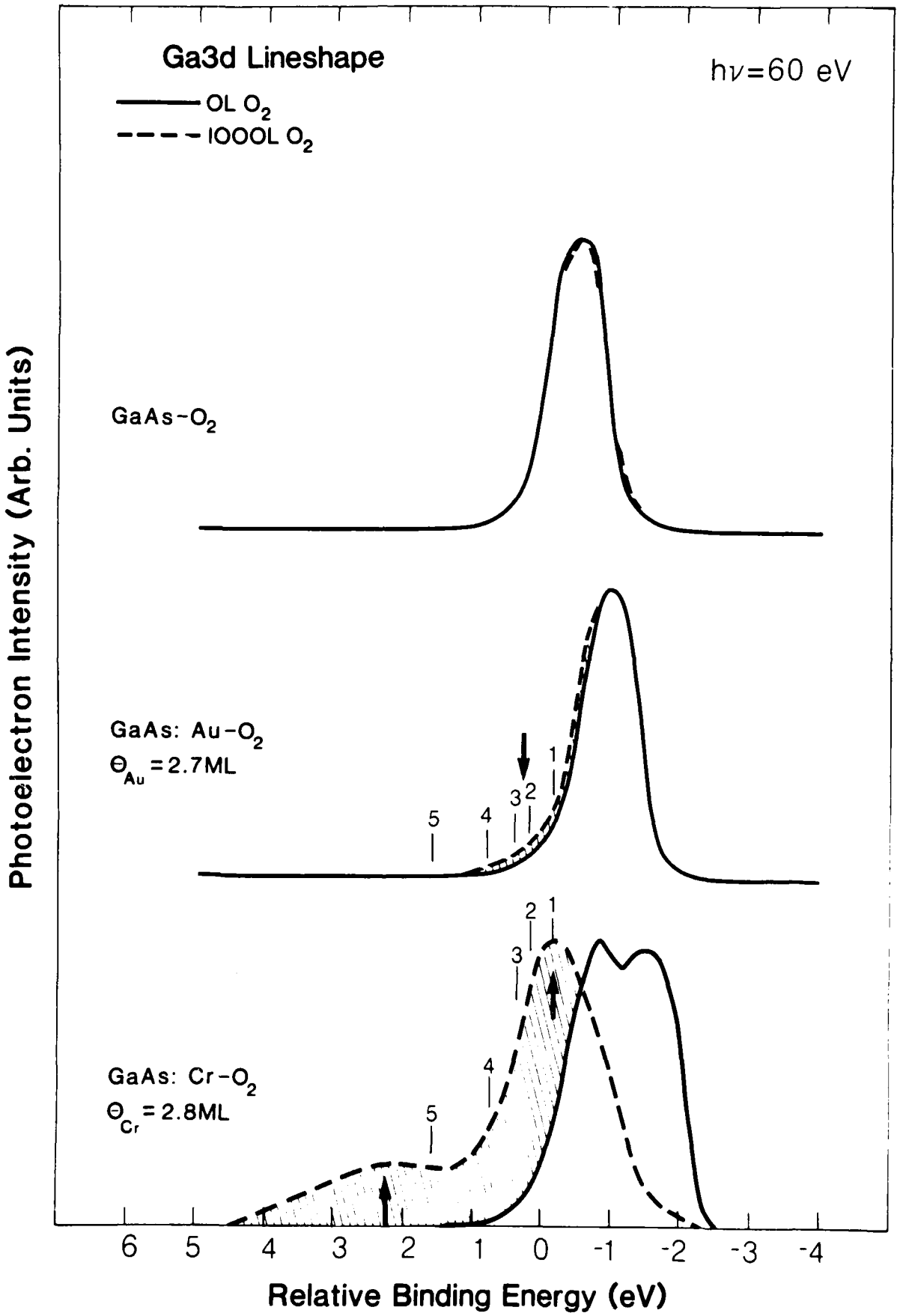
Ga3d Lineshape
hν=60 eV
OL O2
1000L O2
GaAs-O2
GaAs: Au-O2
ΘAu = 2.7ML
GaAs: Cr-O2
ΘCr = 2.8ML
1
2
3
4
5
Photoelectron Intensity (Arb. Units)
6 5 4 3 2 1 0 -1 -2 -3 -4
Relative Binding Energy (eV)

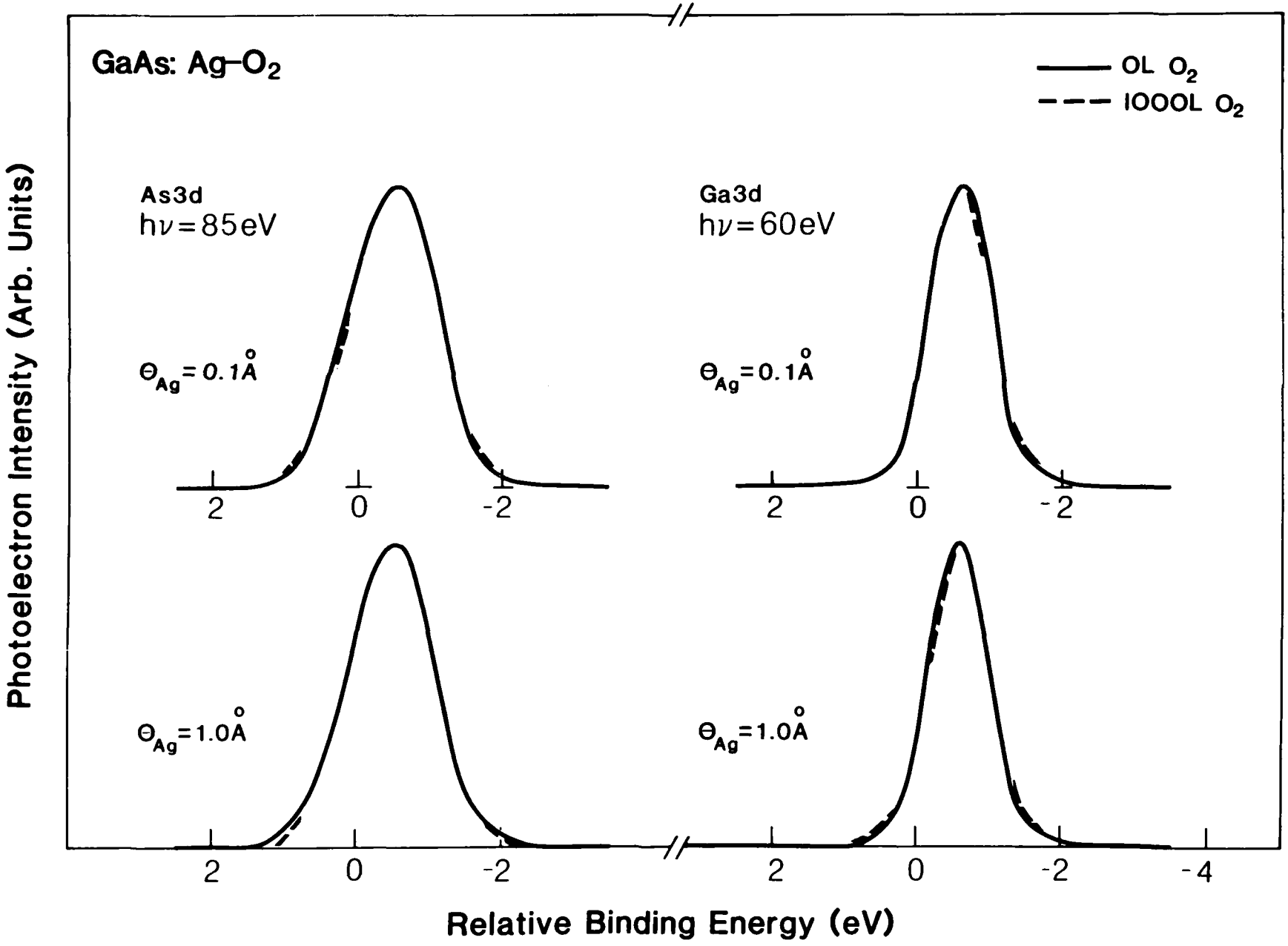
GaAs: Ag–O2
OL O2
1000L O2
As3d
hν=85eV
ΘAg=0.1Å
Ga3d
hν=60eV
ΘAg=0.1Å
ΘAg=1.0Å
ΘAg=1.0Å
2
0
-2
-4
Photoelectron Intensity (Arb. Units)
Relative Binding Energy (eV)

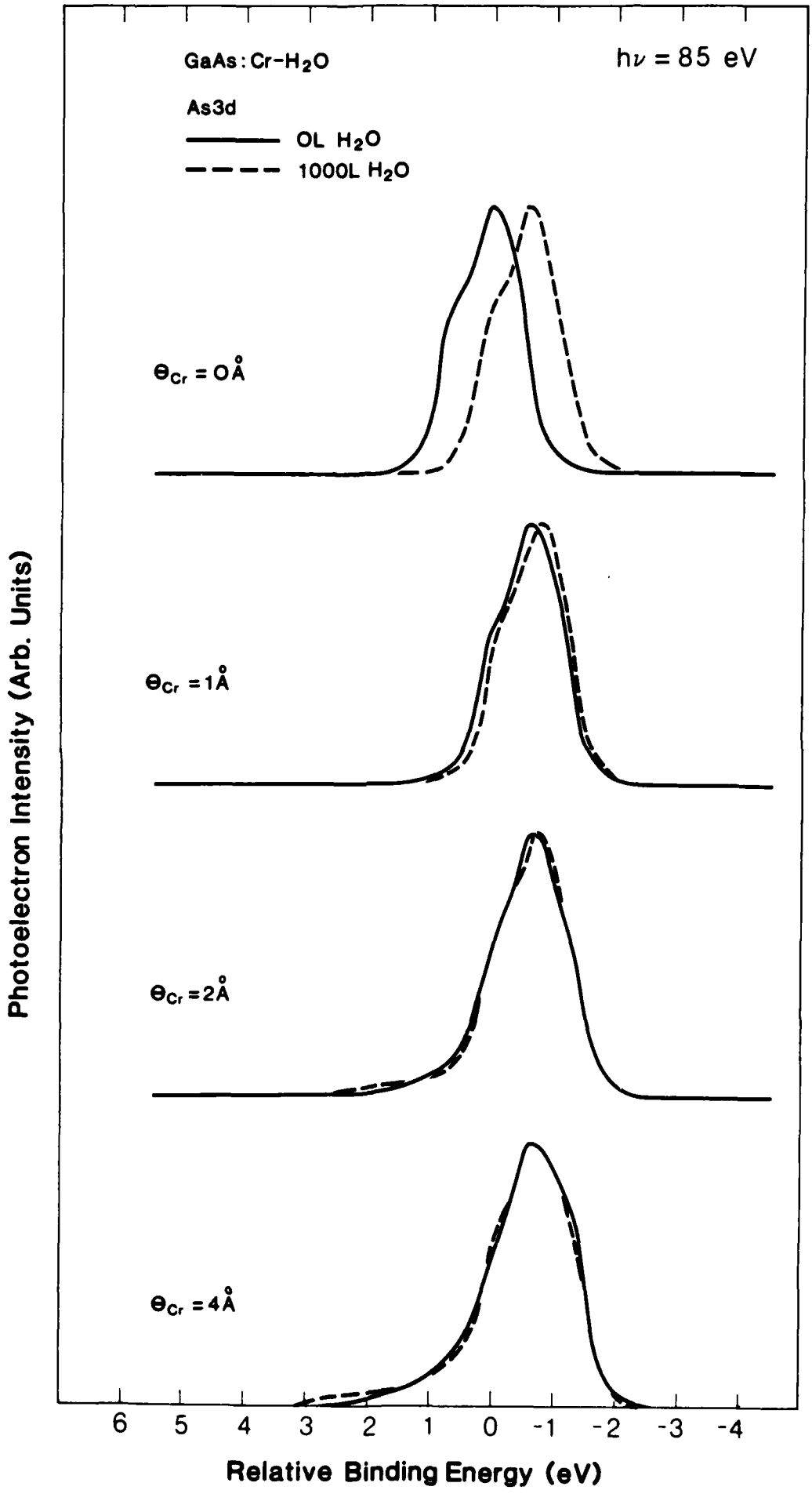
GaAs:Cr-H2O
hν = 85 eV
As3d
OL H2O
1000L H2O
θCr = 0Å
θCr = 1Å
θCr = 2Å
θCr = 4Å
Photoelectron Intensity (Arb. Units)
6
5
4
3
2
1
0
-1
-2
-3
-4
Relative Binding Energy (eV)

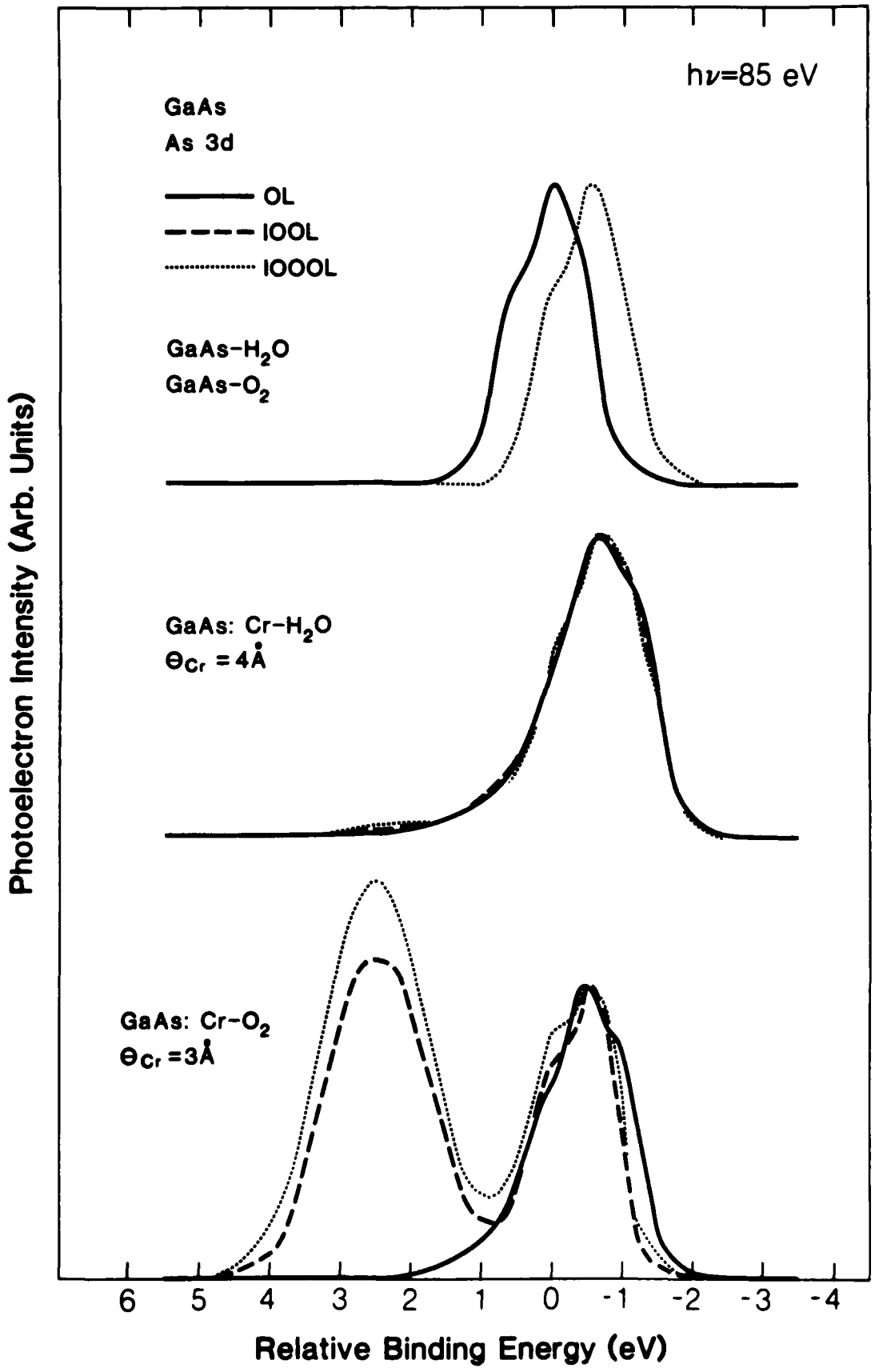
hν=85 eV
GaAs
As 3d
OL
IOOL
IOOOL
GaAs-H2O
GaAs-O2
GaAs: Cr-H2O
ΘCr = 4Å
GaAs: Cr-O2
ΘCr = 3Å
Photoelectron Intensity (Arb. Units)
6
5
4
3
2
1
0
-1
-2
-3
-4
Relative Binding Energy (eV)

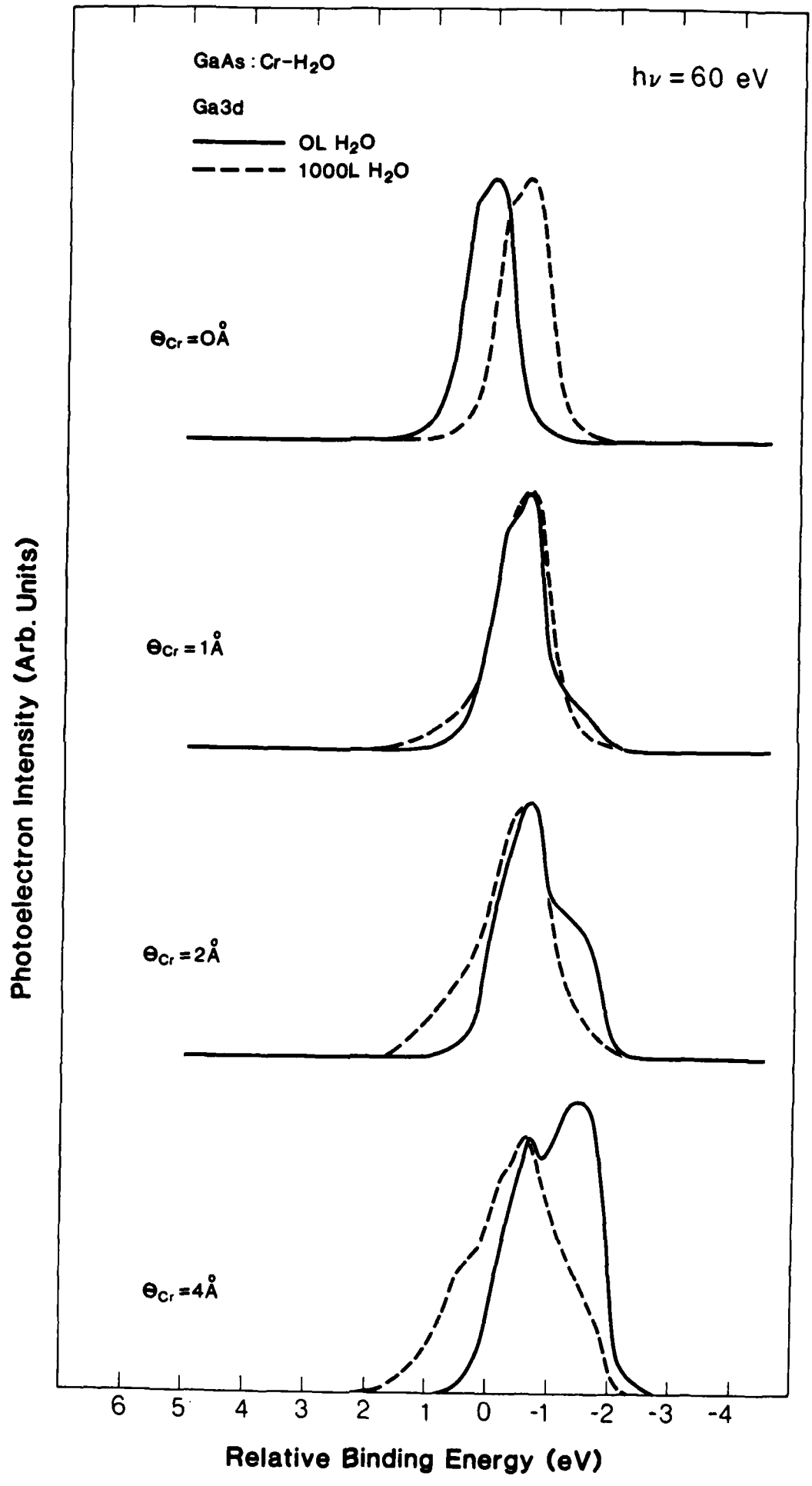
GaAs : Cr–H2O
hν = 60 eV
Ga3d
OL H2O
1000L H2O
θCr = 0Å
θCr = 1Å
θCr = 2Å
θCr = 4Å
Photoelectron Intensity (Arb. Units)
6
5
4
3
2
1
0
-1
-2
-3
-4
Relative Binding Energy (eV)

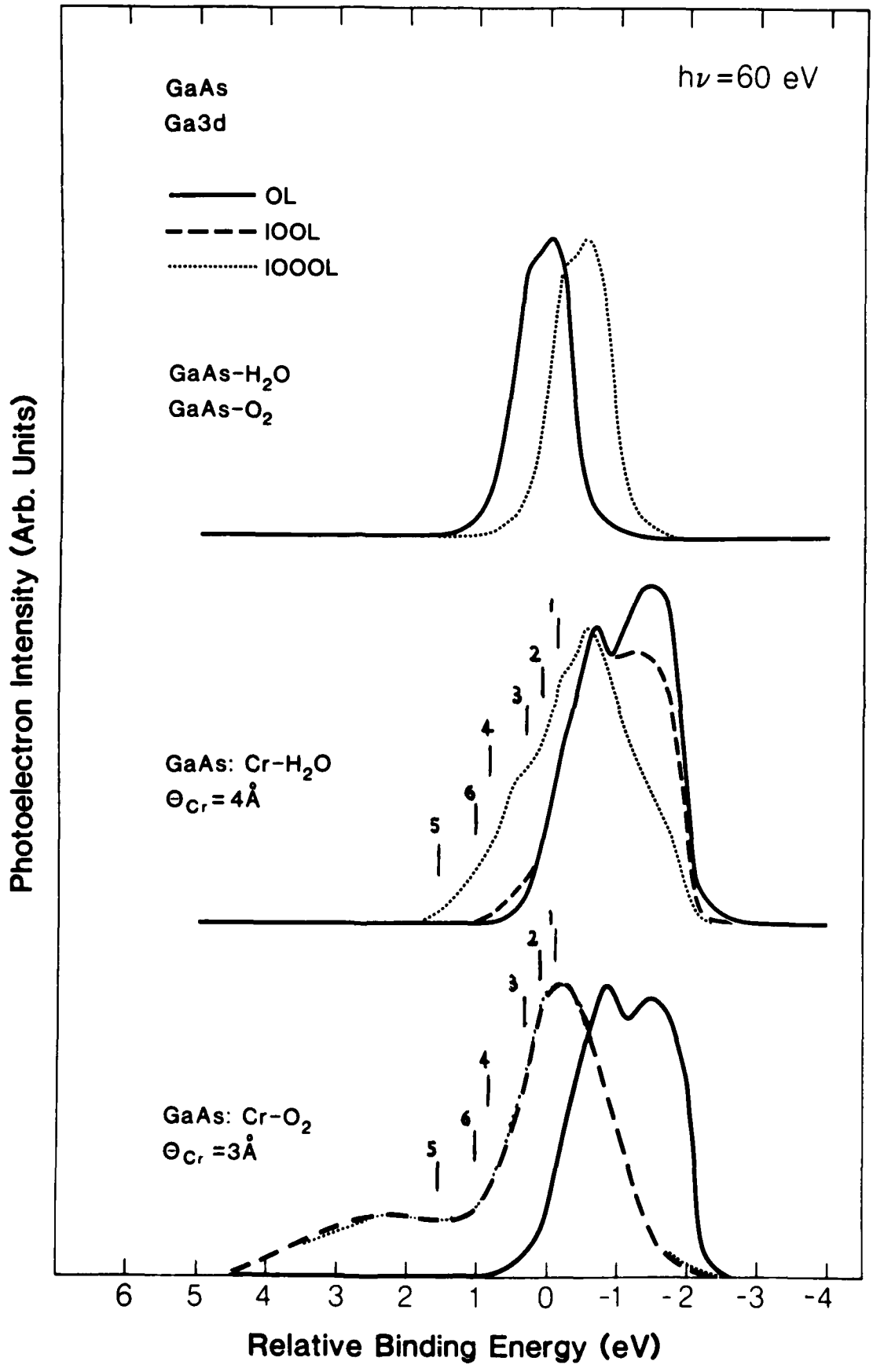
GaAs
Ga3d
hν=60 eV
OL
IOOL
IOOOL
GaAs-H2O
GaAs-O2
GaAs: Cr-H2O
ΘCr=4Å
GaAs: Cr-O2
ΘCr=3Å
1
2
3
4
5
6
Photoelectron Intensity (Arb. Units)
6 5 4 3 2 1 0 -1 -2 -3 -4
Relative Binding Energy (eV)

SUMMARY ABSTRACT

EXPERIMENTAL DETERMINATION OF THE ELECTRONIC STRUCTURE OF SMALL METAL PARTICLES

C. Caprile and A. Franciosi
Department of Chemical Engineering and Materials Science
University of Minnesota, Minneapolis, MN 55455

D. Wielickza
Department of Physics
University of Missouri, Kansas City, MO

C.G. Olson
Ames Laboratory-U.S. Department of Energy
Iowa State University, Ames, Iowa

The electronic structure of small metal particles and the modification of this electronic structure that derive from interaction with a substrate are of prime concern to all of us working in the area of catalysis and chemisorption. In recent years we have conducted a number of chemisorption studies involving metal-semiconductor interactions [1] where one attempts to correlate the changes in adatom and substrate electronic structure (core and valence levels) to the rather complex chemistry of the metal-semiconductor interface. Since large modifications of the metal states are expected also as a result of the increase in cluster size and/or overlayer thickness when a fully inert substrate is employed, the interface scientist is obliged to look for systematic correlation between changes in substrate and adatom electronic features in order to extract the information pertaining to interface chemistry. It is clearly very desirable to compare the results of any chemisorption study on "reactive" substrates with those of similar studies conducted on ideally inert substrates. However, "inert" substrates are hard to come by, and the available experimental information is very scarce. The importance of such studies is emphasized by the discomforting observation that virtually all studies of interface chemistry tend to produce "chemical" shifts of electronic levels and no evidence of size-induced effects in the overlayer states.

In the past the search for an ideally inert substrate has stimulated the use of materials as diverse as amorphous carbon, graphite, silica, layer compunds, etc.[2] Optical and transport studies have been recently supplemented by photoemission spectrosopy studies, that probe directly core and valence states of substrate and overlayer.[3-6] One promising pioneering study has shown the feasibility of synthesizing <u>in situ</u> metal clusters on solid rare

gases[7] and examine the electronic structure through conventional photoemission. Here we summarize the result of a first synchrotron radiation study of Sm clusters grown in <u>situ</u> on solid Xe crystals. Samarium was chosen because an extensive literature exist on the formation of clusters on amorphous carbon [6], on the electronic structure of Sm surfaces [8], and on the chemistry of Sm-semiconductor interfaces.[9-10] Spectroscopically, the Sm 4f emission is a sensitive probe of the local environment, and a valence transition is expected on going from isolated divalent Sm^{+2} atoms to the trivalent bulk.[6] The Sm^{+2} and Sm^{+3} configurations are easily distinguishable in photoemission since they give rise to final states multiplets widely spaced in energy.

A bellow-mounted closed-cycle refrigerator was used as sample manipulator. Films of Al or Sm were evaporated in situ on the polished Cu cold finger prior to cooling. The films (100-500Å thick) were kept at 15K during Xe condensation. Xe pressure in the 10^{-4}-10^{-7} torr range and total exposure in the 10-10^5 L range were explored. We monitored the attenuation of the characteristic substrate emission (Al 2p or Sm 4f levels) as a function of Xe exposure to calculate the thickness of the condensed Xe layer. Surprisingly we observed an exponential attenuation of the substrate emission with constant attenuation length throughout the 0-50L exposure range. Extrapolation to higher Xe coverages and escape depth values from the literature suggest that we were able to synthesize Xe layers in the 5-6000Å thickness range, that such films were stable in ultra-high vacuum on a time scale of several hours, and that the film thickness was uniquely determined by the overall Xe exposure in Langmuirs for a given substrate. Dramatic charging effects of the insulating Xe films were observed at thicknesses above 100Å, and for the cluster studies we used Xe films in the 40-70Å thickness range. Representative photoelectron energy

distribution curves (EDC's) for the 5p 5s and 4d emission from a 70Å Xe film condensed on Sm are shown in fig.1. The spectra have been recorded with a commercial double-pass cylindrical mirror analyzer and a thoroidal grating monochromator at the Synchrotron Radiation Center of the University of Wisconsin-Madison. The energy scale is referred to the substrate Fermi level. Similar results are obtained from Xe films condensed on Al. The only difference is a rigid shift of 1.8 eV to lower binding energies of all Xe spectral features. The shift reflects the variation in substrate work function and the alignment of the insulating Xe states to the vacuum level. We have also analyzed the evolution of the Xe core emission as a function of layer thickness to study relaxation effects induced by metal proximity. On Al we measure relaxation shifts of 0.5eV between the first and the second Xe layer, and of about 0.2eV between the second and the third layer. The shift appear smaller in the Xe-on-Sm case, suggesting a different spatial extension of the screening orbitals.

When a metal is evaporated onto the Xe surface, the small substrate-overlayer interaction results in agglomeration of the deposited film and cluster formation. This is readily visible in the EDC's, since even at the highest coverages explored the Xe emission is always visible. The attenuation of the Xe emission as a function of coverage can be used to estimate the average size of the metal clusters, purview that one makes some simplifying assumption on the cluster morphology. We assumed hemispherical cluster size[11] and through escape-depth dependent core level studies of substrate and metal emission we were able to obtain rough estimates of the average cluster radius. The information on the cluster electronic structure is provided by valence band EDC's after subtraction of the Xe contribution. The result is

shown in fig.2 where we compare the cluster valence emission at increasing metal coverage with the bulk Sm emission (topmost EDC) from a 450Å-thick film deposited on oxidized Ta. The vertical bars indicate the Sm^{+2} final state mutiplet near the Fermi level and the deeper Sm^{+3} mutiplet.[11] The Xenon layer was condensed on a Sm film in an original "sandwich" geometry that minimizes work function-related shifts and simplifies the subtraction of the Xe features. The results of fig. 2 clearly show the expected valence transition from a dominant Sm^{+2} configuration at small cluster size, to a metallic Sm^{+2}/Sm^{+3} ratio (topmost EDC) at larger cluster size. From the modeling of the Xe core emission described previously we estimate an average cluster diameter of about 30±8 Å at Sm coverages of $5x10^{14}$ atoms/cm^2 in fig.2 .[11]

In conclusion, we have presented a simple, straightforward technique to study cluster evolution. From escape-depth-dependent synchrotron radiation photoemission we can estimate cluster distribution and average cluster size. As a by-product of the Xe-metal interaction we obtain information on metal screening and work function[12]. The simplicity of the technique offer promise of wide-range systematic studies in the near future.

This work was supported in part by the Office of Naval Research and by the Microelectronic and Information Sciences Center of Minnesota. The Synchrotron Radiation Center of the University of Wisconsin is supported by NSF Grant No. DMR-80-20164.

REFERENCES

1. For a review of interface results see G. Margaritondo and A. Franciosi, Ann. Rev. Mater. Sci. 14, 67 (1984)

2. Due to space limitations we will not attempt here to summarize the extensive literatute on this subject. See a longer forthcoming paper: C. Caprile, A. Franciosi, D. Wieliczka and C.G. Olson, Phys. Rev. B

3. Y. Takasu, R. Unwin, B. Tesche, A.M. Bradshow, and M. Grunze, Surf. Sci. 77, 219 (1978) and references therein.

4. S.-T. lee, G. Apai, M.G. Mason, R. Benbow and Z. Hurych, Phys. Rev. B23, 505 (1981) and references therein.

5. G.K. Wertheim, S.B. DiCenzo, and S.E. Youngquist, Phys. Rev. Lett. 51, 2310 (1983) and references therein.

6. M.G. Mason, S.-T. Lee, G. Apai, R.F. Davis, D.A. Shirley, A. Franciosi and J.H. Weaver, Phys. Rev. Lett. 47, 730 (1981).

7. J. Colbert, A. Zangwill , M. Strongin, and S. Krummacher, Phys. Rev. B 27, 1378 (1983).

8. G.K. Wertheim and C. Crecelius, Phys. Rev. Lett. 40, 813 (1978); J.W. Allen, L.I. Johansson, I. Lindau, and S.B. Hagstrom, Phys. Rev. B21, 1335 (1980).

9. A. Franciosi, J.H. Weaver, P. Perfetti, A.D. Katnani, and G. Margaritondo, Solid State Commun. 47, 427 (1983).

10. A. Franciosi, P. Perfetti, A.D. Katnani, J.H. Weaver, and G. Margaritondo, Phys. Rev. B29, 5611 (1984).

11. For how to estimate cluster size from escape-depth-dependent core photoemission, see A. Franciosi, D.J. Peterman, J.H. Weaver, and V.L. Moruzzi, Phys. Rev. B25, 4981 (1982).

12. Xe chemisorption on metals is a sensitive probe of the local metal work function; see J.E. Hulse, J. Kuppers, K. Wandelt, and G. Ertl, Appl. Surf. Sci. 6, 453 (1980).

FIGURE CAPTIONS

Fig.1 Emission from the Xe 5p, 5s and 4d levels from a 50Å amorphous film condensed on a clean Sm substrate at 15K.

Fig.2 Valence band emission from Sm clusters deposited in situ on a solid Xe substrate. The spectra are shown after subtraction of the Xe 5p contribution. The topmost spectrum was obtained from a 450Å thick Sm film deposited at room temperature on oxidized Ta. The vertical bars indicate the 4f final state multiplets for the Sm^{+2} and Sm^{+3} configurations. A valence transition from a dominant divalent Sm configuration to a dominant trivalent configuration is seen with incresing cluster size.

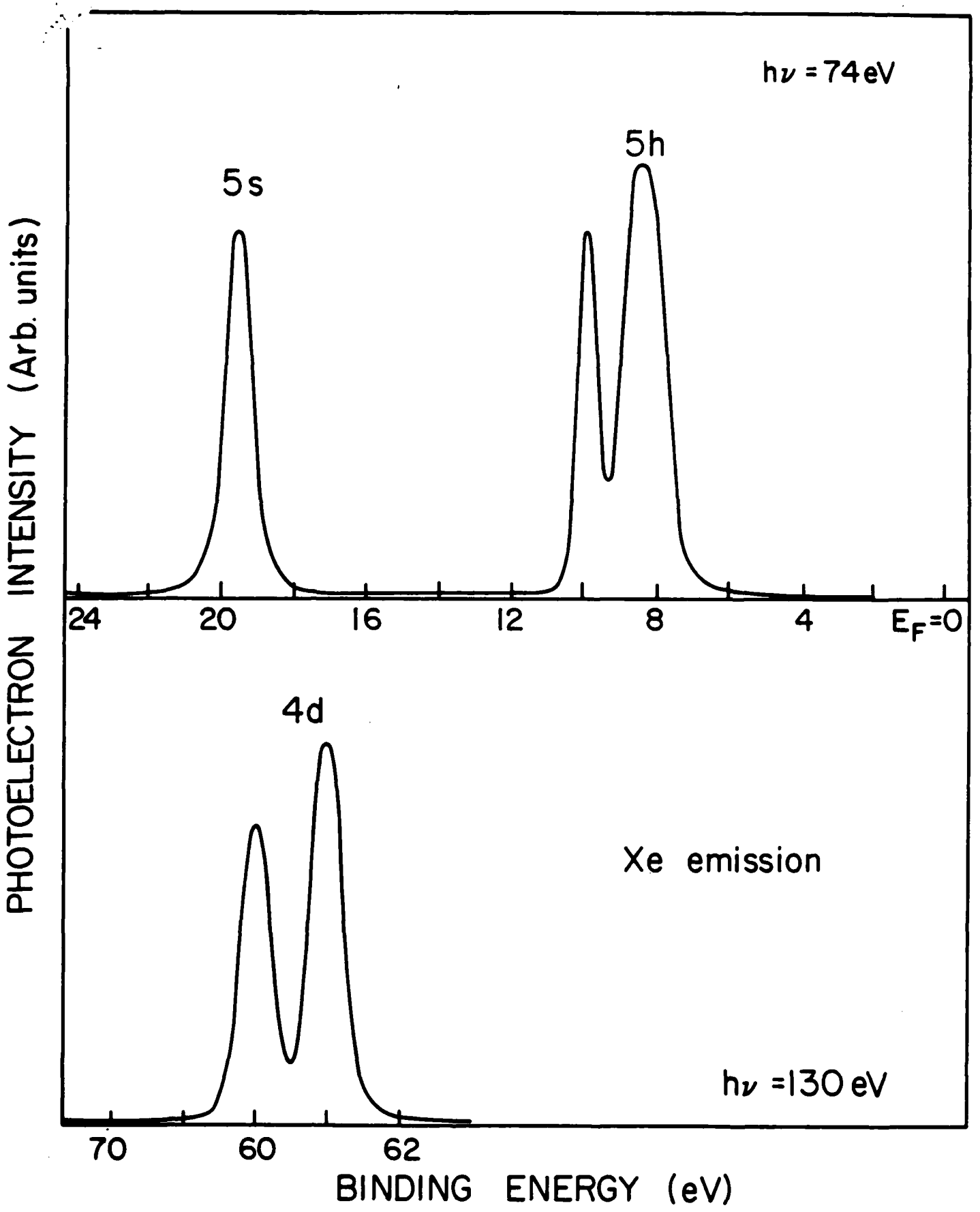
hν = 74 eV
5h
5s
PHOTOELECTRON INTENSITY (Arb. units)
24
20
16
12
8
4
E_F=0
4d
Xe emission
hν =130 eV
70
60
62
BINDING ENERGY (eV)

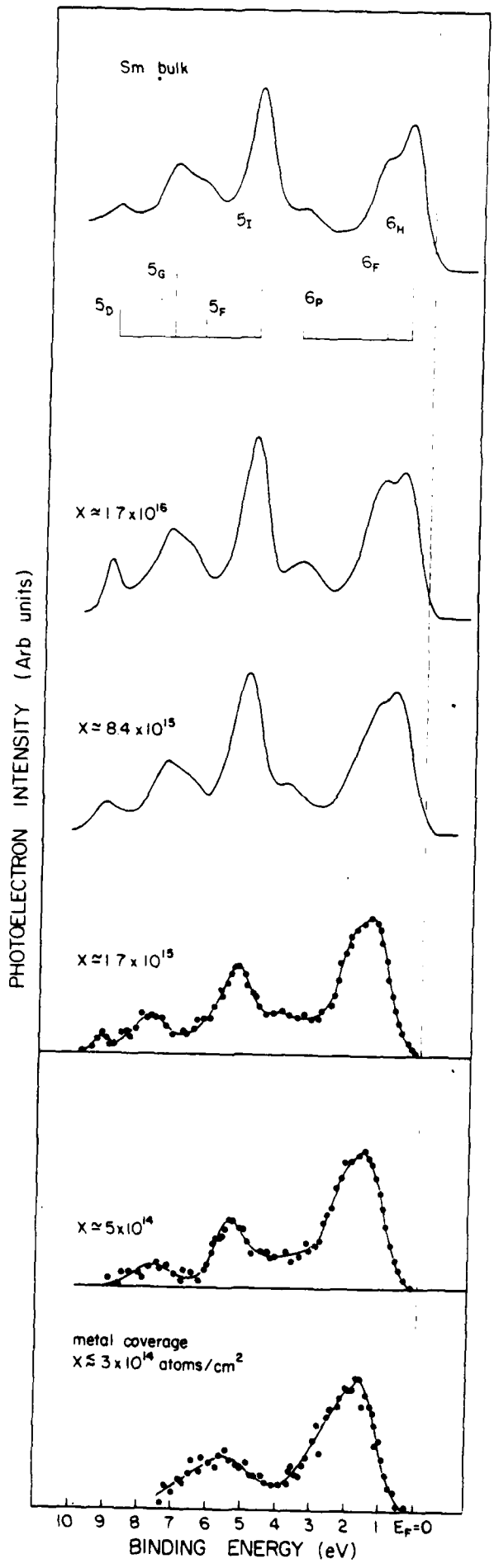
Sm bulk
5_I
6_H
5_G
6_F
5_D
5_F
6_P
X ≃ 1.7 x 10^16
X ≃ 8.4 x 10^15
X ≃ 1.7 x 10^15
X ≃ 5 x 10^14
metal coverage
X ≲ 3 x 10^14 atoms/cm^2
PHOTOELECTRON INTENSITY (Arb units)
10 9 8 7 6 5 4 3 2 1 E_F=0
BINDING ENERGY (eV)

DTIC

END

4-86